

TANEL SÕRMUS

Development of stimuli-responsive and
covalent bisubstrate inhibitors
of protein kinases



DISSERTATIONES CHIMICAE UNIVERSITATIS TARTUENSIS

217

DISSERTATIONES CHIMICAE UNIVERSITATIS TARTUENSIS

217

TANEL SÕRMUS

Development of stimuli-responsive and
covalent bisubstrate inhibitors
of protein kinases



UNIVERSITY OF TARTU

Press

1632

Institute of Chemistry, Faculty of Science and Technology, University of Tartu,
Estonia

The dissertation is accepted for the commencement of the degree of *Doctor philosophiae* in Chemistry on October 27th, 2022, by the Council of Institute of Chemistry, Faculty of Science and Technology, University of Tartu.

Supervisor: Dr Kaido Viht, Institute of Chemistry,
University of Tartu, Estonia

Opponent: Dr Matthias Gehringer

Commencement: December 14th, 2022, at 14:00, room 1020, 14A Ravila St.,
Institute of Chemistry, University of Tartu



European Union
European Regional
Development Fund



Investing
in your future

ISSN 1406-0299 (print)
ISBN 978-9916-27-084-4 (print)

ISSN 2806-2159 (pdf)
ISBN 978-9916-27-085-1 (pdf)

Copyright: Tanel Sõrmus, 2022

University of Tartu Press
www.tyk.ee

CONTENTS

LIST OF ORIGINAL PUBLICATIONS	7
ABBREVIATIONS	8
1. INTRODUCTION	11
2. LITERATURE OVERVIEW	12
2.1 Protein kinases	12
2.1.1 Catalytic domain of protein kinases	13
2.1.2 cAMP-dependent protein kinase	16
2.2 Protein kinase inhibitors	18
2.2.1 Inhibitors of cAMP-dependent protein kinase	21
2.2.2 Bisubstrate inhibitors of protein kinases	22
2.2.3 ARC-type inhibitors	23
2.3 Targeted covalent inhibitors	25
2.3.1 Target residues	27
2.3.2 Electrophile warheads	27
2.3.3 Covalent protein kinase inhibitors	30
2.4 Photochemistry	32
2.4.1 Photocaged bioactive compounds	34
3. AIMS OF THE STUDY	39
4. METHODS	40
4.1 Fluorescence anisotropy assay	40
4.2 Time-gated luminescence intensity assay	41
4.3 The measurement of active PK concentration	44
4.4 Displacement assays	45
5. RESULTS AND DISCUSSION	47
5.1 Construction of activatable and deactivatable bisubstrate PKA inhibitors (Paper I: Sörmus <i>et al</i> , 2019 and Paper II: Sörmus <i>et al</i> , 2022)	47
5.2 Construction of activatable photocaged bisubstrate PKA inhibitor (Paper I: Sörmus <i>et al</i> , 2019)	51
5.2.1 Characterisation of photocaged inhibitors	52
5.2.2 Photocaged inhibitors in cell lysates	54
5.3 Construction of deactivatable bisubstrate PKA inhibitors (Paper II: Sörmus <i>et al</i> , 2022)	56
5.3.1 Photocleavable inhibitor ARC-2121	57
5.4 Construction of a covalent bisubstrate PKA inhibitor (Paper III: Sörmus <i>et al</i> , 2022)	59
5.4.1 Characterization of reversible inhibitors	62
5.4.2 Characterization of covalent inhibitors	64
5.4.3 Reactions of fluorescent dye-labelled covalent inhibitor in cell lysates and cells	66

6. SUMMARY OF RESULTS AND DISCUSSION	69
7. REFERENCES	71
8. SUMMARY IN ESTONIAN	80
ACKNOWLEDGEMENTS	82
PUBLICATIONS	83
CURRICULUM VITAE	136
ELULOOKIRJELDUS	137

LIST OF ORIGINAL PUBLICATIONS

- I. **Tanel Sõrmus**, Darja Lavogina, Erki Enkvist, Asko Uri, and Kaido Viht. Efficient photocaging of a tight-binding bisubstrate inhibitor of cAMP-dependent protein kinase. *Chem. Commun.* **2019**, 55, 11147–11150.
- II. **Tanel Sõrmus**, Darja Lavogina, Erki Enkvist, Asko Uri, and Kaido Viht. Deactivatable bisubstrate inhibitors of protein kinases. *Molecules* **2022**, 27, 6689.
- III. **Tanel Sõrmus**, Darja Lavogina, Anu Teearu, Erki Enkvist, Asko Uri, and Kaido Viht. Construction of covalent bisubstrate inhibitor of protein kinase reacting with cysteine residue at substrate-binding site. *J. Med. Chem.* **2022**, 65, 16, 10975–10991.

Author's Contribution

Paper I: The author participated in planning the experiments. The author performed the synthesis and the biochemical experiments. Cultivation of cells was performed by a co-author. The author was responsible for writing of the manuscript.

Paper II: The author participated in planning the experiments. The author performed the experiments and the synthesis of the photosensitive compounds, co-author performed the experiments and the synthesis of the redox-sensitive compounds. The author wrote the original draft of the manuscript.

Paper III: The author planned most of the experiments. The author performed the synthesis, the biochemical experiments, and most of the Western Blot experiments. Cultivation of cells and microscopy experiments were performed by co-author. The author was responsible for writing of the manuscript.

ABBREVIATIONS

2PE	two-photon excitation
5-TAMRA	5-carboxytetramethylrhodamine
7DP	7 <i>H</i> -pyrrolo[2,3- <i>d</i>]pyrimidine
7DP-Pip	4-(piperazin-1-yl)-7 <i>H</i> -pyrrolo[2,3- <i>d</i>]pyrimidine
Ac	acetyl group
ADP	adenosine 5'-diphosphate
Ahx	6-aminohexanoic acid
AKAP	A kinase anchoring protein
AMP	adenosine 5'-monophosphate
AMPK	AMP-activated protein kinase
ARC	a conjugate of adenosine analogue and oligoarginine; broadly, protein kinase inhibitors developed in the university of Tartu, Institute of Chemistry
ARC-Lum	ARC-based probe possessing protein-induced luminescence signal with microsecond-scale lifetime
ARC-Lum(Fluo)	ARC-Lum probe incorporating a fluorescent dye
ATP	adenosine 5'-triphosphate
Bhc	6-bromo-7-hydroxycoumarin
BNSF	2,7-bis-{4-nitro-8-[3-(2-propyl)-styryl]}-9,9-bis-[1-(3,6- dioxahexyl)]fluorene
Boc	<i>t</i> -butoxycarbonyl
BODIPY	dipyrrrometheneboron difluoride
Bpy	2,2' bipyridine
BTK	Bruton tyrosine kinase
cAMP	3',5'-cyclic adenosine monophosphate
CFP	cyan fluorescent protein
CHO	Chinese hamster ovary
CIMK	chloromethyl ketone
COX	cytochrome c oxidase
CREB	cAMP response element-binding protein
CRG	covalent reactive groups
Cy	cyanine
DMNB	4,5-dimethoxy-2-nitrobenzyl
DMNPE	dimethoxynitrophenylethyl-type photocaging group
Dop	dopamine
EC ₅₀	half-maximal effective concentration
EGFR	epidermal growth factor receptor
EGTA	ethylene glycol tetraacetic acid
EPAC	exchange protein directly activated by cAMP
ErbB	epidermal growth factor family of receptor tyrosine kinases
FA	fluorescence anisotropy
FDA	the U.S. Food & Drug Administration

FMK	fluoromethyl ketone
Fmoc	fluorenylmethyloxycarbonyl
FP	fluorescence polarization
FRET	Förster-type resonance energy transfer
GM	Goeppert-Mayer unit
GSH	glutathione
GSK	glycogen synthase kinase
HEPES	4-(2-hydroxyethyl)-1-piperazineethanesulfonic acid
HER	human epidermal growth factor receptor
HSAB	hard and soft acids and bases theory
I_L	fluorescence intensity of horizontally polarized emissions
I_V	fluorescence intensity of vertically polarized emissions
IBMX	3-isobutyl-1-methylxanthine
IC_{50}	half-maximal inhibitory concentration; in competitive displacement assay: concentration of a competing ligand that causes 50% displacement of a probe
IP20	protein kinase inhibitor peptide (5-24)-amide
IR	infra-red radiation
IvDde	1-(4,4-dimethyl-2,6-dioxocyclohex-1-ylidene)-3-methylbutyl
K_D	dissociation constant
K_i	inhibition constant
K_I	the concentration of inactivator that yields a rate of inactivation equal to $\frac{1}{2} k_{inact}$
k_{inact}	inactivation rate constant of irreversible inhibitor
k_{inact}/K_I	second order rate constant that accounts for the affinity of the initial reversible binding and the maximal rate of covalent bond formation of TCIs
k_{off}	dissociation rate constant
k_{on}	association rate constant
Lo5	Lipinski's rule of five
MAPK	mitogen-activated protein kinase
MEK	mitogen-activated protein kinase kinase; MAP2K
MNI	4-methoxy-7-nitroindoliny
MSK1	mitogen- and stress-activated protein kinase 1
NB	<i>o</i> -nitrobenzyl-type photocaging group
Nda	nonanedioic acid
NDBF	2-methyl-3-nitrodibenzo[<i>b,d</i>]furan
Nic	nicotine (3-[(2 <i>S</i>)-1-methylpyrrolidin-2-yl] pyridine)
NSCLC	non-small cell lung cancers
o/n	overnight
Pan	panitumumab
pdb	protein data bank
PDE	phosphodiesterases
PDK1	3-phosphoinositide-dependent kinase-1

PDT	photodynamic therapy
Phos	phosphate buffer
PK	protein kinase
PKA	protein kinase A; cAMP-dependent protein kinase
PKAc	catalytic subunit of cAMP-dependent protein kinase
PKAr	regulatory subunit of cAMP-dependent protein kinase
PKB	protein kinase B; Akt
PKI	heat stable protein kinase inhibitor peptide
PPG	photoremovable protecting group
PSA	polar surface area
RI	regulatory subunit type I of PKA
RII	regulatory subunit type II of PKA
ROCK	Rho-associated protein kinase
ROS	reactive oxygen species
RSK	ribosomal S6 Kinase
S ₀	ground state
S ₁	lowest excited singlet state
SCI	substrate-competitive inhibitors
SDS-PAGE	sodium dodecyl sulphate-polyacrylamide gel electrophoresis
SGK	serum- and glucocorticoid-inducible kinases
S-S	singlet-singlet transition
STS	staurosporine
<i>t</i> _½	half-life
T ₁	lowest excited triple state
TCEP	tris(2-carboxyethyl)phosphine
TCI	targeted covalent inhibitor
TFA	trifluoroacetic acid
TGLI	time-gated luminescence intensity
THF	tetrahydrofuran
T-S	triplet-singlet transition
Umb	6,8-difluoro-4-methyl-umbelliferone
UV	ultraviolet light
UVA	ultraviolet A (315-400 nm)
UVB	ultraviolet B (280-315 nm)
UV-Vis	ultraviolet and visible light
Vis	visible light
WB	Western Blot
WT	wild-type
YFP	yellow fluorescent protein

1. INTRODUCTION

Protein kinases (PK) are enzymes which catalyse protein phosphorylation and consequently affect almost all cell functions via a myriad of mechanisms. An impaired activity of PKs has been linked to many diseases like cancer. Understanding the structures and interactions of PKs has led to the development of PK inhibitors providing us with more than 70 drugs since the early 2000s. Although majority of the approved PK inhibitor drugs are ATP-competitive, bisubstrate PK inhibitors, which bind the ATP-pocket and peptide binding region simultaneously, can achieve greater affinity and selectivity. In addition to pharmacological perspective, PK inhibitors are valuable chemical probes in PK related research.

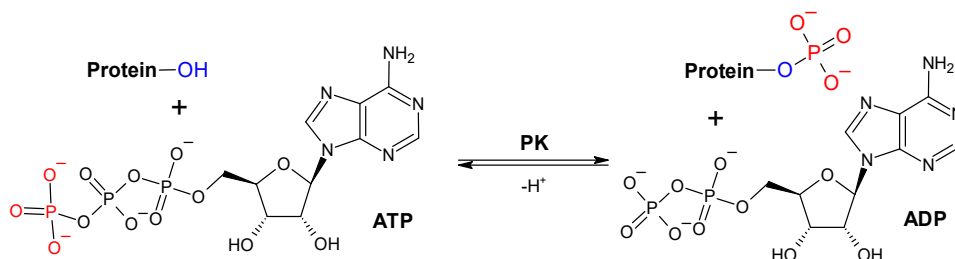
The thesis describes the design, synthesis, and biochemical characterization the first photocaged, the first deactivatable, and the first covalent bisubstrate inhibitors of basophilic protein kinases based on previously measured crystallographic data of ARC-type bisubstrate inhibitors and cAMP-dependent protein kinase (PKA). The bisubstrate nature of the inhibitors enabled to achieve exceptionally large binding affinity changes for the photocaged and deactivatable inhibitors upon applying the stimuli (over 5 orders of magnitude), as well as very high efficiency of covalent modification ($k_{\text{inact}}/K_{\text{I}}$) values for the covalent bisubstrate inhibitors.

This work illustrates how bisubstrate inhibitors can be flexibly modified to gain new features. The principles of covalent binding and on-command activation and deactivation of bisubstrate inhibitors were demonstrated on a quantitative level and can be used in the further design of stimuli-responsive and covalent bisubstrate inhibitors.

2. LITERATURE OVERVIEW

2.1 Protein kinases

Protein kinases (PK) are enzymes which catalyse the reaction of protein phosphorylation. During the phosphorylation reaction PK mediates the γ -phosphoryl group (PO_3^{2-}) from ATP to a hydroxyl group of an amino acid of a substrate protein, forming a phosphoamino acid (**Scheme 1**). These target amino acids are serine (85%), threonine (11.8%), or tyrosine (1.8%) [Schwartz et al. 2011].



Scheme 1. General scheme of protein phosphorylation

Phosphoamino acids are distinctly different from unphosphorylated amino acids since they possess a larger hydration shell and a negative charge greater than 1 at physiological pH. Thus, phosphoamino acids form very strong hydrogen bonds and salt bridges with other amino acids, they diversify protein surfaces, and most importantly generate phosphorylation-dependent-binding sites for other proteins to recognize, which enables signal transduction. A transfer of a single phosphoryl group may result in various inter- and intramolecular interactions, functioning as a switch turning cellular signalling pathways “on” or “off”. Phosphorylation of proteins is one of the most common and important post-translational modifications in eukaryotes. Therefore, PKs play a crucial role in almost every aspect of cellular function by controlling metabolism, transcription, cell division, and programmed cell death, while also participating in immune response and nervous system function [Roskoski 2015].

Table 1. Groups of PKs

number	Group name	Origin of the group name	Number PKs
I	The AGC group	PKA , PKG , PKC	64
II	The CAMK group	CA lcium/cal M odulin-dependent K inases	82
III	The CK1 group	C asein K inases 1	12
IV	The CMGC group	the C yclin-dependent kinases, M AP kinases, G lycogen synthase kinases, C asein	65
V	The STE group	homologs of yeast Sterile 7, Sterile 11, ST erile 20 kinases	49
VI	The TK group	Tyrosyl K inase	95
VII	The TKL group	Tyrosyl K inase- L ike	43
VIII	The RCG group	R eceptor G uanylyl C yclase	5
IX	OTHER		82
X	Atypical		58

There are over 500 PK-encoding genes [Manning et al. 2002; Fabbro et al. 2015; Kanev et al. 2019] in the human genome, which constitutes more than 2.5% of all human genes. Roughly 90% of the PKs are typical and 10% atypical. Atypical PKs have reported to have biochemical activity but lack sequence similarity to the other PKs [Manning et al. 2002]. PKs can also be divided based on the nature of the phosphorylated hydroxylic groups (alcohol or phenol) – protein-serine/threonine kinases (75%), protein-tyrosine kinases (17%), and tyrosine-kinase like kinases (8%). Based on the gene sequences the catalytic domains of PKs have been mapped on a dendrogram (the “kinome tree”) and divided into ten larger groups (**Table 1**) [Manning et al. 2002; Kanev et al. 2019]. The catalytic domains of PKs share a conserved arrangement of secondary structure elements which include activation loop, catalytic loop, and glycine-rich loop among others (**Figure 1A**). About 10% of PKs are inactive or weakly active pseudo-kinases. Pseudo-kinases can bind ATP and have a regulatory function, but they lack at least one of the three catalytic domain motifs listed above [Fabbro et al. 2015].

2.1.1 Catalytic domain of protein kinases

PKs are highly regulated and are activated by regulatory stimuli [Taylor et al. 2012]. PK activation/deactivation mechanisms are diverse and PK specific: some PKs may need multiple other PKs to contribute to their activation (e.g., S6K [Zhang et al. 2013] others do not need phosphorylation for their activation (e.g., ErbB1/2/4 [Gotoh et al. 1992]). Often the phosphorylation of the activation loop is required for PK activity, making the segment a fundamental element of PKs. For example, phosphorylation in the activation loop of PKA (Thr197) fixes the C-helix (His87) and the catalytic loop (Arg165) together and positions them for the phosphorylation reaction (**Figure 1B**). The activation

loop is highly dynamic and phosphorylated either with *cis* or *trans* auto-phosphorylation or by an activating PK. The activation loop begins with a highly conserved DFG sequence and almost always ends with APE sequence but is highly varied in terms of length (**Figure 1B**). In the active “DFG-in” conformation the Asp residue is important for the binding of Mg^{2+} ions (Asp184 in PKA; **Figure 1B**). Mg^{2+} ions act as cofactors of PK and are also needed for the catalysis reaction.

The catalysis of the phosphorylation reaction takes place in the conserved core of the catalytic domain of PKs, which consists of approximately 250 residues. The core of the catalytic domain is located between two lobes of PK – amino-terminal lobe (N-lobe) and carboxyterminal lobe (C-lobe) [Knighton et al. 1991] (**Figure 1A**).

The smaller N-lobe features only a single α -helix (α C helix) and a five-stranded antiparallel β -sheet (β 1- β 5) (**Figure 1C**). The correct positioning of the α C helix, termed “C-helix-in”, is essential for an efficient catalysis and is facilitated by a conserved salt bridge between the active site Lys and a Glu from the α C helix (Lys72 and Glu91 in PKA; **Figure 1C**). The first two strands (β 1 and β 2) of the β -sheet in the N-lobe are joined by a conserved glycine-rich loop (GxGx ϕ G), where ϕ is a hydrophobic residue (**Figure 1C**). The glycine-rich loop plays an important role in positioning of the phosphates of ATP for the catalysis at the outer edge of the ATP-binding site.

The larger C-lobe consists mainly of conserved α -helices (8) and loops, including the activation loop and the catalytic loop (**Figure 1A**). The catalytic loop contains the highly conserved Y/HRD motif with the strictly conserved Asp residue (D166 in PKA) which assists in the transfer of the γ -phosphoryl group from the ATP to the substrate protein (**Figure 1B**).

The N- and C-lobes of PKs are connected by the hinge region (**Figure 1A**). The adenine of ATP is positioned inside the cleft between the N-lobe and C-lobe where it forms hydrogen bonds with the backbone residues of the hinge region [Roskoski et al. 2016]. The catalysis reaction is resolved by opening and closing of the active site cleft, granting the γ -phosphate transfer and the release of the nucleotide. The rate-limiting step of the catalysis reaction is the 20-fold slower ADP dissociation. [Taylor et al. 2004]

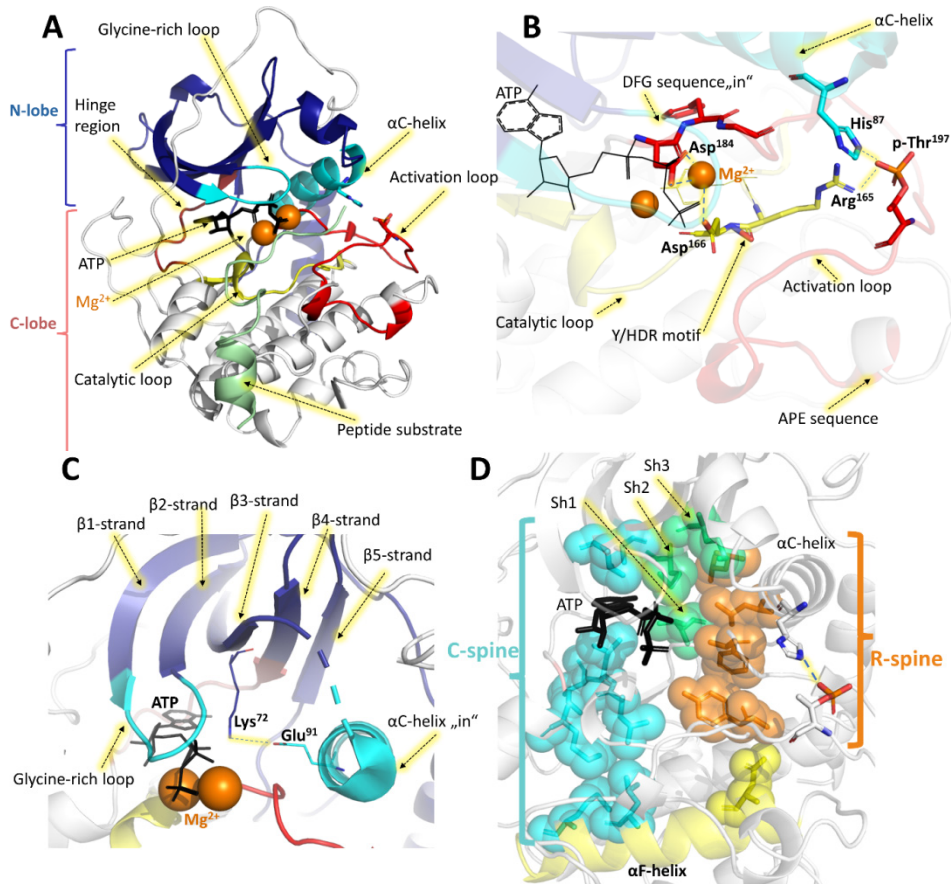


Figure 1. Crystal structure of PKAc in complex with ATP and PKI(5-24)-amide (1ATP). (A) N-lobe displayed in dark blue of which the C-helix and the glycine-rich-loop displayed in teal; C-lobe displayed in white of which the catalytic loop displayed in yellow and the activation loop in red; the hinge region between the lobes displayed in brown. (B) Magnification of the activation loop displaying the DFG-segment “in” conformation. (C) Magnification of the N-lobe displaying the α C-helix “in” conformation. (D) Spines of PKs with C-spine in teal and R-spine in orange connected by the α F-helix of the C-lobe in yellow; the shell residues (Sh1-3) displayed in green.

Catalytic domains of PKs comprise two hydrophobic spines, which connect and align both lobes, the regulatory (R) and catalytic (C) spine (**Figure 1D**). R-spine and C-spine are important for positioning the protein substrate and the ATP, respectively, for catalysis. The R-spine comprises two residues from both lobes and is assembled in active PKs (aligning the β 4 strand, α C helix, the DFG motif, and the α E helix). Usually, activation loop phosphorylation causes the phenylalanine in the DFG motif to flip “in” to complete the R-spine (**Figure 1B**). The C-spine runs parallel to the R-spine and the two spines are connected via the α F helix (**Figure 1D**). The C-spine comprises 8 residues and is completed upon binding the adenine ring of ATP. ATP binding positions the spines

and aligns the PK's catalytic residues optimally for the catalysis [Taylor et al. 2012; McClendon et al. 2014].

Shell amino acids (Sh1, Sh2, Sh3) are also important for PK activity. These amino acids activate and stabilize the PKs (**Figure 1D**). Sh1 occurs in the "back-loop" where it connects the α C helix and β 4-strand. Sh1 is conserved in 90% of PKs and plays an essential role in their catalytic activity [Meharena et al. 2013]. Sh2 is called the gatekeeper residue and it occurs deep in the ATP-binding site before the hinge region at the end of β 5-strand. The gatekeeper residues are often large (3/4 of all PKs) and hydrophobic (4/5 of all PKs). The gatekeeper residue controls the access to the back cleft of the PK which can only be accessed if the gatekeeper residue is small (e.g., Thr or Val [Zuccotto et al. 2010]). The uncommon small gatekeeper residues have enabled the development of drugs with bulky groups which fill the back cleft and thus increase selectivity. Unfortunately, the gatekeeper residue is inclined to mutate in cancer cells for bulkier residue causing drug resistance [Ung et al. 2018]. Sh3 residue occurs in the β 5-strand, two residues upstream of Sh1, and is conserved as a hydrophobic residue in 98% of PKs. Sh2 and Sh3 can compensate each other, but at least one is needed for the catalytic activity [Meharena et al. 2013].

2.1.2 cAMP-dependent protein kinase

cAMP-dependent protein kinase (Protein kinase A; PKA) is a basophilic enzyme which belongs to the AGC group of PKs. PKA was first purified in 1968 and the catalytic subunit of PKA (PKAc α) has served as a prototype for the catalytic domains of PKs [Walsh et al. 1968]. PKA is a heterotetrameric holoenzyme which is catalytically inactive. The PKA holoenzyme is composed of two catalytic subunits (C; PKAc α , PKAc β , or PKAc γ) and a regulatory subunit dimer (R; PKArI α , PKArI β , PKArII α , or PKArII β ; **Figure 2A**). In basal state, the catalytic activity of PKAc is inhibited by the RI or RII with a sub nanomolar affinity ($K_D = 0.23$ nM and 0.27 nM, respectively [Hofmann 1980]). There is a large excess of PKAr in the cells compared to PKAc with most of the PKAr being RII rather than RI in any given tissue (e.g., 17-fold excess of PKAr [Walker-Grey et al. 2017]).

The release of free PKAc from the holoenzyme is regulated by the concentration of a secondary messenger cyclic-AMP (cAMP) [Gold 2019; Smith et al. 2017]. The PKAr dimer contains four cyclic nucleotide-binding domains which bind cAMP resulting in a dissociation of the active PKAc subunits. The cellular levels of cAMP are increased because of intracellular stimuli activating the 7-transmembrane receptors, which in turn activate the adenylate cyclase inside the cell, that starts converting available ATP into cAMP.

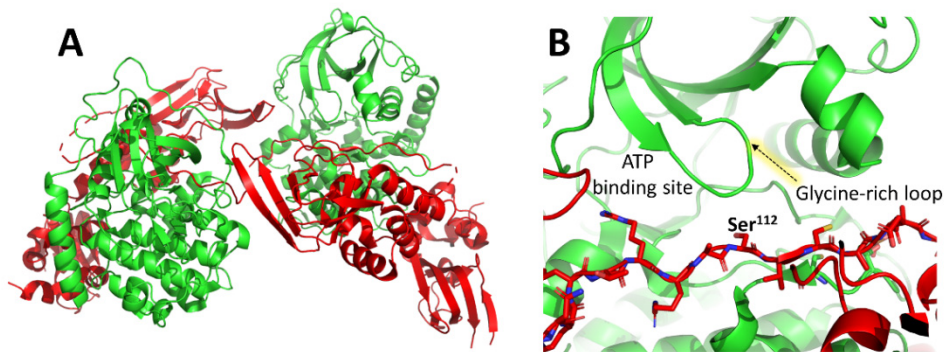


Figure 2. Crystal structure of PKA holoenzyme. **(A)** The crystal structure of the PKA heterotetrameric holoenzyme. The catalytic subunits are depicted in green and the regulatory dimer in red (pdb: 3tnp). **(B)** Magnification of Figure 2A near the phosphorylation site of PKARII.

PKAc has a MW of around 40 kDa and it is mainly encoded by *PRKACA* and *PRKACB* genes, which express the $C\alpha$ and $C\beta$ subunits, respectively. $C\alpha$ is essential to life, as mice with the deletion of *PRKACA* gene die before birth [Skålhegg et al. 2002], while deletion of *PRKACB* gene interestingly leads to protection from certain age-related heart problems [Enns et al. 2010]. $C\alpha$, $RI\alpha$, and $RII\alpha$ are expressed ubiquitously in cells, while $C\beta$ and $RI\beta$ are primarily found in the brain, and $RII\beta$ is expressed in the brain, endocrine tissues, fat, and in the reproductive organs alongside $C\gamma$ [Søberg and Skålhegg 2018].

The PKA holoenzyme is localized in the cells by A kinase anchoring proteins (AKAPs) which restrict the free movement of PKAs. There are over 50 AKAPs which are expressed in essentially all tissue and cell types [Søberg and Skålhegg 2018]. The AKAPs bind the R subunits and are divided as RI-, RII-, or dual-specific AKAPs. Cyclic nucleotide phosphodiesterases (PDEs) also take part in the compartmentalization of active PKAc in cells by restraining intracellular cAMP levels and generating local pools of cAMP [Taskén and Aandahl 2004].

For the catalytic activity, PKAc needs two phosphorylation events – auto-phosphorylation at Ser338 and phosphorylation of Thr197 in the activation segment by PDK1 (**Figure 1B**). The free PKAc is then able to start phosphorylating its substrate proteins in the cytoplasm. In total, there are over 250 PKA-substrates described [Isobe et al. 2017]. RII is also a substrate of PKAc and contains a serine residue that is phosphorylated, unlike RI which is a pseudo-substrate of PKA (**Figure 2B**). PKAc can also migrate to the nucleus, where it phosphorylates the cAMP response element binding protein (CREB), which then activates the transcription of genes. PKAc is transported back to the cytoplasm from the nucleus by the heat stable protein kinase inhibitor (PKI) [Dalton and Dewey 2006] after which PKAr can re-establish its holoenzyme complex with PKAc by outcompeting the PKI. PKI is an endogenous PKAc selective

thermostable protein [Chen and Sabatini 2021; Coover et al. 2016], which also modulates the function of PKAc in addition to the PKAr, especially if cAMP levels have been elevated. PKI has three endogenous isoforms (α, β, γ) that consist of 75, 70, or 75 amino acids, respectively (MW \sim 11 kDa). PKI mimics the structure of PKAr and binds the PKAc with high selectivity and affinity ($K_D = 2$ nM [Demaille et al. 1977]), although only the inhibition domain (1–25) is needed for the high affinity ($K_D \text{ PKI}(5-24) = 2.3$ nM [Herberg and Taylor 1993]). Without the activation loop phosphorylation of Thr197, the binding affinity of PKI for PKAc decreases 10-fold [Steichen et al. 2010]. Synergistic ATPMg binding to PKAc ($K_D \text{ ATP} = 10$ μ M [Whitehouse et al. 1983]) is needed for the tight binding of RI and PKI, without ATPMg a 1000-fold weaker affinity for PKAc is observed ($K_D \text{ RI} = 125$ nM and $K_D \text{ PKI} = 2.3$ μ M [Herberg and Taylor 1993]). RII subunit, on the other hand, does not need ATPMg for the stable holoenzyme formation. The regulation of PKA in the cell is a complex system encompassing a vast number of substrates with the regulation and specificity depending on the concentration of GPCRs, PKAs, AKAPs, PDEs etc.

2.2 Protein kinase inhibitors

PKs were promoted as the major drug targets of the 21st century already 20 years ago when only a few PK inhibitors had been approved by the U.S Food & Drug Administration (FDA) [Cohen, 2002; Roskoski 2015]. This was mostly due to the tremendous therapeutic success of one of the earliest PK inhibitors – imatinib (Gleevec, approved in 2001), which motivated the race to develop PK inhibitors. The patent for imatinib ended in 2016 and its global annual income a year earlier in 2015 was \$4.7 billion [Chen and Kesselheim 2017]. Imatinib proved that the selectivity issues and ATP-competitiveness caused by the conserved ATP-binding site and high cellular concentration of ATP (1–5 mM) do not prevent PK inhibitors from becoming therapeutics. In the 1980s, a natural compound, staurosporine was pursued, which had good potency although lacked selectivity (**Figure 3A**). The first PK inhibitor used as a drug was fasudil, a ROCK kinase inhibitor, which was approved in Japan in 1995 for cerebral vasospasm. In 1999, sirolimus became the first FDA approved PK inhibitor (also the first allosteric PK inhibitor), it is used for the prevention of organ rejection. The second FDA-approved drug was imatinib in 2001 (**Figure 3A**). [Attwood et al. 2021]

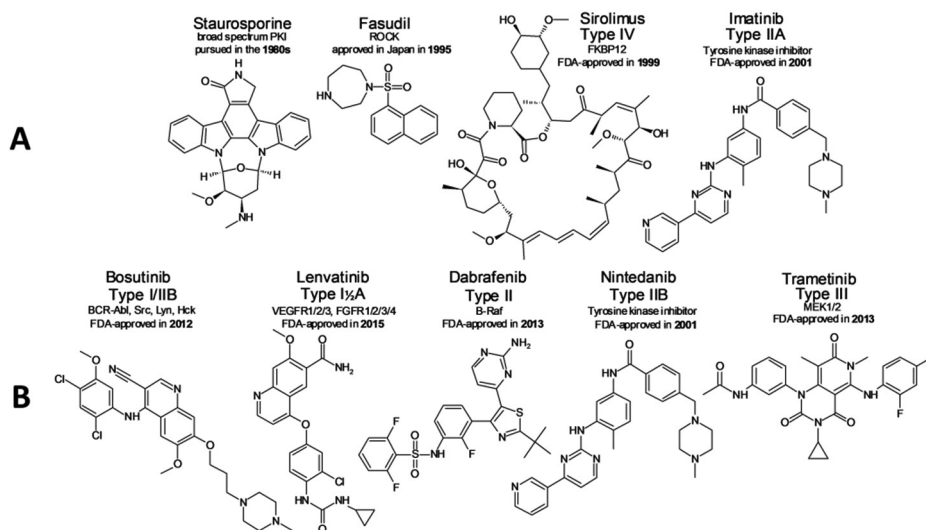


Figure 3. Examples of protein kinase inhibitors. (A) Some of the earliest PK inhibitors; (B) Examples of PK inhibitors of different types [Roskoski 2016].

To date FDA has approved 71 PK inhibitors from which 31 were approved in the last four years (2018-2022) [Roskoski 2022a]. FDA-approved inhibitors target over 20 different PK families and generally have low nanomolar to picomolar K_i values for their target. Also, there is an additional list of PK inhibitors used as drugs, which have been approved by other agencies, making the total count of PK inhibitors approximately 100 [Attwood et al. 2021]. Still, there is an enormous potential for PK inhibitors, since the approved drugs only target primarily 42 PKs (mostly of the TK group) from the total of >500 PKs.

The ATP-binding sites of PKs evolved to bind ATP, which makes them similar and thus the development of specific PK inhibitors more challenging. Many of the approved PK inhibitors are in fact multikinase inhibitors, which may add to their clinical effectiveness but may also lead to various side effects [Roskoski 2021a]. Overall, it is unclear if pursuing a single-molecule selective compound (“magic bullet”) or selectively non-selective compound (“magic shotgun”) in drug discovery is preferred [Roth et al. 2004]. Also, many of the PK inhibitors are used to treat multiple diseases. Imatinib, for example, was initially used to treat chronic myelogenous leukaemia, but it has now become a broad-spectrum inhibitor – it is used for 8 distinct disorders [Roskoski 2021a]. Majority of the PK inhibitors are used for the treatment of oncological illnesses (61 of the 71 FDA approved PK inhibitors).

Lipinski’s rule of five (Lo5) sets ranges for physicochemical parameters to determine whether a substance would be likely to make an orally active drug [Lipinski et al. 2001]. According to Lo5, an orally active drug should have no more than one violation of the following: $MW \leq 500$ (or $5 \cdot 100$); $\text{Log } P \leq 5$; number of H-bond donors ≤ 5 ; number of H-bond acceptors ≤ 10 or $(2 \cdot 5)$.

LogP indicates the hydrophobicity where larger P value indicates a greater hydrophobicity. Additional criteria were added later like counting the rotatable bonds (≤ 10) and rings (≥ 3) or calculating the polar surface area (PSA; $\leq 140 \text{ \AA}^2$). The range limits of Lo5 for MW and cLogp can be exceeded more easily – 27 of the PK inhibitors have a MW higher than 500 and 23 have a greater cLogP than 5. On the other hand, only a few molecules break the laws of having more than 10 H-bond acceptors or more than 5 H-bond donors [Roskoski 2021a]. The average MW of the FDA-approved PK inhibitors is 499 spanning from 306 Da to 1029 Da. Overall, out of the 71 molecules, 54 follow the rules and break only one or none of the Lo5, 13 molecules break 2 rules, and 4 molecules break 3 rules. If the extended criteria of counting rings, rotatable bonds, and PSA are also accounted for, then 10 more molecules deviate from the Lo5.

Table 2. Groups of PKs

Inhibitor type	Binding mode	DFG	ATP-competitive	Reversible
I	Active kinase-ATP pocket	In	Yes	Yes
I½ A/B	Inactive kinase-ATP pocket	In	Yes	Yes
I½ A	- Extends to the back cleft	In	Yes	Yes
I½ B	- Doesn't extend to back cleft	In	Yes	Yes
II A/B	Inactive kinase-ATP pocket	Out	Yes	Yes
II A	- Extends to the back cleft	Out	Yes	Yes
II B	- Doesn't extend to back cleft	Out	Yes	Yes
III	Allosteric (proximal)	Varies	No	Yes
IV	Allosteric (distal)	Varies	No	Yes
V	Bivalent	Varies	Varies	Yes
VI	Covalent	Varies	No	Varies

PK inhibitors can be divided into 7 main groups based on the binding modes of the inhibitor to PK (**Table 2**) [Roskoski 2016]. Types I, I½, and II bind the ATP-binding site directly and typically contain an aromatic system incorporating nitrogen atoms which act as H-bond donors or acceptors. Whereby, type I inhibitors bind to the active PK conformation (with both DFG motive and αC “in”), types I½ and II bind the inactive conformation of PK with the distinction of the DFG motif “in” or “out”, respectively. Type III and IV inhibitors, on the other hand, are allosteric inhibitors, which bind other binding sites either close or distal from the ATP-binding site, respectively. Type V inhibitors are bivalent or bisubstrate inhibitors, which occupy two distinct parts of the PK. Type VI inhibitors are covalent inhibitors which form an irreversible covalent bond with their target enzymes.

The construction of PK inhibitors has been mainly focused on type I, I½, and II inhibitors. Accordingly, most of the FDA-approved PK inhibitors bind the ATP-binding site directly, from which more than 10 target the active

conformation (type I; e.g., **Figure 6A**) and more than 35 target the inactive conformation (types I $\frac{1}{2}$ and II; e.g., **Figure 3**, **Figure 6A**). 8 molecules also form an irreversible covalent bond to their target (type VI; e.g., **Figure 6B-D**) [Roskoski 2022b]. So far only a few drug molecules bind allosteric binding sites (types III and IV; e.g., **Figure 3**) and no bivalent (type V) PK inhibitors have become drugs.

Due to the conserved nature of the ATP-binding site, it may be difficult for ATP-competitive PK inhibitors to achieve selectivity. The substrate protein binding site of PKs, on the other hand, is less conserved and offers better possibilities for achieving selectivity. Protein substrate-competitive inhibitors (SCI) bind to the protein substrate binding site, which is a shallow crevice near the ATP-binding site. The substrate is anchored and positioned in the crevice for the phosphorylation event [de Oliveira et al. 2016]. SCIs must make interactions on the surface of the target PK which is not well-defined and open to solvent. Small ATP-competitive PK inhibitors have the advantage of being pushed into a hydrophobic shell which surrounds them and affords multiple interactions. To have similar number of interactions, SCIs must surround a part of the protein meaning that these molecules need be larger, and thus, frequently violate the Lo5. Further, their delivery to cells is often complicated. SCIs do not readily diffuse across the cell plasma-membrane, instead they are typically taken up into cells by endocytosis trapping them inside intracellular vesicles from where they have difficulty escaping [Teo et al. 2021]. In addition, SCIs which contain mainly of natural amino acid sequences may be susceptible to hydrolysis by cellular proteases.

2.2.1 Inhibitors of cAMP-dependent protein kinase

Although it has been suggested that PKA inhibition might be used in transplantation, brain recovery after ischemic stroke, as an autophagy inducer and inflammatory inhibitor [Liu et al. 2020], to date there are no drugs which specifically target PKA. To determine PKAc's involvement in cellular processes small inhibitors, which bind the ATP-binding site of PKAc, have been used, like KT5720 or H-89 (**Figure 4**; $K_D = 60$ nM and 6 nM, respectively [Liu et al. 2020; Miick et al. 2005; Viht et al. 2007]). Both compounds were initially marketed as selective and potent PKA inhibitors, although now they have been shown to inhibit multiple other PKs in addition to PKAc. KT5720, an analogue of staurosporine is a non-specific inhibitor of PKA and binds multiple PKs (PKB, MEK, MSK1, GSK-3 β , AMPK [Murray 2008]). H-89 was also found to inhibit at least 8 other PKs (PKB, ROCK2, MSK1, SGK, RSK1, RSK2, AMPK, CHK1) and cause a broad effect on the phosphoproteome in PKA-null cells [Limbutara et al. 2019]. The inhibition of PKA activity has also been achieved by cAMP analogues for PKAr to prevent PKAc dissociation (e.g., Rp-8-Br-cAMPS; **Figure 4**) [de Wit et al. 1984]. However, this technique also affects other cAMP targets (e.g., EPAC) and requires high cellular concentrations of the inhibitor ($c > 10$ μ M) to effectively inhibit PKA activation [Liu et al. 2020].

Thus, drawbacks such as necessity for a high cellular concentration and non-specific binding hinder the usage of small inhibitors of PKA.

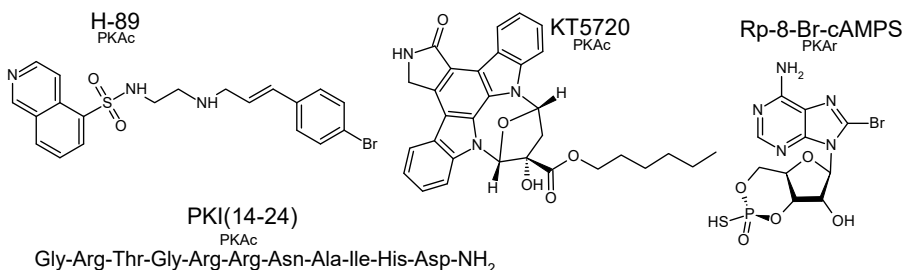


Figure 4. Examples of PKA inhibitors

Peptide analogue inhibitors based on the PKI have been developed, which provide a more selective inhibition profile. Synthetic peptide analogues, like PKI(6-22)-amide, PKI(5-24)-amide, and PKI(14-24)-amide (**Figure 4**) have been synthesised with nanomolar affinities towards PKAc ($K_D = 7.4$ nM, 19 nM, and 340 nM, respectively [de Boer et al. 2005]). Different modifications have been added to peptidic segments to help them enter the cells, like myristylation [Eichholtz et al. 1993] or introducing hydrocarbon-stapled modifications [Manschwetetus et al. 2019].

2.2.2 Bisubstrate inhibitors of protein kinases

Bisubstrate PK inhibitors constitute two fragments which occupy two distinct substrate sites of the PK simultaneously. Bisubstrate PK inhibitors are heterobifunctional – they contain two distinct pharmacophores linked via a spacer. One of the moieties binds the ATP-binding site, and the other moiety binds the peptide substrate-binding site. The bisubstrate PK inhibitors have an advantage of generating more interactions with its target PK, which can net an increased affinity and selectivity. The incorporation of two different moieties into one compound leads to a significant increase in binding affinity. The binding free energy of both moieties can be added up, with the extra free energy of linking from entropic gain [Lavogina et al. 2010; Turnbull 2005] (equation 1).

$$\Delta G_1 + \Delta G_2 + \Delta G_{linking} = RT \ln K_D, \quad (1)$$

where K_D is the dissociation constant of the ligand-receptor complex. Upon a linear increase of the free binding energy, the K_D value decrease is exponential. Thus, it is not unusual for bisubstrate PK inhibitors to have K_D values in the low picomolar range. High affinity is the greatest strength of bisubstrate inhibitors in addition to possible high selectivity towards specific PK targets, and tolerance towards ATP-binding site mutations [Lee et al. 2021]. Bisubstrate inhibitors could provide much better chances to fulfil the “magic bullet” strategy of

targeting only a specific PK compared to the small ATP-competitive PK inhibitors. Bisubstrate inhibitor strategy has made way for many selective and high affinity inhibitors [Lavogina et al. 2010; Lee et al. 2021]. Avidity, known as functional affinity, is the accumulated strength of multiple affinities summed up from multiple binding interactions and is mainly used to describe the binding of antibodies, since they harbour multiple domains [Lee et al. 2021]. Avidity can be used to describe bisubstrate inhibitors too. On the other hand, bisubstrate inhibitors have an inherent difficulty to satisfy the MW requirement of Lo5. As discussed above, most of the FDA-approved PK inhibitor drugs abide the Lo5, so the intrinsically high MW discourages development of bisubstrate inhibitors. What is more, similarly to SCIs, large structures which incorporate poly-peptidic fragments may limit the bioavailability.

2.2.3 ARC-type inhibitors

ARC inhibitors are bisubstrate PK inhibitors, which have been developed in Dr Asko Uri's lab in the University of Tartu for the past 30 years. ARCs used to stand for adenosine oligo-arginine conjugates, but the meaning has since been widened to cover conjugates of adenosine analogues and peptide mimetics. ARCs comprise an ATP-binding site-targeting moiety which was connected to the substrate peptide mimetic (e.g., oligo-D-arginine) fragment via a hydrophobic linker (**Figure 5**).

ARC inhibitors overcome some of the setbacks of bisubstrate inhibitors. For example, the 1st generation ARCs comprised L-amino acids and their replacement with D-amino acids significantly increased their binding affinity and intracellular stability (ARC-902; **Figure 5**) [Enkvist et al. 2006]. The crystal-structure guided design of ARC-inhibitors has led to several improved properties like increased affinity and selectivity of compounds. The affinity and selectivity were improved by varying the ATP binding site moiety: e.g., ARC-902 and ARC-1411 possess a 100-fold K_D difference towards PKAc (**Figure 5**) [Vaasa et al. 2009; Ivan et al. 2016]. A longer linker incorporating a chiral spacer was utilized to direct the oligoarginine fragment of the inhibitor into a more favourable position. The chiral spacer also forms hydrogen bonds with the glycine-rich loop increasing the affinity and selectivity of the ARCs: e.g., ARC-1034 and ARC-1012 possess a 40-fold K_D difference towards PKAc (**Figure 5**) [Lavogina et al. 2009]. Using different ATP-binding site moieties and oligo-aspartate fragments in ARC structures (e.g., oligo-aspartates or their isomeric peptoid counterparts) high-affinity inhibitors of acidophilic PKs have been developed (ARC-1502; **Figure 5**) [Enkvist et al. 2012]. ARCs have also displayed the ability to enter the cell, either in a form of a prodrug (ARC-1849; **Figure 5**) [Viht et al. 2015], by virtue of comprising a polyarginine sequence [Vaasa et al. 2010; Enkvist et al. 2006], or an extra hydrophobic modification (ARC-1143, **Figure 5**) [Kriisa et al. 2015; Nonga et al. 2021].

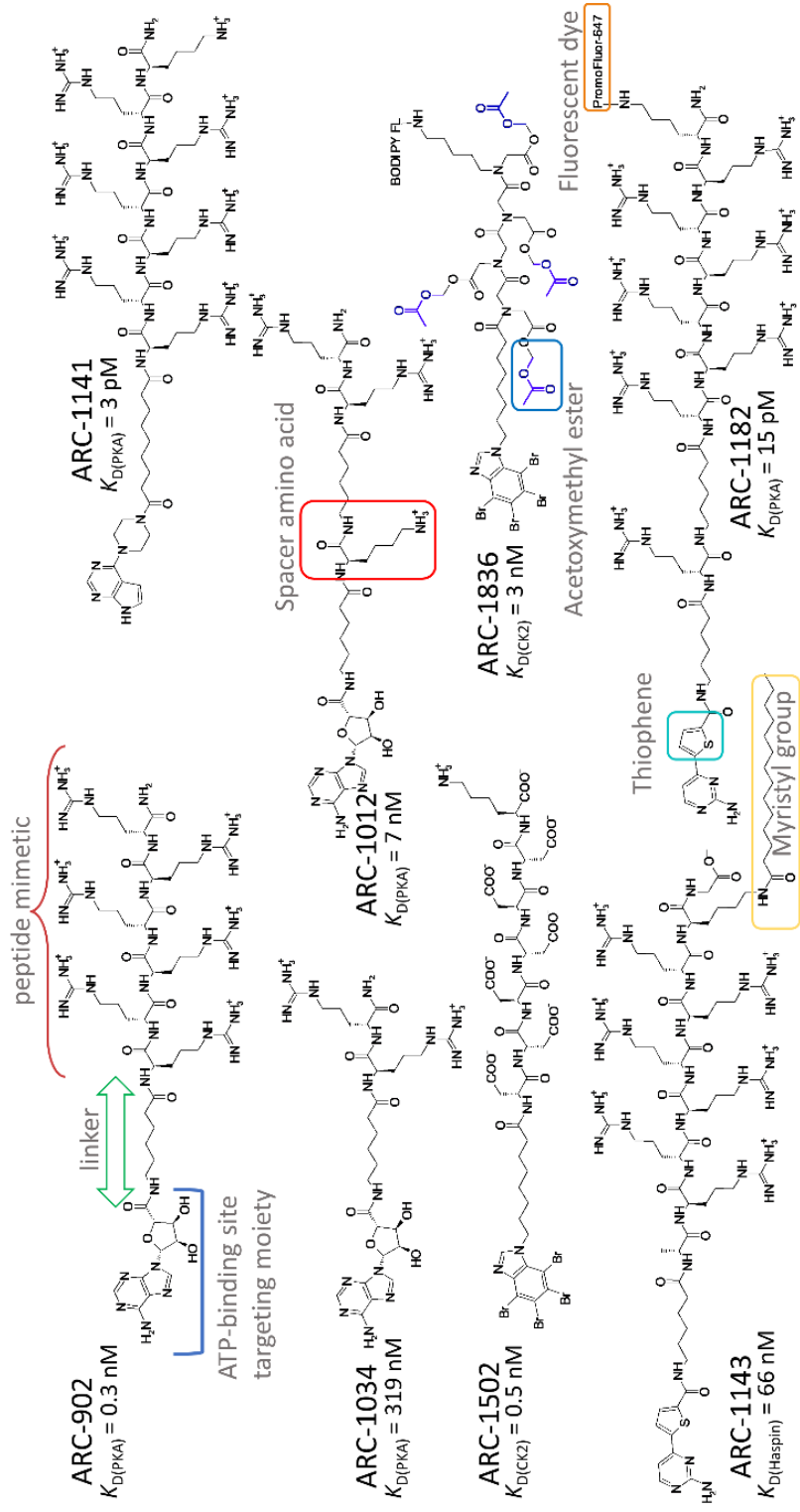


Figure 5. Example structures of ARCs.

The discovery that ARC-inhibitors, which incorporate thiophene structures, emit long lifetime luminescence upon excitation when they are bound to PKs, led to the development of ARC-Lum probes (ARC-1182, **Figure 5**) [Vaasa et al. 2009]. A fluorescent dye equipped to an ARC inhibitor can amplify the long lifetime luminescence intensity via FRET (ARC-1182, **Figure 5**). Convenient methodology to determine the K_D -values of tight-binding inhibitors using nanomolar concentrations of PKs has been developed using ARC-Lum probes (discussed further under **METHODS**).

2.3 Targeted covalent inhibitors

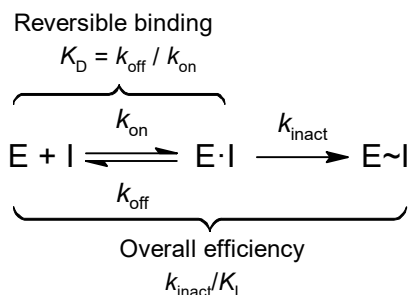
Targeted covalent inhibitors (TCIs) are inhibitors equipped with a reactive electrophile, which forms an irreversible (or reversible) covalent bond with a specific amino acid of their target enzyme. Only a few decades ago, the development of TCIs as drugs was disfavoured because of potential toxicity risks and safety concerns. Drugs which function via a covalent mechanism have been around for over a century, although they were discovered serendipitously rather than via rational design. Aspirin, the first covalent drug, was already marketed in 1899, although the covalent mechanism of action was established retrospectively in 1975 [Roth et al. 1975] (acetylation of a serine residue in COX [Shimokawa and Smith 1992]). Penicillin, the first antibiotic, was discovered in 1928. It covalently binds an active site serine residue in bacterial enzyme DD-transpeptidase preventing the synthesis of the cell wall [Waxman and Strominger 1983]. Omeprazole, first proton pump inhibitor made in 1979, had its mechanism elucidated a few years before approval in 1988 (forms a disulfide bond with a cysteine residue of a proton pump, which leads to the inhibition of secretion of gastric acid) [Lindberg et al. 1986]. The main reason covalent inhibitors had previously been avoided was the presence of a reactive functional group and a fear that it might form an immunogenic protein-drug adduct causing allergic response and hypersensitivity [Utrecht 2009; Zhang et al. 2011].

It has been claimed that around 30% of all marketed drugs form a covalent bond with their target enzyme [Sutanto et al. 2020]. Eight of the 71 FDA-approved PK inhibitors are TCIs. Ibrutinib (Imbruvica, approved in 2013) was one of the first PK inhibitors designed to intentionally form an irreversible bond with its target enzyme, rendering its target – Bruton tyrosine kinase (BTK) definitively inactive (ibrutinib, **Figure 6D**). Now ibrutinib is used in the treatment of four different diseases and its revenue in 2021 was \$5.4 billion [AbbVie Reports 2022], repeating the success of imatinib and spiking the interest in TCIs.

Covalent inhibition has several advantages over reversible inhibitors. (1) TCIs function with non-equilibrium kinetics meaning that after the covalent modification there is no competition with natural ligands (like ATP for PKs). (2) Covalent inhibitors have an infinite residence time, which enables prolonged duration of action – enzyme activity can be restored only by *de novo* protein

synthesis. This also means TCIs have improved efficiency, and lower and less-frequent dosing of the drug is needed, which reduces the risk of side effects. (3) TCIs are less affected by mutations, which cause drug resistance if the protein binding site is changed due to a mutation which leads to a less efficient reversible binding (unless the targeted amino acid is mutated). (4) TCIs can target proteins without a well-defined and/or shallow binding sites [Sutanto et al. 2020].

TCIs have a two-step mechanism of inhibition (**Scheme 2**). First, the inhibitor reversibly binds the target protein forming an inhibitor-protein complex. Also, the electrophilic warhead is fixed into a favourable position in relation to the targeted amino acid residue. Second, a covalent bond is formed between the electrophile and the nucleophile. The formation of the reversible complex is characterized with dissociation constant K_D and the formation of the irreversible covalent bond is characterized with k_{inact} . The latter constant describes the maximum rate of inactivation achieved at infinite concentration of the inactivator.



Scheme 2. Two-step mechanism of covalent inhibition between inhibitor (I) and target enzyme (E)

The overall efficiency of the covalent modification can quantitatively be described by the second order rate constant k_{inact}/K_I (M/s). k_{inact}/K_I accounts for both the reversible and covalent steps. A larger ratio of k_{inact}/K_I typically implies higher potency, meaning that high binding affinity and reactivity are favoured [Strelow 2017; Roskoski 2021b; Abdeldayem et al. 2020]. K_I is defined as the concentration of inhibitor that yields the half-maximal rate of the covalent bond formation ($K_I = \frac{1}{2} k_{inact}$). K_I can be considered equal to K_D for inhibitors which have a much slower rate of reaction with their target compared to the rate of dissociation ($k_{inact} \ll k_{off}$). [Zhai et al. 2020] K_I can be calculated:

$$K_I = \frac{k_{off} + k_{inact}}{k_{on}}. \quad (2)$$

As the two-step mechanism shows, the covalent inhibition is time-dependent and does not follow classical equilibrium kinetics. Since longer exposure times

lead to an increased inhibitor-protein adduct formation, IC_{50} , EC_{50} , and K_D are not the appropriate parameters for comparing TCIs.

Rational TCI development often follows the process of optimizing a reversible inhibitor and modifying it with an electrophilic warhead. The reactivity of the warhead can be later optimized to minimize off-target labelling [Pęczka et al. 2022]. Selectivity towards the target protein can be achieved via the first step of the covalent reaction mechanism – the reversible binding. Interestingly, excellent selectivity profiles often occur upon short-term treatment with TCIs, whereas an extended exposure has been shown to increase off-target reactions [Lanning et al. 2014]. In fact, poor metabolic stability of the warhead might be preferred to avoid time-dependent side reactions – Zaro *et al* purposely made a warhead that would be hydrolysed in the cell to decrease the slower off-target reactions [Zaro et al. 2016].

2.3.1 Target residues

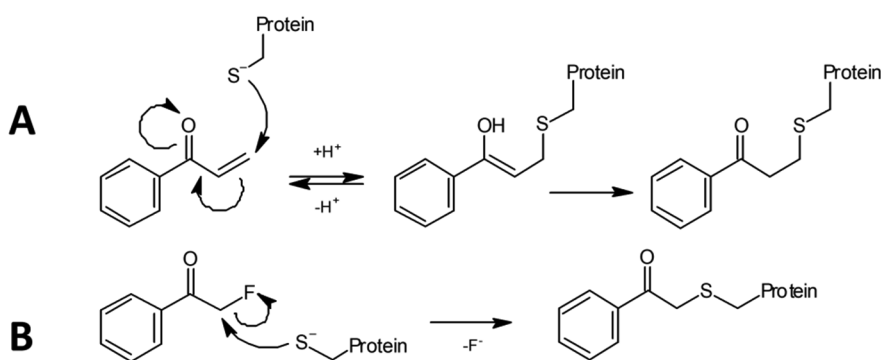
The preferentially targeted nucleophilic amino acid in proteins is cysteine since it is highly reactive (the strongest nucleophile from the 20 natural amino acids) and the third least abundant amino acid (only 2.2% of protein amino acid residues) [Miseta and Csutora 2000]. All the eight covalent FDA-approved PK inhibitors react with a cysteine residue. Thiolates of cysteines are highly polarizable and thus soft bases. Although, the protonated thiol is only moderately reactive, it can easily be deprotonated ($pK_a \sim 8.6$ for cysteine) making it a strong nucleophile that can be targeted with multiple electrophiles [Sardi et al. 2013]. The pK_a of a thiol can shift several orders of magnitude depending on the environment the cysteine residue is in the protein – pK_a values of 2.5 to 11.1 have been reported [Gehringer and Laufer 2019]. An acquired mutation of cysteine is an excellent target for TCIs. Other amino acid residues have also been targeted (e.g., lysine [Pettinger et al. 2017], serine, or tyrosine [Bum-Erdene et al. 2020]). Buried lysines for example, have been targeted since they can become quite acidic (pK_a as low as 5.3 [Pettinger et al. 2017]) and are often present in active centres. The lysines on the surface of PKs, on the other hand, usually remain protonated (pK_a 10.4). The reactivity of any amino acid depends highly on their microenvironment, and amino acids with lower intrinsic reactivities make their targeting more challenging, especially because the measurement of pK_a values might not be trivial.

2.3.2 Electrophile warheads

Chemo-selective covalent reagents, which react in a one-step mechanism and ambiguously label the most reactive and accessible amino acid residues, cannot be used as covalent reactive groups (CRG) in TCIs [Gehringer and Laufer 2019]. The CRG's innate reactivity must not be too high, otherwise it leads to excessive nonspecific off-target labelling and is scavenged by cellularly abundant nucleophiles like glutathione (GSH; $c_{\text{cellular}} = 0.5\text{-}10$ mM) [Wu et al. 2004;

Johnson et al. 2010]. However, the CRG must be reactive enough to rapidly form the covalent bond after precise positioning in proximity to the appropriate nucleophilic residue of the target enzyme.

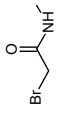
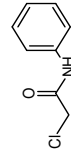
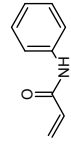
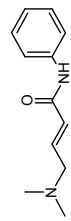
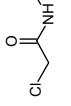
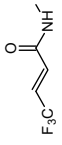
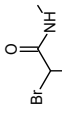
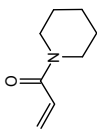
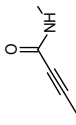
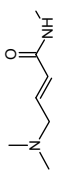
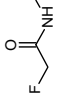
Different reaction types have been defined for the CRGs, but addition-elimination and nucleophilic substitution are by far the most prevalent reaction types [Péczka et al. 2022]. These reaction types are not specific, can be applied to various amino acids, and their reactivity can be tuned by tailoring the warhead [Péczka et al. 2022]. Other mechanisms, on the other hand, may offer higher selectivity – e.g., aromatic electrophilic substitution occurs only by tyrosine and tryptophane and oxidative mechanisms occur only for cysteine and methionine [Péczka et al. 2022].



Scheme 3. Reaction between thiol of a cysteine residue and an electrophilic warhead via the (A) Michael addition reaction mechanism and (B) S_N2 reaction mechanism.

The most prevalent warheads are α,β -unsaturated carbonyl compounds reacting with cysteine residues via the Michael addition reaction [Jackson et al. 2017] (**Scheme 3**). Following the hard and soft (Lewis) acids and bases (HSAB) theory, the soft acrylamides reacting via the Michael addition are suitable for the soft, highly polarizable cellular nucleophiles (thiols) [Reed 2008]. Unfunctionalized acrylamide is only weakly reactive towards thiol nucleophiles, but since its structure is highly modifiable it has become an attractive option for TCI development (**Table 3**). Substitutions at the α or β carbon of acrylamide can adjust its reactivity and the reaction reversibility. The covalent reaction can be made reversible if an electron withdrawing group is used next to the acryl group [Sutanto et al. 2020]. The *N*-substitutions also play role in acrylamide reactivity, for example, the *N*-alkyl or *N*-aryl substituent can highly differ in reactivity. In fact, all 8 covalent FDA-approved PK inhibitors use a form of α,β -unsaturated carbonyl CRG that react with a cysteine residue of their target PK via the Michael addition reaction resulting in a thioether formation.

Table 3. Pseudo-first order kinetics of GSH addition reactions

							
$t_{1/2}$ (h)	0.001 ^c	<0.08 ^a	0.40 ^a	0.53 ^b	0.88 ^a 1.24 ^b	1.20 ^b	3.2 ^a
							
$t_{1/2}$ (h)	4.0 ^a	4.4 ^a	16.7 ^a	33 ^a	41 ^a	>60 ^a	>78 ^b

^a Measured at 37°C; 100 mM Phos, pH 7.4; 1 mM electrophile and 10 mM GSH. [Flanagan et al. 2014]

^b Measured at 37°C; 100 mM Phos, pH 7.4; 1 mM electrophile and 10 mM GSH [Shindo et al. 2019]

^c Measured at 25°C; pH 7.4 [Schwöbel et al. 2010]

Other widely used electrophiles participate in the S_N2 , Pinner, and S_NAr reactions. α -halo-substituted carbonyls, for example, react with the S_N2 mechanism (**Scheme 3**). The reactivity of α -halo-substituted carbonyls increases down the periodic table ($F < Cl < Br < I$) with the fluoride substituted substance being least reactive. In this case, the polarity of the C-X bond is reinforced by the electron-withdrawing effect of the carbonyl, which results in a highly electrophilic α -carbon. Like for acrylamides, it is possible to tune the reactivity of α -halo-substituted carbonyls via a combination of steric and inductive effects. The α -halo-substituted carbonyls have also been widely used in TCI development, like fluoromethyl ketones (FMK) [Cohen et al. 2007; Garske et al. 2011; Coover et al. 2016] and chloromethyl ketones (ClMK) [Perez et al. 2009].

2.3.3 Covalent protein kinase inhibitors

To date there are eight FDA-approved covalent PK inhibitors (**Figure 6B-D**). Yet these PK inhibitors mainly target only two families of PKs. Primary target for three of the covalent PK inhibitors is BTK, while the other five PK inhibitors find their targets among the 4 members of the epidermal growth factor receptor (EGFR) family (ErbB1/2/3/4).

The EGFR family contains four polyomymous members: (i) ErbB1/HER1/EGFR, (ii) ErbB2/HER2, (iii) ErbB3/HER3, and (iv) ErbB4/HER4. These ErbB targeting drugs are used to treat non-small cell lung cancers (NSCLC; 85% of all lung cancers) and breast cancer. For example, an estimated 20% of breast cancers overexpress ErbB2. The 1st generation EGFR tyrosine kinase inhibitors (TKI) were reversible inhibitors based on the 4-anilinoquinazoline scaffold and compete with ATP for its binding site (**Figure 6A**) [Hossam et al. 2016] These TKI inhibitors were FDA-approved for the treatment of NSCLC. EGFR activating mutations which favoured the tumour development (e.g., L858R and exon 19 deletion) increased the binding affinity for ATP and also for the EGFR inhibitors. NSCLC patients initially had good responses to the 1st generation EGFR inhibitors but were inclined to develop resistance to the drugs via the gatekeeper point mutation (T790M). To overcome the mutation resistance, 2nd generation inhibitors were developed by incorporating reactive moieties to the 1st generation inhibitors (**Figure 6B**). Afatinib, dacomitinib, and neratinib are covalent, 2nd generation TKIs and they react with a non-catalytic Cys797 in the EGFR active site. The 2nd generation drugs inhibit the EGFR T790M mutant but also inhibit the wild-type which leads to dose-limiting side effects. This problem was solved with the 3rd generation TKIs which incorporate a pyrimidine scaffold (**Figure 6C**) [Tumbrink et al. 2021]. Osimertinib e.g., has been approved for treating NSCLC patients with the activating EGFR mutation or the T790M drug resistance mutation. The 3rd generation TKIs overcome the gatekeeper (T790M) mutation and have mutant selectivity over the wild type (WT) due to more selective reversible binding for the mutant EGFR and faster covalent bond formation rate compared to the 2nd generation EGFR drugs [Zhai et al. 2020]. The usage of irreversible EGFR inhibitors becomes problematic with the

Cys797 mutation (C797S) or oxidation, problems not affecting the reversible inhibitors (**Figure 6A**).

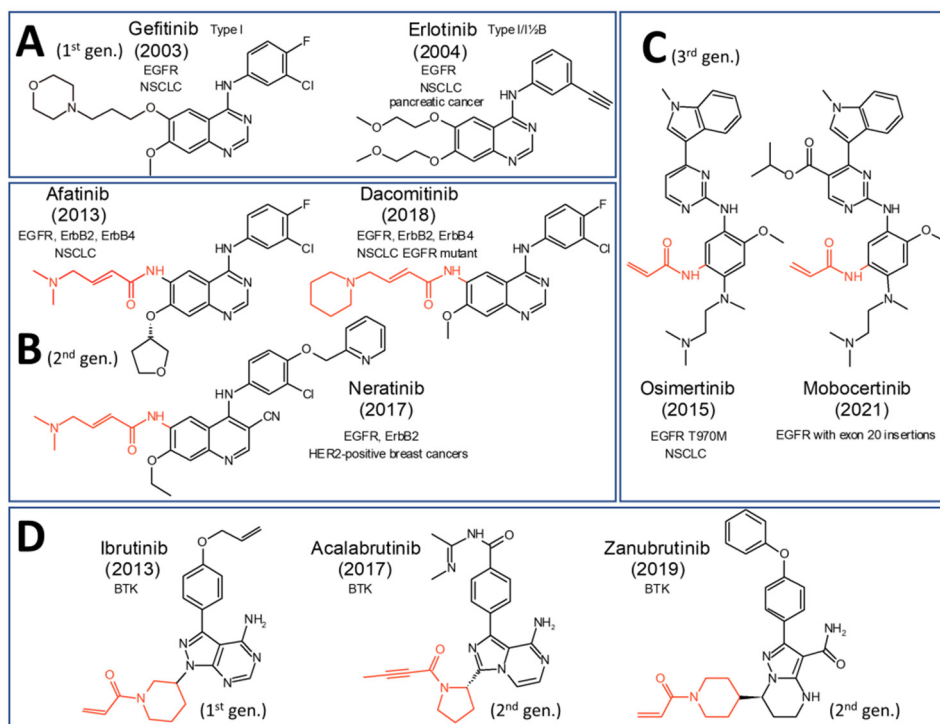


Figure 6. FDA-approved covalent PK inhibitors. (A) 1st, (B) 2nd, (C) 3rd generation EGFR inhibitors; (D) 1st and 2nd generation BTK inhibitors. Inhibitor name, year of FDA-approval, primary targets, and conditions they are used for are added to the inhibitors. The electrophilic warheads of the covalent inhibitors are depicted in red.

BTK is the other PK family that FDA has approved covalent PK inhibitors for (**Figure 6D**). Activating mutations make BTK constitutively active which leads to promoting downstream proliferative processes. BTK inhibitors are approved for the treatment of B-cell malignancies. The TCIs for BTK target the Cys481. Both 1st and 2nd generation BTK inhibitors function via the covalent mechanism (**Figure 6D**). The 1st generation BTK drug, ibrutinib was revolutionary since it brought about the treatment of B-cell malignancies without the need for chemotherapy that is based on general cytotoxic agents. However, various side effects made prominent that further development is needed for more selective BTK inhibitors. 2nd generation BTK inhibitors were developed and have an increased selectivity and fewer off-target toxicities. In clinical practice, the BTK drug is chosen by considering which side-effects would be more tolerable for the patient (e.g., ibrutinib is not recommended for patients with cardiovascular

diseases; acalabrutinib not for patients with headaches) [Ran et al. 2022]. Usage of 1st and 2nd generation BTK drugs may lead to an acquired resistance due to the C481S mutation. 3rd generation BTK inhibitors are reversible inhibitors and potent for both BTK and BTK^{C481} mutants. Although, several of them are in development, none have yet received the FDA approval. As evident, covalent PK inhibitors drugs can lead to improved cancer treatment and provide fewer side-effects and a smaller drug dosage. Unless the cysteine which is targeted by the covalent inhibitor is mutated, the drug can be beneficial against other acquired mutations.

2.4 Photochemistry

Electromagnetic radiation is quantified into elementary particles called photons, that have a discrete amount of energy depending on their frequency. Photons are the smallest particles of light; they are massless and move at the speed of light. The energy of a photon which is transferred (ΔE) to a substance upon absorption depends on the photon's frequency (ν) and hence also on the wavelength (λ):

$$\Delta E = h\nu, \quad (3)$$

$$\nu = \frac{c}{\lambda}, \quad (4)$$

where h is the Planck's constant, and c is the speed of light. For the photon to be absorbed, the photon's energy must be equal to the energy needed for the excitation. Energy absorption results in the molecule being excited to one of the discrete excited states (S_1 , S_2 etc.; **Figure 7**) [Lakowicz 2006]. Structures that absorb light can be characterized by the excitation coefficient (ϵ), which describes how strongly a chemical species absorbs light. The higher the excitation coefficient, the higher the probability to absorb photons at a certain wavelength (λ). How the rate of biological, chemical, and physical processes depends on the wavelength of light can also be described by the action spectrum.

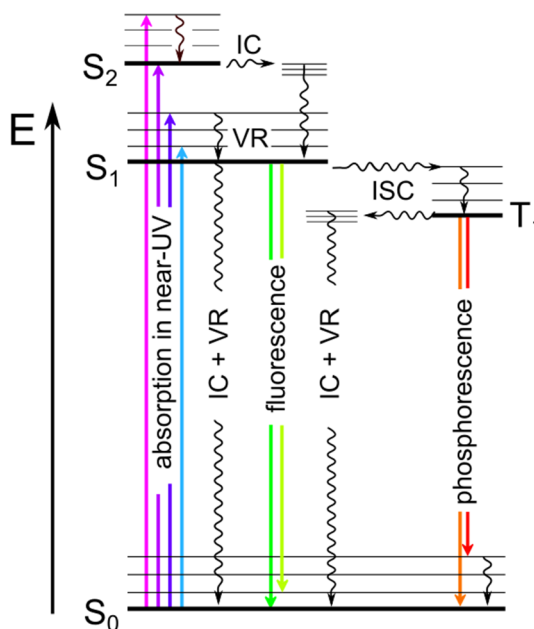


Figure 7. Jablonski's diagram, displaying the different molecular states (S_0 – the ground state; S_1 , S_2 , and T_1 – excited singlet and triplet states) and photophysical processes – absorption, internal conversion (IC), vibrational relaxation (VR), fluorescence, intersystem crossing (ISC), and phosphorescence. Thicker and thinner vertical lines represent the electronic energy minima and vibrational energy states, respectively [Lakowicz 2006].

Light absorption is a very fast process (10^{-15} s). It is followed by the energy being dispersed between other vibrational energy states via inner conversion (10^{-12} - 10^{-6} s) and intra-system crossing ($S \rightarrow T$ 10^{-12} - 10^{-6} and $T \rightarrow S$ 10^{-9} - 10^1). An excited molecule has multiple ways to dispose the excess energy and return to the ground state. The relaxation to the ground state can occur via photophysical processes. Photophysical processes do not involve chemical bond rearrangements and can be divided into non-radiative processes, which generate heat (vibrational and rotational relaxation; 10^{-13} - 10^{-12} s) and radiative processes, which generate light such as fluorescence (10^{-9} - 10^{-7} s) and phosphorescence (10^{-6} - 10^{-3}). [Klån and Wirz 2009]

In addition, the relaxation to the ground state (S_0) can occur via primary photochemical processes where chemical bonds are rearranged and the parent compound is photolyzed into a photoproduct. Photolysis is scission of a chemical bond due to light and it can be initiated by UV, Vis, or IR. Further chemical changes that may follow the photolysis are called secondary photochemical processes and do not require an additional absorption of light.

In nature, photochemical processes can be beneficial (in accordance with the need of organisms) or harmful (photodamage). For example, D-vitamin is produced in the human skin as a response to UV light (280 nm), and the light-

induced E-Z isomerization of opsin in the retina of the eye is linked to signal transduction. On the other hand, the residual UVB light (260-320 nm) reaching the surface of earth may endanger living organisms. The most widespread UVB chromophores in the skin are nucleic- and amino acids, and thus the most common photoreaction the photodimerization of two pyridine bases in the DNA. [Klàn and Wirz 2009]

Photochemical and photophysical processes can also be characterized by quantum yield. Quantum yield $\Phi_x(\lambda)$ is the ratio of a photo-chemical or -physical processes (n_x) and the absorbed photons (n_p):

$$\Phi_x(\lambda) = \frac{n_x}{n_p}. \quad (5)$$

According to the *Kasha's rule*, polyatomic molecules luminesce only from the lowest excited state (S_1 or T_1), hence quantum yields do not depend on the wavelength of excitation. All relaxation processes have a quantum yield and are competing. Excited molecule uses the fastest mechanism to return to the ground state, may it be vibrational relaxation, fluorescence, phosphorescence, or photolysis. By multiplying the quantum yield (Φ) and the molecular extinction coefficient (ϵ), the efficiency ($\Phi \cdot \epsilon$) of said relaxation process can be calculated [Klàn and Wirz 2009]. Chemical bond rearrangement can be the primary mechanism of relaxation depending on the structure of the molecule. The structures of photocleavable groups are designed to restrict molecule's vibrational and rotational movements with ridged conjugated aromatic systems, and a cleavable bond, which produces a good leaving group.

2.4.1 Photocaged bioactive compounds

Photocaging groups or photoremovable protecting groups (PPG) are photosensitive functional groups also known as photocleavable, photoactivatable, photolabile, photo-releasable groups, or photo-triggers [Silva et al. 2019]. PPGs are usually used to mask the activity of a biomolecule by diminishing it with PPG coupling. Then, upon irradiation with UV-Vis, the PPG can be removed with spatial and temporal precision, and the biological activity is restored. PPGs were first reported 60 years ago [Barltrop and Schofield 1962; Patchornik et al. 1970] and were adopted to biology 20 years later [Engels and Schlaeger 1977; Kaplan et al. 1978]. Since then, PPGs have been used to photocage molecules (or ions) of all sizes from protons and metal ions [Momotake et al. 2006] to neurotransmitters [Palma-Cerda et al. 2012], peptides, and proteins [Mangubat-Medina and Ball 2021; Rakauskaitė et al 2020].

Similarly, photo-switching groups are also used control bioactivity of compounds. The most common photo-switches are based on the azobenzene scaffold, which go through a photo-responsive double-bond isomerization between *cis* and *trans* configurations (**Figure 8A**). Although most of azobenzene photo-switches respond to UV-light, it is also possible to make red-shifting azo-

benzene photo-switches [Dong et al. 2015]. Photo-switching groups do not produce side products; however, it might be more difficult to achieve large changes in affinity compared to PPGs which are cleaved off.

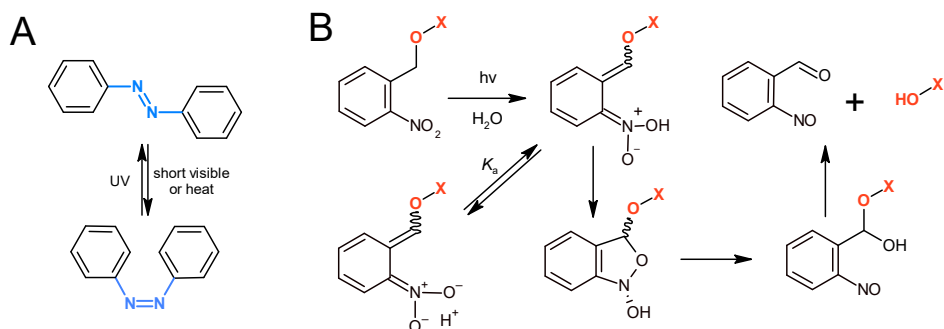


Figure 8. Reaction mechanisms of photosensitive compounds. (A) Reversible azobenzene type photo-switch. (B) Principal reaction mechanism of irreversible nitrobenzene type photolysis [Klan et al. 2013].

Photocaged molecules have been used in many applications, for example, the development of light-sensitive pro-drugs and drug delivery systems [Poelma et al. 2016; Silva et al. 2019; Rapp and DeForest 2021], photoactivatable antibiotics [Velema et al. 2013], manipulating PK activity with photo-switchable peptides [Yi et al. 2014], etc.

Most PPGs are cleaved under UV-light. However, UV-light is not applicable for many medicinal applications since absorption and scattering hinder the penetration of short wavelengths through the skin. The main absorber in the epidermis is melanin that protects aromatic amino- and nucleic acids from UVA (320-380 nm). Visible light is also largely absorbed by melanin, haemoglobins, flavines, and carotenoids. Red and infrared light, on the other hand, penetrate the tissue quite well (3-5 mm at 600 nm and 6-10 mm at 800 nm) and are mostly only absorbed by melanin [Zhou et al. 2016]. Photodynamic therapy (PDT) is a treatment that uses reactive oxygen species (ROS), produced by photosensitizers, to kill cancer cells. Photosensitizers are taken up by tumour cells and start producing ROS from oxygen upon exposure to light [Kou et al. 2017]. The optical window for activating the photosensitizers used in PDT (600–900 nm) is set by water (under 900 nm) and oxyhaemoglobin (over 600 nm), the strongest chromophore in blood. However, the photons of red and infrared light have low energy and the handling of compounds sensitive to red light is more complicated. Two-photon excitation (2PE) is an alternative to one-photon excitation and makes it possible to excite chemical species at double excitation wavelength. 2PE occurs when a molecule absorbs two photons simultaneously. 2PE efficiency can be described by two-photon cross-section δ , which is measured in Goepfert-Mayer units ($1 \text{ GM} = 10^{-50} \text{ cm}^4 \cdot \text{s} \cdot \text{photon}^{-1}$).

molecule⁻¹) [Klán et al. 2013]. For biological applications, the 2PE cross-section should be at least $\delta > 0.1$ GM [Brieke et al. 2012]. 2PE needs a very high light intensity that can only be achieved with special light sources.

A PPG should have a high extinction coefficient (ϵ) and the wavelength of excitation should be higher than 300 nm. The photolysis reaction should occur with a high chemical yield and quantum yield (Φ). The higher the quantum efficiency ($\epsilon\Phi$), the more efficient the photolysis. A $\epsilon\Phi$ over $100 \text{ M}^{-1}\text{cm}^{-1}$ is considered good, over $1000 \text{ M}^{-1}\text{cm}^{-1}$ excellent, but values over $10\,000 \text{ M}^{-1}\text{cm}^{-1}$ are not unusual either [Momotake et al. 2006; Vickerman et al. 2021]. The molecule equipped with a PPG should be photolabile. The photocaged molecule should be thermally stable, soluble, and available in high purity. Since PPGs are usually large hydrophobic groups, attaching one may have a large effect on solubility and membrane permeability. The photolysis products should be poor chromophores with a low toxicity. The irradiation time should be minimal to avoid unwanted photoreactions and degradation. Depending on the application, the PPG should have a wide 2PE cross-section.

A variety of PPG structures have been used, each having their distinct advantages and disadvantages (**Table 4, Figure 9**). A widely used photocaging group is *o*-nitrobenzyl (*o*-NB; **Table 4, Figure 9a**) and its methoxy derivatives (DMNPE; **Table 4, Figure 9b**) [Goeldner and Givens 2005]. The photolysis mechanism of *o*-NB proceeds via a cyclic intermediate and produces a leaving group which contains a newly formed carbonyl and a nitroso group (**Figure 8B**) [Klán et al. 2013]. *o*-NB is widespread due to its simplicity. The downside of the *o*-NB is its slow photolysis kinetics and potentially toxic side products (e.g., *o*-nitrobenzyl aldehyde). Structural modifications have been able to overcome some of the disadvantages of *o*-NB. Increasing the size of the aromatic system and adding substitutions increases the wavelength of excitation and allows for compounds with high photolysis efficiencies, high quantum yields (NDBF; **Table 4, Figure 9c**) [Momotake et al. 2006], and excellent 2PE properties (BNSF; **Table 4, Figure 9d**) [Gug et al. 2008]. Nitroindolines type photocaging groups have been developed as an alternative to *o*-NBs and are stable but usually have low efficiency (MNI; **Table 4, Figure 9e**) [Goeldner and Givens 2005]. Coumarine-4-ylmethyl derivatives have fast photolysis, high ϵ at longer wavelengths than 350 nm, are stable, have good fluorescent properties, and 2PE properties (Bhc; **Table 4, Figure 9f**) [Fedoryak and Dore 2002]. Substitutions in the coumarin structure can be used to improve its properties. There are also metal-containing photocaging groups where the metals coordination changes upon irradiation which enables the release of metal ions, gaseous inorganic molecules (e.g., NO or CO), or organic molecules ($[\text{Ru}(\text{bpy})_2(\text{nic})_2]^{2+}$; **Table 4, Figure 9g**) [Filevich et al. 2010]. As an alternative to 2PE, PPG-s which are cleavable in the phototherapeutic window region have been developed (BODIPY and Cy; **Table 4, Figure 9h and 9i**) [Sitkowska et al. 2020; Nani et al. 2015]. Making molecules absorb light at higher wavelengths has an inherent drawback of making them larger and more hydrophobic.

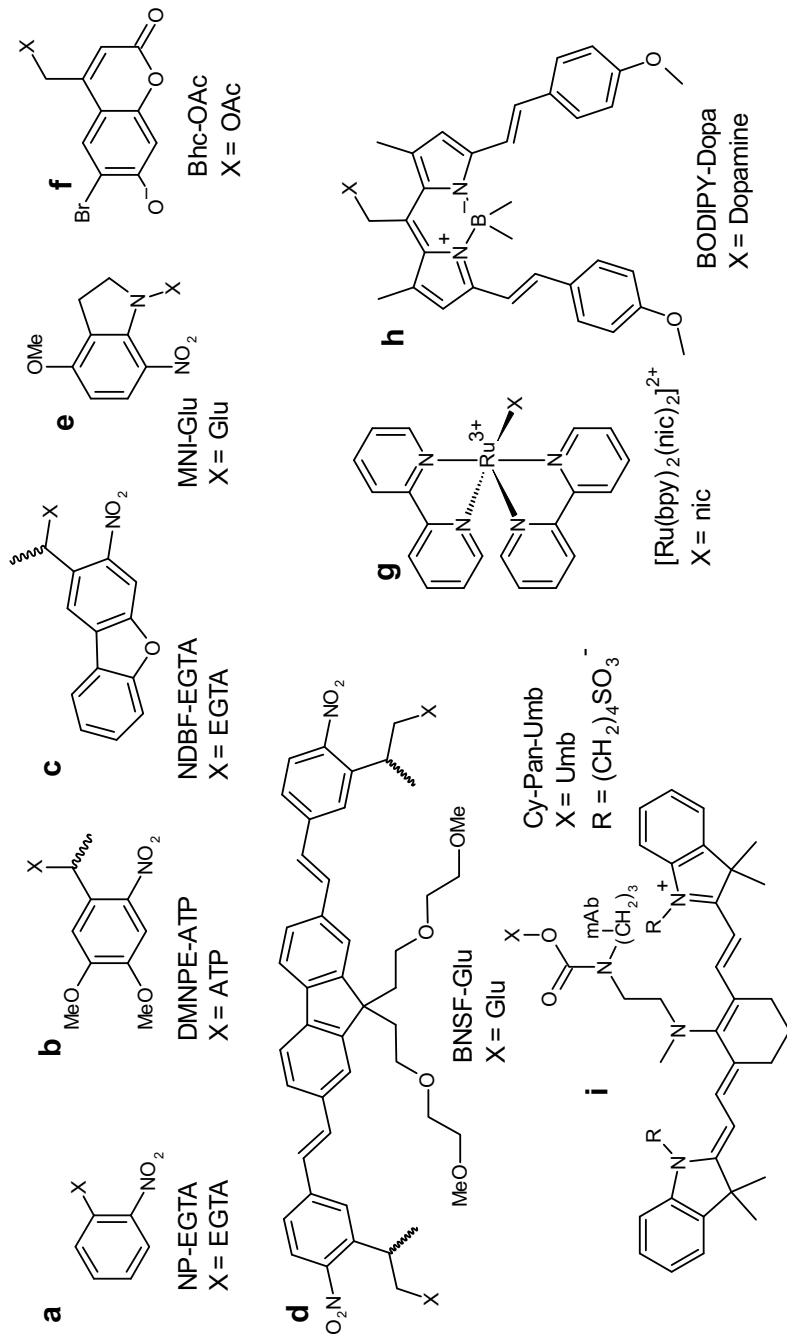


Figure 9. Selection of various photocaging groups

Table 4. Examples of different types of photocaged compounds

Photocaged compounds	λ_{max} [nm]	ε [$\text{M}^{-1}\text{cm}^{-1}$] (λ [nm])	Φ	$\varepsilon \cdot \Phi$ [$\text{M}^{-1}\text{cm}^{-1}$] (λ [nm])	$k_{\text{photolysis}}$ [s^{-1}]	2PE δ [GM]
a. NB-EGTA ¹	260	974 (347)	0.23	224 (347)	68 000 (Ca^{2+})	0.001
b. DMNPE-ATP ²	249 350	17 200 (249) 5100 (350)	0.07	350 (347)	18 pH 7.0	0.03
c. NDBF-EGTA ³	330 400	18 400 (330) 1 720 (400)	0.7	12 880 (330)	20 000 (Ca^{2+})	0.6 (720 nm)
d. BNSF-Glu ⁴	415	63 960 (415)	0.25	16 000 (415) 7500 (354)	not reported	5.0 (800 nm)
e. MNI-Glu ²	350	not reported	0.085	380 (347)	2 700	0.06 (730 nm)
f. Bhc-OAc ⁵	370	15 000 (370)	0.036	540 (370)	not reported	0.72 (720 nm)
g. [Ru(bpy) ₂ (nic) ₂] ²⁺ ⁶	453	4300 (453) 500 (532)	0.23	989 (453)	17 · 10 ⁹	0.01-0.1 (800 nm)
g. BODIPY-Dop ⁷	643	61 000 (650)	not reported	not reported	not reported	not reported
j. Cy-Pan-Umb ⁸	676	51 500 (676)	0.29	15 000 (676)	not reported	not reported

¹[Ellis-Davies and Kaplan 1994]; ²[Goeldner and Givens 2005]; ³[Momotake et al. 2006]; ⁴[Gug et al 2008]; ⁵[Fedoryak and Fore 2002]; ⁶[Filevich et al. 2010]; ⁷[Sitkowska et al. 2020]; ⁸[Nani et al. 2015]

3. AIMS OF THE STUDY

The aims of the study were crystal structure guided design, synthesis, and biochemical characterization of:

- 1) Light-activatable bisubstrate PKAc inhibitor
- 2) Deactivatable bisubstrate PKAc inhibitor
- 3) Irreversible covalently binding bisubstrate PKAc inhibitor

4. METHODS

4.1 Fluorescence anisotropy assay

Fluorescence anisotropy (FA) assay is based on the change of molecule rotational orientation during the time between absorption and emission events. In FA assays fluorophores are excited with linearly polarized light and thereafter the extent of polarization of the emitted light is measured using polarizers (vertical \parallel and horizontal \perp). The polarization of the emitted light is affected by rotational diffusion and depends on the angle the fluorophore has rotated during its excitation lifetime. Small molecules rotate quickly and thus the emitted radiation is less polarized, while large molecules rotate slowly and emit highly polarized light (**Figure 10**). As a result, large molecules or fluorophores attached to or complexed with large molecules have high FA values.

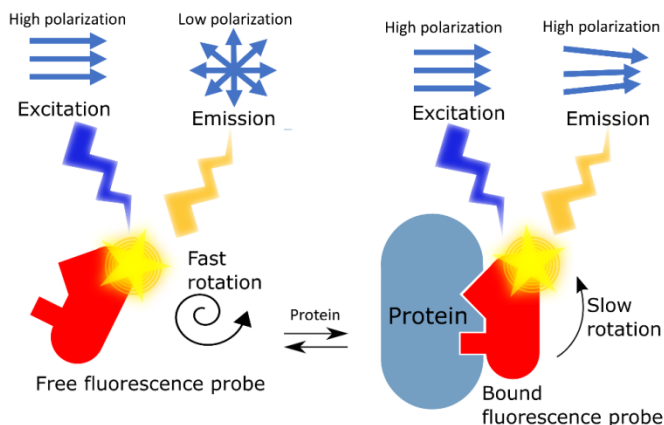


Figure 10. Principle of fluorescence anisotropy

Fluorescence polarization (FP) represents the same phenomenon as FA, and both can be used interchangeably although the use of FA is recommended since in FA the difference in intensities ($I_{\parallel} - I_{\perp}$) is normalized by the total intensity ($I_T = I_{\parallel} + 2I_{\perp}$). FA and FP are calculated by:

$$FA = \frac{I_{\parallel} - I_{\perp}}{I_{\parallel} + 2I_{\perp}}, \quad (6)$$

$$FP = \frac{I_{\parallel} - I_{\perp}}{I_{\parallel} + I_{\perp}}, \quad (7)$$

where I_{\parallel} and I_{\perp} are the fluorescence intensities of vertically and horizontally polarized emissions, respectively. If a small fluorescent probe (1–2 kDa) rotates

freely in solution, it emits depolarized light but if it binds a large molecule like a PK, its rotational freedom decreases, and the emitted light remains highly polarized.

FA based assay is simple, fast, and easily automated, although it might be difficult to use it in biologically complex systems. In FA binding or displacement assays the probe cannot be in large excess since unbound probe decreases the FA values. Using low affinity fluorescent probes ($K_D > 10$ nM) might require the use large amounts of PK which increases the experimental costs.

4.2 Time-gated luminescence intensity assay

Another method to determine the binding affinities of inhibitors is the time-gated luminescence intensity (TGLI) method. The TGLI method is based on the differences in the lifetimes of background fluorescence and the long-lifetime photoluminescence signals (**Figure 11**). The photoluminescence intensity is measured after a short delay (e.g., 50 μ s) after the flash excitation to ensure that most of the background luminescence has been faded. The window of measurement depends on the fluorophores luminescence lifetime (e.g., 200 μ s) resulting in a time-gated measurement. Signal-to-noise ratio of TGLI measurements can be further improved with repeated measurements.

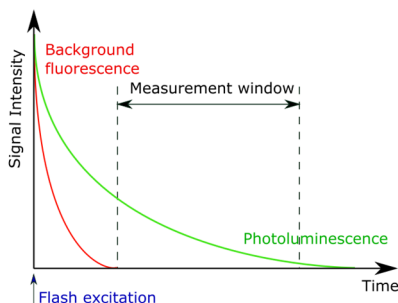


Figure 11. Time-gated luminescence intensity

ARC-Lum(Fluo) probes can be used as TGLI probes for TGLI measurements [Enkvist et al. 2011] (**Figure 12**). ARC-Lum(Fluo) probes are bisubstrate inhibitors that incorporate 1) a thiophene- or selenophene-comprising heteroaromatic system in the ATP-binding site targeting moiety and 2) a fluorescent dye (**Figure 12A**). In 2011 Enkvist et al. [Enkvist et al. 2011] described a phenomenon where PK was able to stabilize and shield the excited thiophene-or selenophene-containing probe from quenching. As a result, the probe started emitting phosphorescence when in complex with the PK (**Figure 12B,C**). In case of an unbound probe, however, the long-lifetime photoluminescence was quickly quenched by the solvent and dissolved oxygen. The phosphorescence emission of a bound probe can be magnified by transferring its energy to a fluorescent dye that also increases the emission wavelength resulting in a long-lifetime photoluminescence signal.

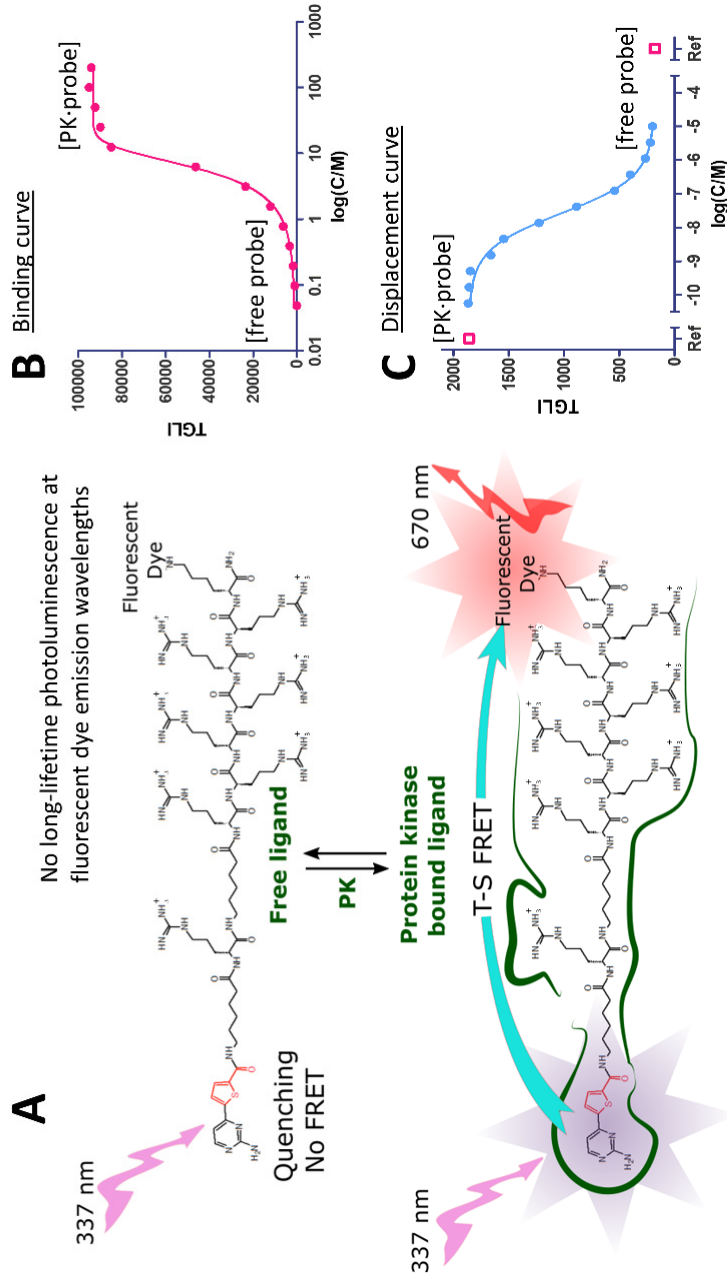


Figure 12. (A) The principle of ARC-Lum(Fluo) probes in a binding assay. The thiophene containing fragment in the structure of the ARC-Lum(Fluo) probe is shown in red. A fixed concentration of ARC-Lum(Fluo) probe was used when measuring (B) a binding curve with PKAα varying its concentration, and (C) a displacement curve with a fixed PKAα concentration and varying the displacer concentration.

This energy transfer is possible due to a phenomenon known as the Förster-type resonance energy transfer (FRET) which describes non-radiative energy transfer between two chromophores (FRET donor and acceptor) via dipole-dipole coupling (**Figure 13A**). In case of ARC-Lum(Fluo)s FRET takes place between the ATP-binding site moiety (donor) and the fluorescent dye (acceptor) (**Figure 13B**). The excitation of ARC-Lum(Fluo) probes is done at short wavelengths (337 nm) and the emission wavelength is dependent on the fluorescent dye (e.g., 647 nm). The S-S FRET occurs whether the probe has bound the PK or not, it has a relatively short lifetime and is decayed before the TGLI measurement window starts. Triplet state is stabilized in the ATP-binding site; therefore, the T-S FRET is more prominent when the PK and ARC-Lum(Fluo) complex has formed. In this case the long-lifetime photoluminescence signal can be measured during the measurement window.

For FRET to work, there must be an overlap between the donor emission spectrum and the acceptor excitation spectrum. In addition, the donor and the acceptor must be close in space (1–10 nm), since FRET efficiency (E) is highly dependent on the distance between the donor and the acceptor (r) – with an inverse 6th-power:

$$E = \frac{1}{1 + \left(\frac{r}{R_0}\right)^6}, \quad (8)$$

where R_0 is the Förster donor-acceptor distance, at which the energy transfer efficiency is 50%. Thus, ARC-Lum(Fluo) probes can be used in displacement assays to measure the affinities of unknown inhibitors. Similarly to the FA measurements, the PK-probe complex results in a high output signal while the free probe does not produce a signal. In case of FA based assay, the excess free probe decreases the dynamic range but for TGLI the free probe does not interfere with the signal output. The TGLI measurements using ARC-Lum(Fluo) probes provide a more accurate method for the affinity measurements with tight-binding inhibitors, since it is possible to use very small amounts of PK (e.g., 1 nM) and large amounts of probe (e.g., 10-200 nM). On the other hand, excitation at low wavelengths (337 nm) can cause photodamage, especially when photocaged compounds are being measured.

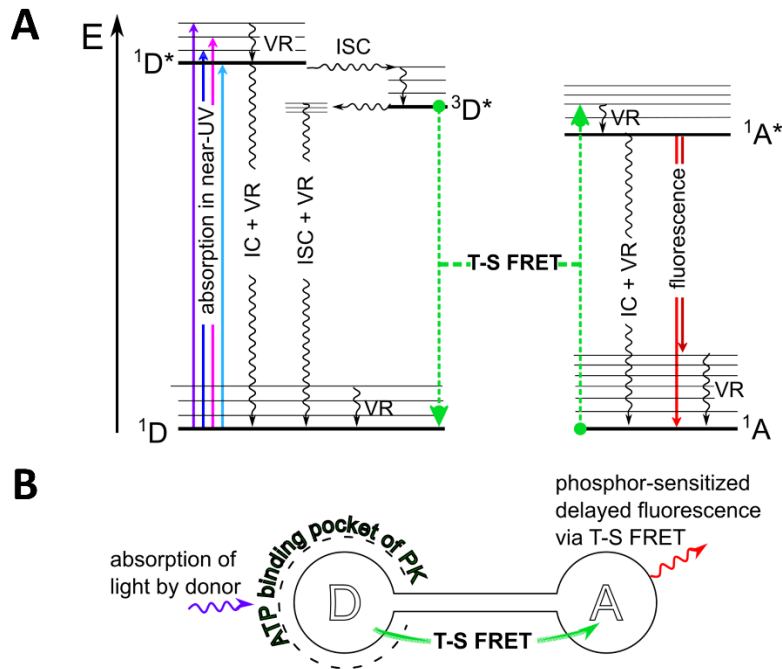


Figure 13. Jablonski's diagram (A) of photophysical processes displaying the phosphor-sensitized fluorescence via triplet-singlet Förster-type resonance energy transfer in ARC-Lum(Fluo) protein kinase complex (B)

4.3 The measurement of active PK concentration

Both FA and TGLI based assays can be used in binding experiments to measure the concentration of active PK or displacement experiments to measure the binding of a competing PK inhibitor. This is done by measuring a series of intensities at different PK or inhibitor concentrations, using the measured TGLI or FA values to plot a binding curve, and calculating IC_{50} and/or K_D values.

In this work the active enzyme concentration was always measured prior to the biochemical experiments with the recombinant PKs. 2-fold dilution series of PK was pipetted (typically starting from 200 to 400 nM concentrations) to which a fluorescent probe was added (typically with a 10 or 20 nM concentration).

The active PK concentration was calculated with the following equation:

$$r = (1 - M) \cdot r_{\text{probe}} + M \cdot r_{\text{complex}}, \quad (9)$$

$$M = \frac{Q \cdot [\text{complex}]}{1 + [\text{complex}] \cdot (Q - 1)}, \quad (10)$$

$$Q = \frac{I_{complex}}{I_{probe}}, \quad (11)$$

$$[complex] = P_t + K_{D1} + k \cdot x - \sqrt{\frac{(P_t + K_{D1} + k \cdot x)^2 - 4P_t \cdot k \cdot x}{2P_t}}, \quad (12)$$

$$K_{D1} = \frac{[probe][PK]}{[probe - PK]}, \quad (13)$$

$$k = \frac{C_{active}}{x}, \quad (14)$$

where r is the measured FA value, r_{probe} is the FA value of the free fluorescence probe, $r_{complex}$ – the FA value of the complex of the enzyme and fluorescence probe; I_{probe} and $I_{complex}$ are the intensities of the fluorescence probe and the complex of the enzyme and fluorescence probe, respectively; P_t is the total concentration of the fluorescence probe, K_{D1} is the dissociation constant of the complex of the enzyme and fluorescence probe, x is the nominal concentration of the enzyme ($C_{active} + C_{non-active}$), and C_{active} is the total concentration of the active enzyme.

4.4 Displacement assays

Two different methods were used to calculate the IC_{50} and K_D values – the TGLI and the FA method. The IC_{50} values were calculated using the following equation:

$$Y = Y_{min} + \frac{Y_{max} - Y_{min}}{1 + 10^{(\log IC_{50} - X) \cdot H}}, \quad (15)$$

where Y is the value of TGLI or FA, Y_{min} is the minimum value of the TGLI or FA signal, Y_{max} is the maximum value of the TGLI or FA signal, IC_{50} is the half-maximal concentration of the displacement, X is the logarithm of the inhibitor concentration, and H is the Hill slope.

The K_D values from the TGLI measurements were determined by the following equation:

$$Y = Y_{min} + M \cdot [EP_f], \quad (16)$$

where Y is the measured TGLI, Y_{min} is the background signal, M is the molar luminescence intensity of the enzyme and fluorescence probe complex, and $[EP_f]$ is the equilibrium concentration of the enzyme and fluorescence probe

complex, which was calculated from the following the solution to cubic equation [Wang 1995]:

$$[EP_f] = \frac{P_f \cdot \{2\sqrt{(a^2 - 3b)} \cos\left(\frac{\Theta}{3}\right) - a\}}{3 \cdot K_{D1} + \{2\sqrt{(a^2 - 3b)} \cos\left(\frac{\Theta}{3}\right) - a\}}, \quad (17)$$

$$a = K_{D1} + K_{D2} + 10^X + P_f - E, \quad (18)$$

$$b = K_{D1}(10^X - E) + K_{D2}(P_f - E) + K_{D1} \cdot K_{D2}, \quad (19)$$

$$c = -K_{D1} \cdot K_{D2} \cdot E, \text{ and} \quad (20)$$

$$\Theta = \arccos \frac{-2a^3 + 9ab - 27c}{2\sqrt{(a^2 - 3b)^3}}, \quad (21)$$

where P_f is the total concentration of the fluorescence probe, K_{D1} is the dissociation constant of the enzyme and fluorescence probe, K_{D2} is the dissociation constant of the enzyme and inhibitor, X is the logarithm of the total concentration of the competing inhibitor, E is the concentration of the active enzyme.

The K_D values from the FA measurements were determined by the equations 9 and 10, where Q is the quotient of the bound and free fluorescent probe intensities. The equilibrium concentration of the enzyme and the fluorescent probe complex was calculated according to the equation 17.

5. RESULTS AND DISCUSSION

5.1 Construction of activatable and deactivatable bisubstrate PKA inhibitors (Paper I: Sörmus *et al*, 2019 and Paper II: Sörmus *et al*, 2022)

Bisubstrate inhibitors present unique possibilities of structure modulation due to their characteristics of binding to two different binding sites. Investigation of how bivalent binding could be controlled by stimulus-responsive moieties was conducted. The PPG was integrated (1) to a hot spot of the inhibitor (to drastically decrease binding affinity; *PAPER I*) or (2) to the linker region (to maximally sustain the affinity; *PAPER II*). As a result, the binding affinity could be increased or decreased using external stimuli like light (**Figure 1 in PAPER II**). As an alternative to the light-deactivatable inhibitor, a redox-deactivatable inhibitor was also developed.

When the aim is to decrease the affinity of a bioactive compound by photocaging, an appropriate position for the photocaging group must be found to maximally decrease the bioactivity of the parent compound. Photocaged inhibitors can be sufficiently activated even via an incomplete photolysis reaction. If, for example, only 50% of the uncaged product is released, the IC_{50} of the final mixture is 2-fold higher compared to the fully uncaged product. However, this also means that even a minor contamination (e.g., 0.1%) with the transformation product of the batch of the inhibitor considerably decreases the dynamic range of activity change of the activatable inhibitor (e.g., arising from premature activation/inactivation).

In contrast to the photoactivatable inhibitors, when constructing a deactivatable inhibitor, the photocaging group must conversely not diminish the binding affinity initially, but only after the photolysis. The photolysis breaks the inhibitor into smaller entities, which then constitute significantly lower binding affinities compared to the parent compound. Efficient deactivation of an inhibitor relies on a very clean and high-yielding chemical (or photochemical) transformation. For example, a 99% transformation of a deactivatable inhibitor would cause a 100-fold IC_{50} increase, which is much less than would be observed after a complete conversion into the completely inactive state. On the other hand, contaminations of deactivatable inhibitors have marginal effect on the IC_{50} change, which makes the preparation and handling of deactivatable inhibitors more convenient. In the present work, to avoid unwanted photolysis, the synthesis and biochemical experiments with the novel light-sensitive inhibitors were performed under red light. Also, the inhibitors were purified with the UV detector of HPLC switched off and their peaks were collected according to the previously determined retention times.

Previously measured co-crystal structures of PKA α with ARC-inhibitors were used to design the structures of the inhibitors. PKA α was chosen as the

target PK since it has been considered a prototype PK for which many crystal structures are available, including co-crystal structures of many PKA α /ARC-type inhibitor complexes. PKAc has been photocaged on cysteine residues (C199 and C343) [Curley and Lawrence 1998; Chang et al. 1998, Gao et al. 2015], and on Thr197 [Zou et al. 2002].

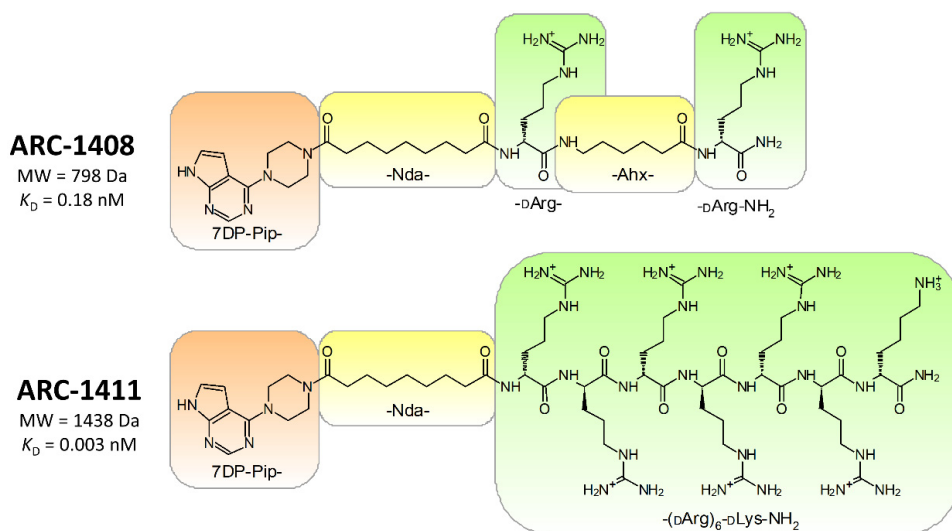


Figure 14. Structures of lead compounds, previously developed in our group, **ARC-1408** and **ARC-1411** [Ivan et al. 2016]. The ATP-binding site moiety, 7DP-Pip, is shown in **orange** boxes; linkers, Nda and Ahx, in **yellow** boxes; D-arginine and D-lysine residues in **green** boxes.

Previously published PKAc inhibitors **ARC-1408** and **ARC-1411** were used as the lead compounds. Both **ARC-1408** and **ARC-1411** comprise the 4-(piperazin-1-yl)-7H-pyrrolo[2,3-d]pyrimidine (7DP-Pip) moiety, and D-arginines which are connected via flexible and hydrophobic linkers (**Figure 14**). **ARC-1408** comprises two D-arginine residues and an elongated linker; one arginine is a spacer arginine in between the two linkers and the other one is in the C-terminus. **ARC-1411** has only one linker and comprises a hexa-D-arginine and a D-lysine, which increase its binding affinity as well as MW. The four extra D-arginines in **ARC-1411** result in a nearly 100-fold lower K_D value compared to **ARC-1408**. A significant fraction of the binding energy of **ARC-1408** and **ARC-1411** originate from strong interactions between the ATP-binding site and 7DP-Pip – multiple hydrophobic interactions and H-bonds with hinge region residues Glu121 and Val123 (**Figure 15**). The D-Arg residues reach out of the ATP-binding site and interact with amino acids on the surface of the PK.

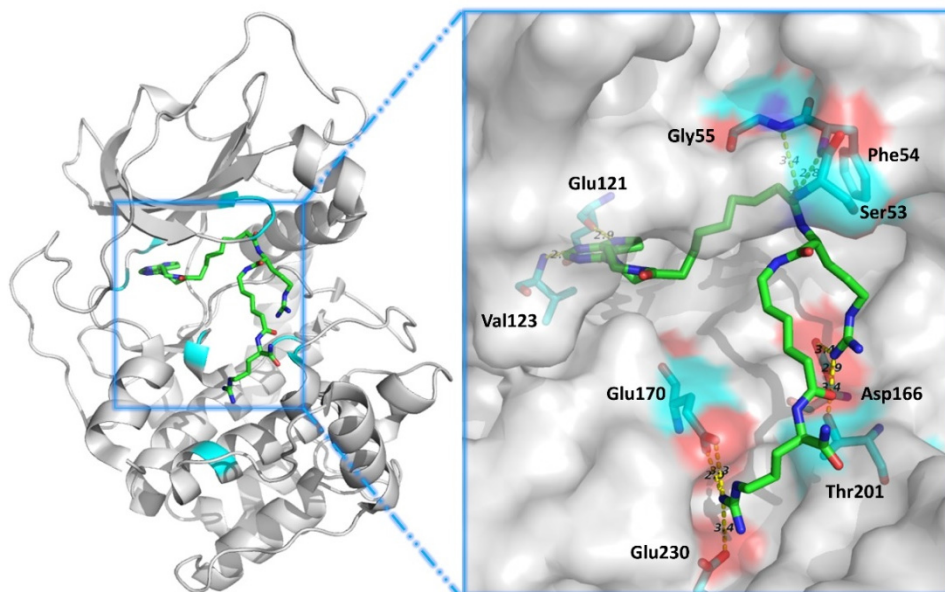


Figure 15. Crystal structure of ARC-1408 in complex with PKA α (pdb: 5izf). PKA is shown as **grey** cartoon (left) or surface (right); ARC-1408 as **green** sticks.

2-Methyl-3-nitrodibenzo[*b,d*]furan (NDBF) was chosen as the photosensitive moiety to be used in the photocaging strategies since it has many suitable qualities for efficient photolysis: high quantum yield ($\Phi = 0.7$) and extinction coefficient ($\epsilon_{330\text{nm}} = 18\,400\text{ M}^{-1}\text{ cm}^{-1}$). In addition, NDBF has fast cleavage kinetics, an absorption maximum reaching up to the visible region (420 nm), and a possibility for 2PE ($\delta = 0.6\text{ GM}$). [Momotake et al. 2006]

We developed a short 3-step transition metal free route to compound **IV**, an electrophilic precursor of NDBF for photocaging 7-deazapurine moiety (**Scheme 4**). For the construction of the photocleavable inhibitor, chiral NDBF- β -amino acid was synthesised (compound **XI**) and for that an enantioselective synthesis route was developed, which was based on a previously published general method for enantioselective synthesis of β -amino esters via chiral *N*-*tert*-butanesulfinyl imines (**Scheme 4**) [Brinner et al. 2009].

5.2. Construction of activatable photocaged bisubstrate PKA inhibitor (Paper I: Sörmus *et al*, 2019)

ARC-1408 was used as a lead compound to construct a photocaged bisubstrate inhibitor due to its high binding affinity for PKA α for its MW (K_D PKA α = 0.18 nM; MW = 798 Da) [Ivan *et al.* 2016]. The C-terminal D-Arg of **ARC-1408** forms charge-assisted hydrogen bonds with Glu170 and Glu230 and the spacer D-Arg interacts with Asp166 and Thr201 (**Figure 15**). Hence, these three positions are important for protein-inhibitor interactions and were considered for the attachment of the photocaged moiety – N7 of 7DP, C-terminal D-Arg, and spacer D-Arg.

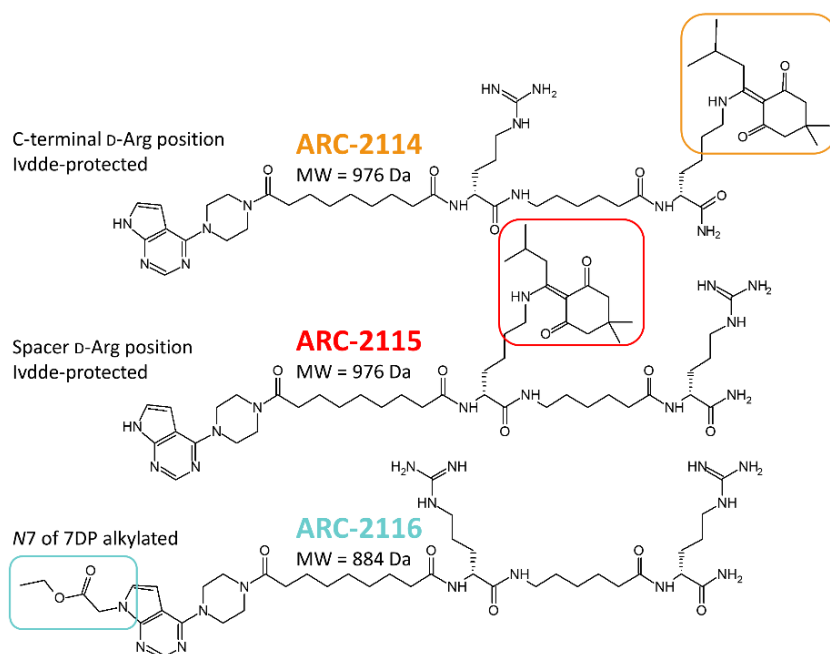


Figure 16. Structures of **ARC-2114**, **ARC-2115**, and **ARC-2116**. The derivatized positions are shown with coloured boxes: Ivdde in the structure of **ARC-2114** and **ARC-2115** in orange and red boxes, respectively; EtOAc in the structure of **ARC-2116** in teal box.

Attaching a single photocage to one of the D-Arg residues would not be effective since the flexible D-Arg chain is likely to reposition, adopt a different conformation, and not disrupt the other interactions with the protein. Photocaging the 7DP fragment not only blocks certain H-bonding interactions but adds steric bulk that debilitates the access of the strongly interacting 7DP-Pip to the ATP-binding site. To confirm these considerations on a quantitative basis,

three model compounds were synthesised bearing non-cleavable bulky groups attached to the positions discussed (**Figure 16**). In **ARC-2114** and **ARC-2115**, the C-terminal and the spacer D-Arg were replaced by IvDde-protected D-lysines, respectively. In **ARC-2116**, N7 of 7DP was alkylated. As expected, the derivatization of the ATP-binding site moiety had the largest effect on the binding affinity (**ARC-2116**, 10 000-fold difference; **Table 5**). Substitution of the D-Arg residues had a much smaller effect on the binding affinity, although changing the C-terminal D-Arg proved to be more impactful (**ARC-2114**, 67-fold difference) compared to the spacer D-Arg (**ARC-2115**, 16-fold difference). Thus, the fragment of choice for photocaging a bisubstrate inhibitor **ARC-1408** proved to be the aromatic moiety targeting the ATP-binding site of PK. Next, NDBF was attached to N7 of the 7DP-Pip of **ARC-1408**, yielding **ARC-2112** (**Scheme 4, Figure 17A**).

Table 5. Schematic structures of ARCs and their K_D values in complex with PKA α as determined by FA¹- or TGLI²-based assays. 7DP-Pip, 4-(piperazin-1-yl)-7H-pyrrolo[2,3-d]pyrimidine; Ahx, 6-aminohexanoic acid; Nda, nonanedioic acid; NDBF, 2-methyl-3-nitrodibenzo[b,d]furan; IvDde, 1-(4,4-dimethyl-2,6-dioxocyclohex-1-ylidene)-3-methylbutyl).

<i>Compound</i>	<i>Schematic Structure</i>	<i>K_D, nM</i>	<i>Irradiated K_D^{app}, nM</i>
ARC-2114	7DP-Pip-Nda-DArg-Ahx-DLys(IvDde)-NH ₂	12 ± 1 ¹	
ARC-2115	7DP-Pip-Nda-DLys(IvDde)-Ahx-DArg-NH ₂	2.9 ± 0.2 ¹	
ARC-2116	EtOCOCH ₂ -7DP-Pip-Nda-DArg-Ahx-DArg-NH ₂	1700 ± 230 ¹	
ARC-1408	7DP-Pip-Nda-DArg-Ahx-DArg-NH ₂	0.18*	
ARC-2112	NDBF-7DP-Pip-Nda-DArg-Ahx-DArg-NH ₂	>15 000	0.76 ± 0.25 ¹
ARC-1411	7DP-Pip-Ahx-[DArg] ₆ -DLys-NH ₂	0.003*	
ARC-2123	7DP-Pip-Nda-DAla-Ahx-[DArg] ₆ -NH ₂	0.005 ± 0.001 ²	
ARC-2113	NDBF-7DP-Pip-Nda-DAla-Ahx-[DArg] ₆ -NH ₂	1900 ± 500 ¹	<0.1 ¹

*[Ivan et al. 2016]

5.2.1 Characterisation of photocaged inhibitors

It was convenient to express the affinities of the inhibitors post-fragmentation as apparent K_D values (K_D^{app}). Apparent affinity is used to describe the affinity of the mixture of compounds after fragmentation and its calculation is based on the concentration of the initially intact inhibitor. Use of K_D^{app} enabled to quantitatively express the extent of deactivation of the inhibitors by the decrease of affinity on K_D -scale.

The affinities of the novel compounds were expressed as the corresponding K_D or K_D^{app} values of their complexes with PKA α pre- and post-irradiation, respectively (**Table 5**). **ARC-2112** was not able to displace the probe from the PKA α complex even at 0.1 mM concentration. Irradiation of **ARC-2112** under Hg vapour lamp brought about photolysis, liberated **ARC-1408**, and provided a 20 000-fold affinity increase towards PKA α (**Figure 17B**).

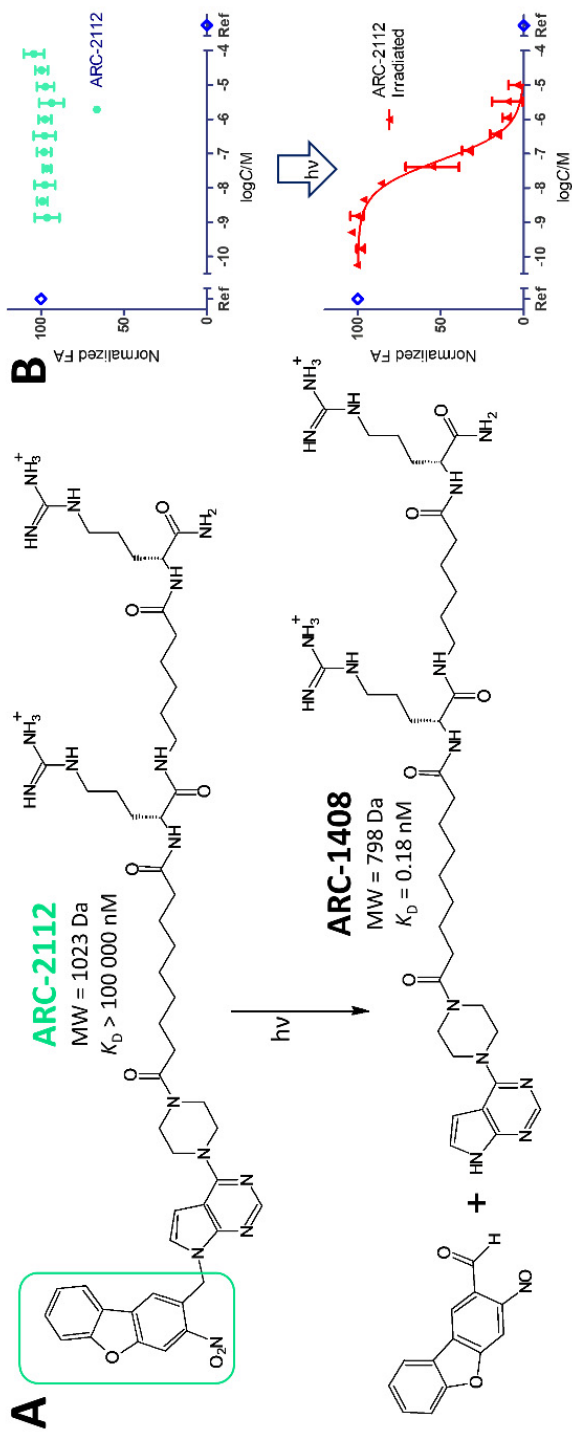


Figure 17. Photolysis of **ARC-2112**. **(A)** The proposed photolysis reaction of **ARC-2112**. **(B)** Displacement FA assay with **ARC-2112** pre- and post-irradiation using recombinant PKA α ($c = 3\ \text{nM}$) and **ARC-583** as the probe ($c = 2\ \text{nM}$).

To see if the photocaging strategy would work on a bisubstrate inhibitor with stronger interactions with the protein substrate-binding region of PKA α , hexa-D-arginine inhibitor **ARC-2123** was prepared. The structure of **ARC-2123** was based on **ARC-1411** but also incorporated an extra DAla-Ahx fragment in the linker region which elongated the linker similarly to **ARC-1408** (**Figure 14,18A**). The K_D value of **ARC-2123** in complex with PKA α was determined to be 5 pM, close to the affinity of **ARC-1411** ($K_D = 3$ pM [Ivan et al. 2016]; **Table 5**). Thereafter, a photocaged variant of **ARC-2123** was synthesised – **ARC-2113** (**Scheme 4; Figure 18A**). **ARC-2113** showed a modest residual affinity towards PKA α ($K_D = 1.9$ μ M; **Table 5**). The 380 000-fold affinity decline upon photocaging (i.e., the ratio of **ARC-2123** vs **ARC-2113**) is remarkable and demonstrates that bisubstrate inhibitors with picomolar affinity can be efficiently deactivated by the attachment of a single photocaging group.

5.2.2 Photocaged inhibitors in cell lysates

Next, **ARC-2113** was used for on-command disruption of the PKA holoenzyme in the presence of other intracellular components. A lysate of CHO cells (C9H6) which express genetically modified fusion proteins PKA β -CFP and PKA α -YFP was used [Ivan et al. 2016; Lissandron et al. 2005; Vaasa et al. 2010; Koschinski and Zaccolo 2017]. The holoenzyme dissociation was monitored by a decrease of FRET between the donor CFP and the acceptor YFP.

Before photolysis, **ARC-2113** was not able to induce FRET change at the highest used concentration of 10 μ M (**Figure 18B**). After 1 min irradiation with a 398 nm LED array the FRET signal decreased and produced a similar dose-response curve to **ARC-1411** (**Figure 18B**). Thus, the photocage had been efficiently removed and the liberated inhibitor worked as efficiently as **ARC-1411** in the cell lysate.

To conclude, the photocaged inhibitors **ARC-2112** and **ARC-2113** possessed no effect on the activity of PKA α at micromolar concentration range and the binding affinities of the uncaged compounds could be quickly (within 1 min) restored with irradiation at 400 nm. The affinity change pre- and post-irradiation was over 5 orders of magnitude.

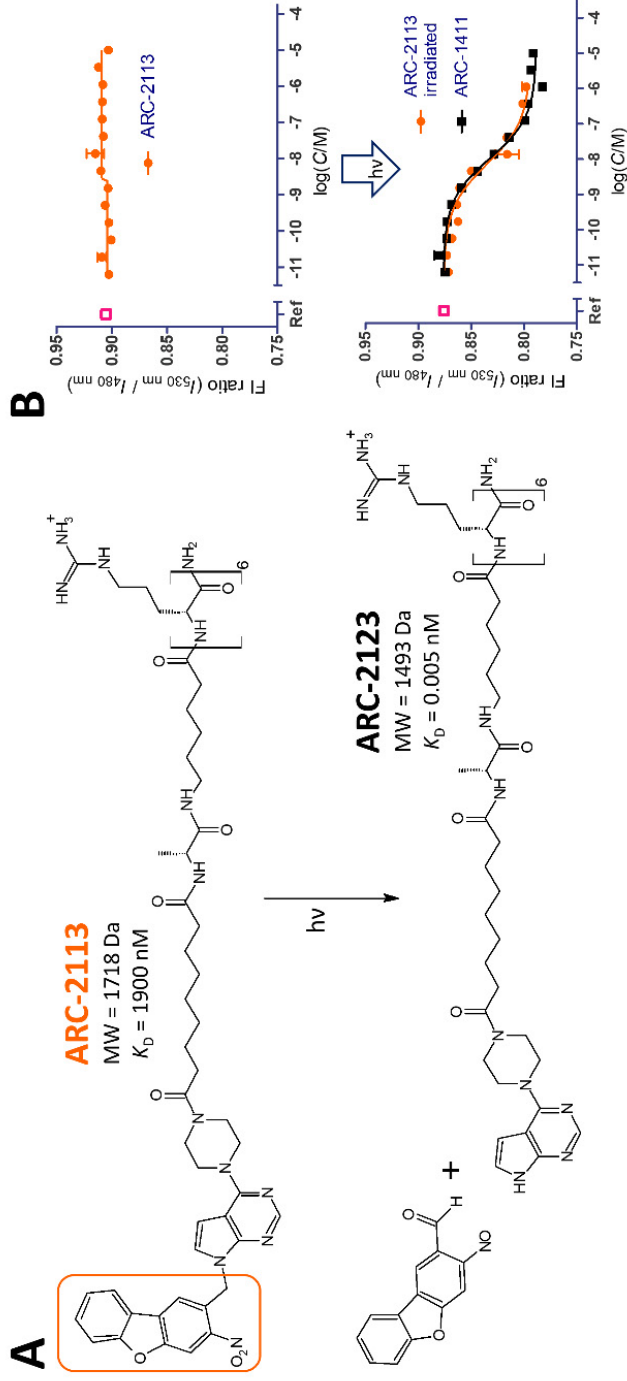


Figure 18. Photolysis of **ARC-2113**. (A) The proposed photolysis reaction of **ARC-2113**. (B) Disruption of PKA holoenzyme by **ARC-2113** pre- and post-irradiation inside C9H6 cell lysate expressing PKArl β -CFP and PKA α -YFP. Reference point (Ref) indicates the neat lysate. FRET was measured after 1 h incubation.

5.3 Construction of deactivatable bisubstrate PKA inhibitors (Paper II: Sörmus *et al.*, 2022)

The designs of the deactivatable inhibitors (**ARC-2121** and **ARC-2194**) were based on the structure of **ARC-1411** (**Figure 14**) due to its exceptionally high affinity towards PKA α ($K_D = 3$ pM) and other basophilic PKs [Ivan *et al.* 2016]. To synthesise the novel redox-cleavable inhibitor, **ARC-2194** (**Figure 19A**), the Nda linker in the structure of **ARC-1411** was replaced with a self-immolative disulfide linker of similar length [Deng *et al.* 2020]. The disulfide linker of **ARC-2194** did not marginally decrease the binding affinity towards PKA α ($K_D = 7 \pm 1$ pM; **Table 6**). Addition of an excess of tris(2-carboxyethyl)phosphine hydrochloride (TCEP) to **ARC-2194** reduced the disulfide bond rapidly and quantitatively. In less than 1 minute **ARC-2194** was converted to compounds **1a** and **1b** (**Figure 19B**). This conversion was followed by a slower self-disintegration of **1a** and **1b** into final products **2a** (7DP-Pip) and **2b** (hexa-D-arginine-amide; **Figure 19A,B**), respectively. The final products were expected to be very weak inhibitors of PKA α , since the analogues of **2a** [Caldwell *et al.* 2008] and **2b** [Enkvist *et al.* 2006] displayed IC₅₀ values in micromolar and millimolar range, respectively. After two hours, most of **1a** had converted to **2a**, but during this timeframe the time-dependent shift of displacement curves was not observed. This implied that the IC₅₀ values of **1a** and **2a** were in the same concentration region. Thus, the full effect of deactivation of **ARC-2194** was already realized in under a minute, after the first reductive cleavage step.

The K_D^{app} calculated from the displacement curve of **ARC-2194** after TCEP-treatment (**Figure 19C**) was 4.5 orders of magnitude higher compared to the K_D value of untreated **ARC-2194**. Also, the K_D^{app} of reduced **ARC-2194** was practically identical to the K_D value of **2a** (**Table 6**), displaying that **ARC-2194** was quantitatively disassembled in the used conditions. This conclusion is also consistent with the HPLC-MS monitoring of the cleavage reaction (**Figure 19B**).

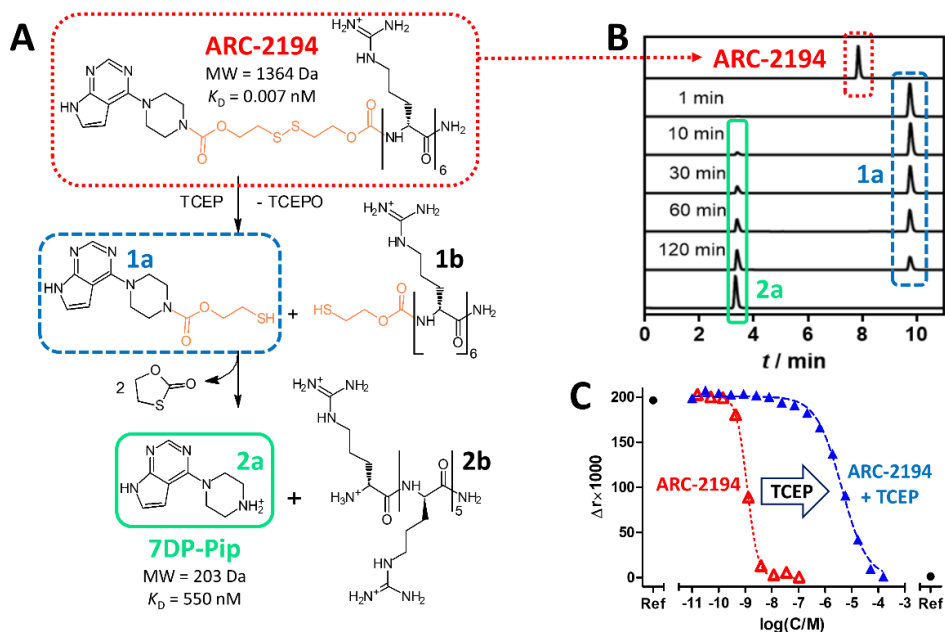


Figure 19. Degradation of ARC-2194 in redox conditions (A) theoretical reaction mechanism of dissociation into **1a** and **1b**, which simultaneously transform into **2a** and **2b**; (B) monitored by HPLC; (C) monitored by a displacement assay.

Table 6. K_D values of PKA α complexes with characterized compounds

Compound	Sequence Structure	K_D , nM	K_D^{app} , nM
ARC-1411	7DP-Pip-Nda-[DArg] ₆ -dLys-NH ₂	0.003 ± 0.001 ^a	
H-89		13 ± 3 ^{a,b}	
ARC-2194	7DP-Pip-COO[CH ₂] ₂ S-S(CH ₂) ₂ COO-[DArg] ₆ -NH ₂	0.007 ± 0.001 ^a	350 ± 30 ^{b,d}
ARC-2121	7DP-Pip-Nda-NDBFβaa-[DArg] ₆ -NH ₂	0.019 ± 0.007 ^a	0.6 ± 0.3 ^{a,c}
2a	7DP-Pip	550 ± 150 ^b	
3c ; (ARC-2167)	NDBFβaa-[DArg] ₆ -NH ₂	650 ± 130 ^b	
3a + 3c ; (1:1) (ARC-2104 + ARC-2167)	7DP-Pip-Nda-NH ₂ + NDBFβaa-[DArg] ₆ -NH ₂		190 ± 60 ^b
3a ; (ARC-2104)	7DP-Pip-Nda-NH ₂	460 ± 210 ^b	

^aTGLI (10 nM ARC-1063, 1 nM PKA α), ^bFA (2 nM ARC-583, 3 nM PKA α); ^cirradiated for 2 min under 365 nm LED; ^dTCEP treatment

5.3.1 Photocleavable inhibitor ARC-2121

For the light-cleavable compound, the replacement of Nda in the structure of **ARC-1411** with NDBF group was not considered due to steric reasons. Instead, photocleavable chiral β-amino acid incorporating the NDBF in the side chain was designed and synthesised. The β-amino acid was introduced between the

linker and the hexa-D-arginine moiety, yielding **ARC-2121**. According to the published route [Klán et al. 2013] the photodegradation of **ARC-2121** (**Figure 20A**) would yield two main products: **3a** (ARC-2104) and **3b**, a derivative of hexa-D-arginine-amide, which had nitrosodibenzofuranyl group attached to the N-terminus via malonic acid residue. **3a** and **3c** (ARC-2167), an analogue of the photolysis product, were synthesised.

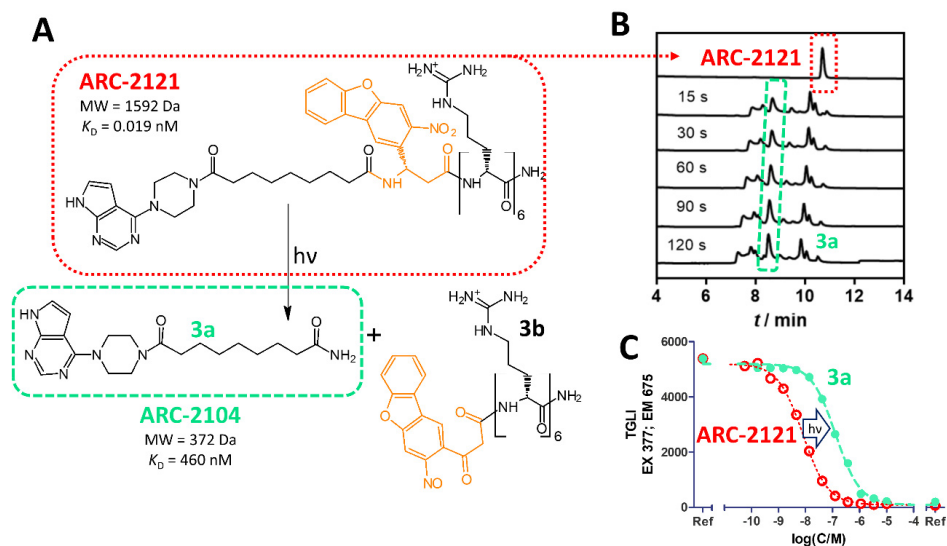


Figure 20. Photolysis of **ARC-2121** (A) theoretical reaction mechanism of photolysis into **3a** and **3b**; (B) monitored by HPLC; (C) monitored by a displacement assay.

The binding affinity of **ARC-2121** only marginally decreased with the addition of the β -amino acid with the bulky NDBF side chain ($K_D = 19 \pm 7$ pM; **Table 6**) compared to **ARC-1411**. The irradiation of the assay mixtures in 384-well microplate was performed with a custom-made device with an array of 365 nm LED-s fixed at distances corresponding to this microplate format. The HPLC-MS monitoring of the photochemical reaction did not detect **ARC-2121** after 15 s of irradiation, and no significant changes in the chromatogram were observed after 30 s of irradiation (**Figure 20B**). It was decided to irradiate the samples for 2 minutes as the displacement curves of **ARC-2121** did not change with a longer irradiation time.

The 2-min treatment of **ARC-2121** (with UV-radiation, 365 nm) did not result in a dramatic change in the binding affinity, unlike with the redox-sensitive **ARC-2194** or the photocaged **ARC-2112** (in *PAPER I*). Instead, the irradiated **ARC-2121** still possessed very high apparent affinity toward PKA α , as shown by 30-fold higher apparent K_D^{app} value (0.6 ± 0.3 nM; **Table 6**; **Figure 20C**). If **ARC-2121** had been cleanly photolyzed into 1:1 mixture of **3a** and **3b** (**Figure 20A**), the apparent affinity of the irradiated inhibitor would have

decreased by at least 10 000-fold, close to the K_D^{app} value for the 1:1 mixture of the theoretical products **3a** and **3c** ($K_D = 190 \pm 60$, **Table 6**). However, the photolysis of **ARC-2121** turned out to yield a complex mixture of products from which only **3a** could be identified by HPLC-MS. It is possible that the high residual K_D^{app} of irradiated **ARC-2121** resulted from the combination of the formation of excessively active products and incomplete photolysis. It is possible that the photolysis of **ARC-2121** stopped (e.g., due to inner filter effect) before a quantitative conversion and small fraction of **ARC-2121** was present in the final mixture that was undetectable by HPLC-MS. If the cleavage of the inhibitor had yielded completely inactive fragments, a 30-fold decrease of K_D^{app} would correspond to about 3% of the residual **ARC-2121** in the solution. It is also possible that excessively potent inhibitors formed in secondary reactions (including the possibility of recombination of the fragments to yield novel bisubstrate inhibitors).

5.4 Construction of a covalent bisubstrate PKA inhibitor (Paper III: Sörmus *et al*, 2022)

It was investigated if and how the bisubstrate inhibitors, which reach out of the ATP-binding site, could be used to make a covalent bond to cysteines distal from the ATP-binding site. The design of the covalent bisubstrate inhibitor was guided by the previously published results of X-ray crystallographic study on the complex of **ARC-1408** and PKA α (**Figure 21**) [Ivan *et al.* 2016]. **ARC-1408** was used as the lead compound, as mentioned above, it possesses high affinity towards PKA α ($K_D = 0.18$ nM) and a moderate molecular weight (MW = 798 Da, **Figure 14**). PKA α possesses two cysteine residues with one of them located in the activation-loop (Cys199). Cys199 is far from the ATP-binding site and is unavailable for small ATP-binding site targeting inhibitors. However, as evident from the co-crystal structure of the complex of **ARC-1408** with PKA α , the distance between Cys199 and the C-terminal D-Arg of **ARC-1408** is only 10 Å. This distance has been considered within suitable range for designing a covalent inhibitor [Wang *et al.* 2019].

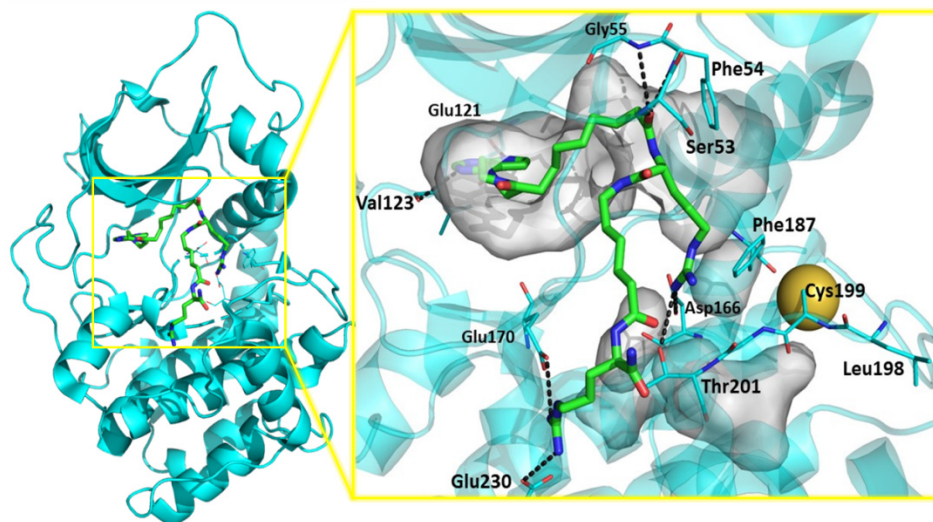


Figure 21. Binding interactions of **ARC-1408** with PKA α . Co-crystal structure of the complex of **ARC-1408**; sticks; C atoms – green, N atoms – blue, O atoms red) and PKA α (Protein Data Bank ID 5izf; cyan cartoon) [Ivan et al. 2016]. Sulfur atom of Cys199 is depicted as a yellow sphere.

The comparative analysis of X-ray crystallographic data of PKA α complexes demonstrated that the placement of a fragment of **ARC-1408** overlaps with placement of a fragment of PKI(5-22) and a fragment of the PKA β II (Figure 22). What is more, the amino acid residues of PKI(5-22) or PKA β II on the C-terminal side of this overlapping region approach the Cys199 of PKA α .

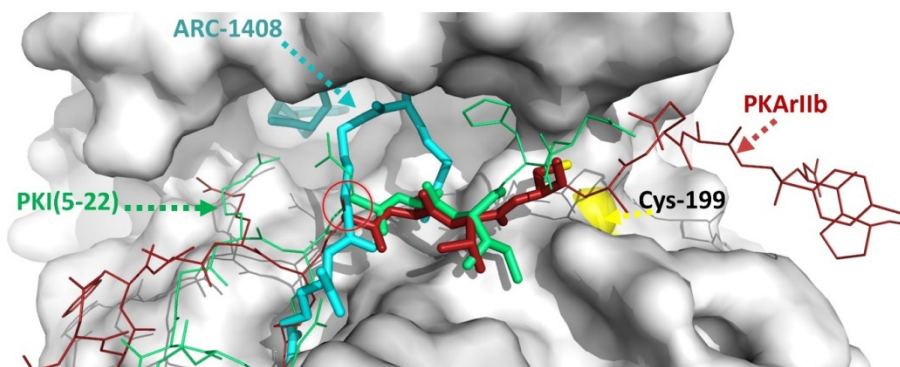
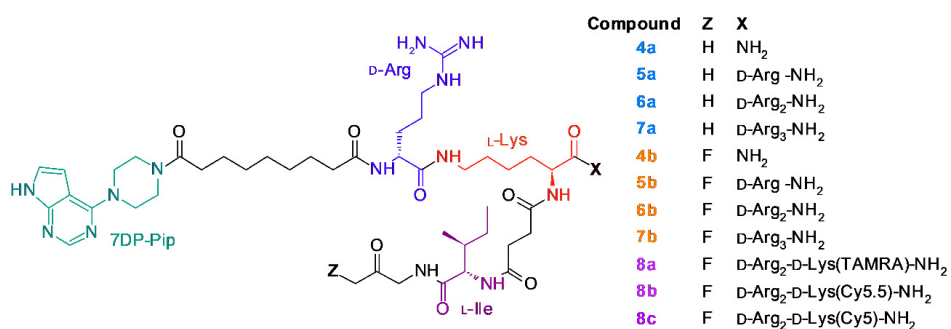


Figure 22. Superimposed images of crystal structures of PKA α in complex with **ARC-1408** or PKI(5-22) or PKA β II. The overlay of three crystal structures: complexes of (1) PKA α (grey surface) with **ARC-1408** (teal sticks; pdb: 5izf); (2) PKA α with PKI(5-22) (green lines; 1atp), and ATP (not shown); (3) PKA α with PKA β II (red lines; 3tnp). Red circle indicates the overlap of **ARC-1408** with PKI(5-22) and PKA β II. Sulfur atom of Cys199 (PKA α) is depicted as a yellow sphere.

Based on this idea, a hybrid molecule in which a side-arm derived from the peptide chain of PKI(5-22) (or PKArII β) is attached to **ARC-1408** was designed and synthesized. The Ahx linker in **ARC-1408** was replaced with an L-lysine residue which preserved the linker length between the D-arginine residues but provided an extra amino group for the side-arm (**Scheme 5**). From there on, succinic acid was used as a short linker to connect the α -amino group of L-Lys to L-Ile. It was expected that L-Ile residue would be in a similar position to L-Ile of PKI(5-22) (**Figure 22**) and give similar interactions with PKA α . Finally, FMK electrophile was attached to the carboxyl group of L-Ile residue. FMK was chosen as the warhead since it had been successfully used to target the same cysteine residue (C199) of PKA α by Coover et al. [Coover et al. 2016].



Scheme 5. Structures of compounds synthesized in the current work; 7DP-Pip depicted in green, D-Arg in blue, L-Lys in red, L-Ile in purple. The ARC codes of the covalent inhibitors are depicted in orange, their reversible derivatives depicted in blue, and the fluorescently labelled derivatives of **6a** (ARC-2156) are depicted in purple.

Starting from the commercially available racemic 1-fluoro-3-chloropropan-2-ol, the precursor for FMK was synthesized over seven steps, which could be attached to the rest of the inhibitor on solid phase. A series of inhibitors tagged with FMK group was synthesized by varying the number of D-arginine residues at the C-terminus of the inhibitors (**Scheme 5**). Also, the analogous non-reactive control compounds were synthesized for reference, all lacking the fluorine atom on the methyl ketone moiety (**Scheme 5**).

5.4.1 Characterization of reversible inhibitors

The reversible compounds **4a** (ARC-2161), **5a** (ARC-2163), **6a** (ARC-2156), and **7a** (ARC-2165) possessed K_D values in nano- and picomolar range (**Table 7**, **Figure 23A**). Overall, the binding affinity strongly depended on the count of C-terminal D-arginine residues. Each D-arginine decreased the K_D value by approximately an order of magnitude, whereas the attachment of the second C-terminal D-arginine residue caused the largest increase in the binding affinity. The dissociation rate (k_{off}) of the reversible inhibitors from their complex with PKA α was measured. For the smaller compounds, **4a** and **5a**, the dissociation was complete after a few minutes. Unlike, for the larger compounds, **6a** and **7a**, the dissociation was much slower, taking 30 and 40 min, respectively (**Table 7**, **Figure 23B**). Again, a strong correlation between the count of C-terminal D-arginine residues in the inhibitor and their dissociation times – the more D-arginine residues, the slower was the dissociation.

The selectivity profile of the reversible **6a**, which comprised 2 C-terminal D-arginines, was analyzed in a commercial inhibition assay in a panel of 140 PKs. **6a** ($c = 100$ nM) revealed the highest inhibitory potency for PKA α (residual activity of $2 \pm 1\%$). Additionally, three other basophilic PKs of the AGC group were inhibited by more than 90%: ROCKII, PKB α , and PKB β (residual activities of $8 \pm 1\%$, $8 \pm 3\%$, and $9 \pm 2\%$, respectively). In total, 12 PKs were inhibited by more than 50%, from which 9 belonged to AGC, 2 to CAMK, and 1 to CMGC group.

Table 7. Characterization of reversible and covalent compounds. K_D , k_{off} , and k_{inact} values using PKA α ; k_{on} , K_I , and k_{inact}/K_I were calculated.

	C-terminal D-Args	K_D [nM]	k_{off} [s ⁻¹]	k_{on} [M ⁻¹ s ⁻¹] ^c	K_I [nM] ^d	k_{inact} [s ⁻¹]	k_{inact}/K_I [M ⁻¹ s ⁻¹]
4a (ARC-2161)	0	$(4.2 \pm 0.4) \cdot 10^{-9}$	$(1.4 \pm 0.3) \cdot 10^{-1}$	$3.3 \cdot 10^7$			
4b (ARC-2162)	0				$4.2 \cdot 10^{-9}$	$(3.3 \pm 0.2) \cdot 10^{-5,a}$	$7.9 \cdot 10^3$
5a (ARC-2163)	1	$(6.3 \pm 1.0) \cdot 10^{-10}$	$(2.4 \pm 0.5) \cdot 10^{-2}$	$3.8 \cdot 10^7$			
5b (ARC-2148)	1				$6.3 \cdot 10^{-10}$	$(7.7 \pm 0.7) \cdot 10^{-5,a}$	$1.2 \cdot 10^5$
6a (ARC-2156)	2	$(1.9 \pm 0.1) \cdot 10^{-11}$	$(2.6 \pm 0.1) \cdot 10^{-3}$	$1.4 \cdot 10^8$			
6b (ARC-2158)	2				$2.3 \cdot 10^{-11}$	$(5.8 \pm 1.2) \cdot 10^{-4,b}$	$2.5 \cdot 10^7$
7a (ARC-2165)	3	$(4.9 \pm 0.1) \cdot 10^{-12}$	$(1.0 \pm 0.1) \cdot 10^{-3}$	$2.2 \cdot 10^8$			
7b (ARC-2166)	3				$6.8 \cdot 10^{-12}$	$(4.2 \pm 0.6) \cdot 10^{-4,b}$	$6.2 \cdot 10^7$

^aDisplacement experiments (5 nM PKA α , 10 nM inhibitor, 200 nM ARC-1063), ^bWestern Blot, ^ccalculated according to $k_{on} = k_{off}/K_D$; ^dcalculated according to equation 3.

5.4.2 Characterization of covalent inhibitors

The reaction rate of covalent compounds **4b** (ARC-2162), **5b** (ARC-2148), **6b** (ARC-2158), and **7b** (ARC-2166) with recombinant PKA α was measured by preincubating them for a given period. At fixed time points, the reaction was stopped by adding an excess amount of the TGLI probe. The added probe would replace the unreacted covalent inhibitor in the complex with the PK and the measured TGLI signal correlated with the amount of unreacted PKA α in the solution. The plot of TGLI-signal vs reaction time showed a clear time-dependent decrease of TGLI signal with all FMK-modified compounds (**Figure 23C**). This showed that the PK was indeed being covalently modified.

The compounds with fewer D-arginines (**4b** and **5b**) reacted very slowly with PKA α as the reaction was not complete even after 8 h. Addition of the second C-terminal D-arginine residue to the inhibitor structure (**6b**) gave the largest gain in binding affinity and decreased the reaction half-life from 2.5 h down to 19 min. Reaction rates for **6b** and **7b** were very similar, although **7b** comprised an extra D-arginine. The obtained time dependencies were analyzed to calculate k_{inact} values of the covalent inhibitors (**Table 7**).

The reaction times of the smaller FMK-containing inhibitors with PKA α were rather long (**4b** and **5b**, half-lives of reaction of more than 2.5 h) if compared to the fast off-rate of the corresponding reversible complexes, established with the corresponding reference compounds (**4a** and **5a**, half-lives of dissociation less than 1 min). Therefore, the reaction between PKA α and **4b** or **5b** was rapidly quenched upon addition of excess amount of the TGLI probe and the off-rates of these compounds could be ignored when deriving k_{inact} values from data presented in **Figure 23C**.

On the other hand, in case of the larger inhibitors which comprise more D-arginine residues, the difference between the off-rate of unreacted inhibitor and the rate of chemical reaction with PKA α was smaller ($t_{1/2}(\text{reaction}) \sim 20$ min; $t_{1/2}(\text{dissociation}) \sim 5 - 10$ min). Thus, the reaction half-lives of **6b** and **7b** with PKA α were also measured using Western Blot (WB). The reaction half-lives measured using TGLI assay and WB were in good agreement (**Figure 23E**, **Table 7**).

The K_{I} values of the covalent inhibitors were calculated using the k_{inact} values, k_{off} , and k_{on} according to equation 2. The $k_{\text{inact}}/K_{\text{I}}$ values of **6b** and **7b** (**Table 7**) are higher than these of the FDA approved EGFR targeted covalent inhibitors (e.g., afatinib $k_{\text{inact}}/K_{\text{I}} = 1.5 \times 10^7$ [Schwartz et al. 2014]) and much higher than these of the peptidic covalent inhibitors of PKA (e.g., $k_{\text{inact}}/K_{\text{I}} = 6.2 \times 10^3$; $k_{\text{inact}}/K_{\text{I}} = 5.0 \times 10^2$ [Coover et al. 2016; Bramson et al. 1982]). The high $k_{\text{inact}}/K_{\text{I}}$ ratios of the covalent bisubstrate ARC-inhibitors mostly originate from the nano- to picomolar K_{D} values of these compounds.

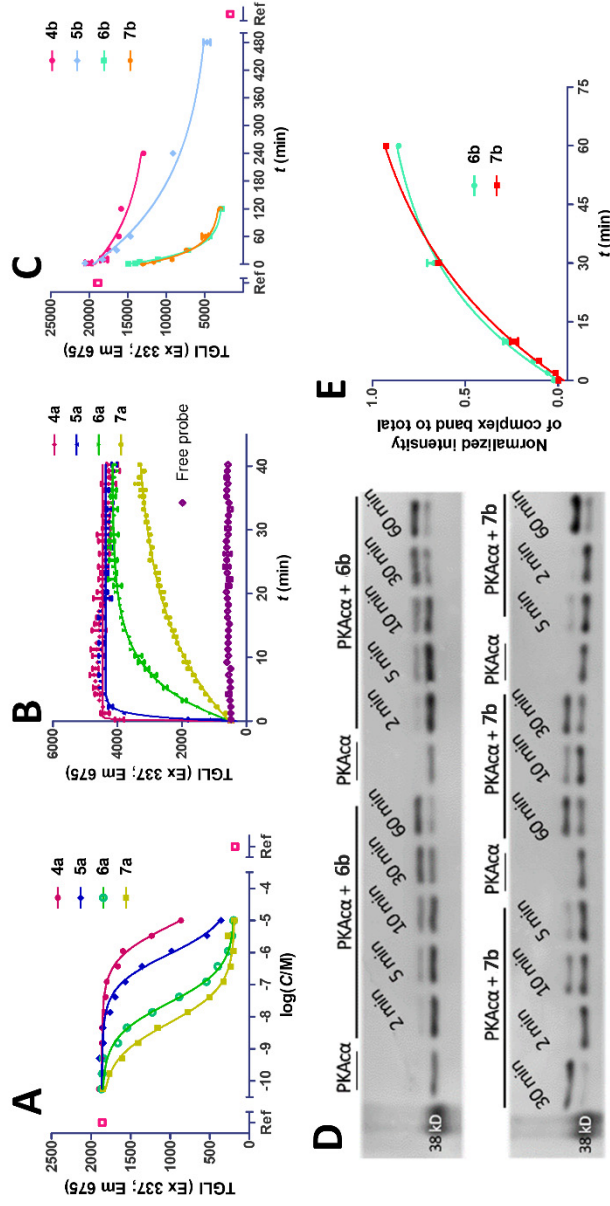


Figure 23. Biochemical evaluation of compounds reversible and covalent compounds using TGLI-based assays. The probe used in all experiments was ARC-1063 ($K_D = 0.015$ nM) [Enkvist et al. 2011]. TGLI values for ARC-1063 with PKA α (higher TGLI) or without PKA α (lower TGLI) were used as references (Ref). **(A)** equilibrium displacement of TGLI probe (20 nM) from complex with PKA α (1 nM) by reversible inhibitors; **(B)** measurement of dissociation kinetics of reversible inhibitors; 5 nM PKA α and 10 nM inhibitor were incubated for 1 h, measurement was started after the addition of 200 nM displacing probe; **(C)** monitoring the reaction of covalent inhibitors (10 nM) with PKA α (5 nM). At fixed time points, excess TGLI probe (200 nM) was added to an aliquot of the reaction mixture to titrate the unreacted PKA α . Higher number of excitation flashes was used which resulted in a relatively higher TGLI signal compared to **(A)** and **(B)**. **(D)** Time course of reaction between PKA α and **6b** or **7b** monitored with WB using fluorescence detection (Li-Cor). PKA α ($c = 5$ nM) and inhibitor ($c = 50$ nM) were incubated for a fixed time, thereafter SDS was added to stop the reaction; **(E)** normalized intensities of bands corresponding to PKA α -inhibitor (**6b** and **7b**) conjugate. The normalized intensity was calculated as follows: $I_{\text{normalized}} = I_{\text{upper band}} / (I_{\text{upper band}} + I_{\text{lower band}})$.

The intrinsic reactivity of FMK warhead was determined in a reaction between **6b** (0.15 mM) and GSH (10 mM) in 100 mM potassium phosphate buffer at pH 7.4. FMK displayed a moderate-high reactivity ($t_{1/2\text{GSH}} = 0.74$ h at 30°C; $t_{1/2\text{GSH}} = 0.37$ h at 37°C). Also, FMK bearing **6b** was slowly decomposing in phosphate buffer (pH 7.4; $t_{1/2\text{deg}} = 1.31$ h at 30°C; $t_{1/2\text{deg}} = 0.95$ h at 37°C). Although, the reaction of **6b** with PKA α ($t_{1/2\text{PKA}\alpha} = 0.32$ h; 30°C) was twice as fast as the unspecific reaction with GSH ($t_{1/2\text{GSH}} = 0.74$ h; 30°C), the reaction was slower compared to previously published peptidyl FMK targeting the same Cys199-residue ($t_{1/2\text{PKA}\alpha} = 0.07$ h; 30°C) [Coover et al. 2016]. This suggests the FMK electrophile in the structure of **6b** is not optimally positioned for the reaction with Cys199. The reactions of **4b** and **5b** with PKA α were much slower ($t_{1/2\text{PKA}\alpha} = 5.76$ h and 2.52 h, respectively) than with GSH ($t_{1/2\text{GSH}} = 0.74$ h) or the FMK degradation ($t_{1/2\text{deg}} = 1.31$ h). This implies that **4b** and **5b** were bound to the ATP-binding site and were not able to position their warheads in suitable distance and geometry to efficiently react with Cys199.

The covalent modification of PKA α at Cys199 residue was also confirmed using LC-MS/MS analysis of trypsinated **6b**-PKA α adduct. The peptide fragment of PKA α , which incorporated modified Cys199 (TWTLC¹⁹⁹GTPEY-LAPEIILSK) with mass difference corresponding to the attached **6b** (MW +1235 Da) was detected. The modification was unambiguously localized to Cys199. Modification of the other cysteine residue of PKA α , Cys343, was not detectable which showed that the reaction with Cys199 was specific.

5.4.3 Reactions of fluorescent dye-labelled covalent inhibitor in cell lysates and cells

For monitoring the formation of the irreversible PK-inhibitor adduct in complex biological matrices, the structure of **6b** was modified to enable introduction of a fluorescent dye. During the peptide synthesis, D-Lys was attached to the C-terminus of **6b** and thereafter the obtained compound was labelled with the (1) 5-carboxytetramethylrhodamine (5-TAMRA) dye and yielded **8a** (ARC-2154), (2) Cy.5.5 dye and yielded **8b** (ARC-2168), or (3) Cy5 dye and yielded **8c** (ARC-2160).

Compound **8a** (TAMRA-labelled) was added to different cell lysates (of U2OS, HeLa, and PC3 cells) and incubated at 30 °C. After 1 h, the reaction was stopped by adding loading buffer which contained sodium dodecyl sulfate (SDS). Next, the proteins were separated on dodecyl sulfate–polyacrylamide gel electrophoresis (SDS-PAGE), transferred onto a nitrocellulose membrane, and analyzed by WB. The WB analysis showed that the covalent inhibitor can inhibit PKAc selectively in the cell lysate in a concentration dependent manner, meaning that if the covalent inhibitor prefers its target enzyme, PKAc, but will react with other components if in excess (**Figure 24A**). An experiment where cell lysates were spiked with different PKs (AKT3, MSK1, AurA, AurB, ROCKII) displayed that the covalent inhibitor **8a** preferred to first react with PKAc in all the samples, and thereafter it could react to the spiked PKs, which

had a cysteine residue in an analogous position to Cys199 of PKA α (AKT3, AurA, and MSK1).

8b (Cy5.5-labelled) was used cell experiments, to see if the inhibitor was able to penetrate the cell membrane (HeLa cells). Here, the lysate was made after the inhibitor had already been incubated with live cells; also, forskolin was added to initiate the PKA holoenzyme dissociation via the concentration increase of cAMP. As seen from the WB images, **8b** was able to penetrate the at higher, 5 μ M concentration, but not at the lower, 1 μ M concentration (**Figure 24B**). However, the **8b** reacted with multiple cellular components similarly to the previously performed lysate experiments with **8a** where the too high inhibitor concentration promoted off-target reactions. Also, in live cells, PKAc was not the main target. These results suggest that at 5 μ M applied concentration the inhibitor efficiently accumulates in the cells to a concentration that far exceeds the average concentration of PKAc in HeLa cells (200 nM) [Nonga et al. 2021]. In this case, arising from the high reactivity of FMK warhead and non-specificity of binding, the inhibitor targets and reacts with multiple proteins, of which some may be more abundant in the cells compared to PKAc. At 1 μ M concentration of the inhibitor in the incubation medium such accumulation does not occur, that was reflected by faint fluorescence signal corresponding to labelled proteins. It should be noted that inside live cells differences in localization between the internalized inhibitor and its target proteins contribute on the overall selectivity of reaction. According to the results of WB analysis the non-labelled **6b** at applied 5 μ M concentration did not target PKAc in live HeLa cells (data not shown). Thus, tagging the inhibitor with a hydrophobic Cy5.5 dye remarkably improved membrane-penetrative properties of the compound, yet the mechanism (endocytosis or direct penetration of the plasma membrane) by which the bisubstrate inhibitor enters the cell requires further studies.

8c (Cy5-labelled) was used to further visualize efficiency of cellular uptake and the intracellular localization of the labelled covalent inhibitors. At 5 μ M concentration, **8c** internalized efficiently into live HeLa cells regardless of the incubation time (15-min, 1-h, or 2-h) or the presence of forskolin (**Figure 24C**). The total fluorescence intensity in the wells containing cells treated with 5 μ M **8c** was significantly higher than for cells treated with 1 μ M **8c** ($P < 0.05$); the effect of forskolin was insignificant for all pairwise comparisons of signals with vs without forskolin. The decrease of incubation time from 2 h to 1 h was insignificant for 5 μ M, yet it was significant for treatment with 1 μ M **8c**. Overall, this data confirms that the covalent bisubstrate inhibitors developed within this study can be used for intracellular targeting, although the selectivity of the compounds needs to be tuned for the precise targeting of the PK of interest. The cell membrane-penetrative properties of compounds should be improved and quantified to enable the application of bisubstrate covalent inhibitors at lower concentrations in cellular assays.

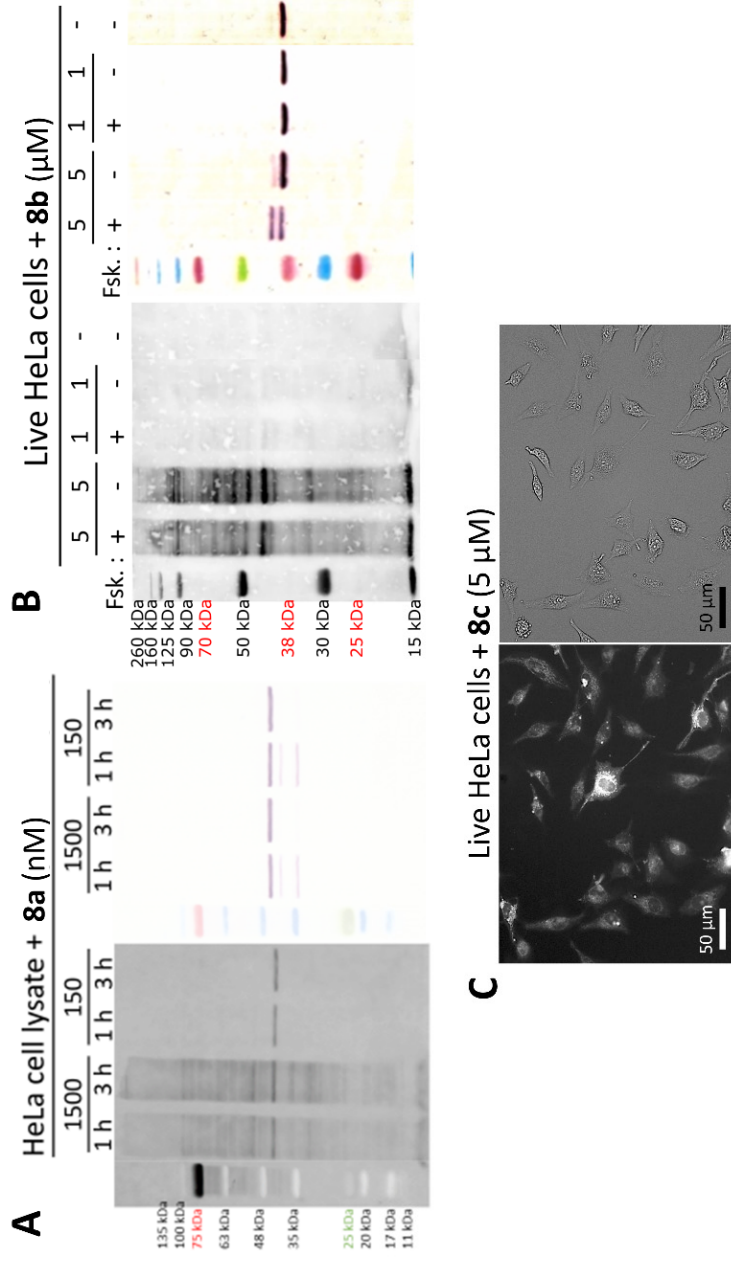


Figure 24. Membrane fluorescent imaging, WB experiments, and microscopy. **(A)** Membrane fluorescent imaging and WB experiments with **8a** at various final total concentrations in PC3 cell lysate, 1 h incubation; left: fluorescence (TAMRA), right: immunostaining; cAMP ($50 \mu\text{M}$) and IBMX ($25 \mu\text{M}$) were added to the lysate.; **(B)** Membrane fluorescent imaging and WB experiments with **8b**; left: fluorescence (Cy5.5), right: immunostaining with PKAc antibody; 5 or $1 \mu\text{M}$ **8b** incubated on pre-lysis HeLa cells for 2 h in the presence/absence of forskolin ($30 \mu\text{M}$); **(C)** Cellular uptake of **8c** into live HeLa cells following treatment with $5 \mu\text{M}$ concentration and 2 h. left – Cy5 fluorescence; right: – Bright field. Scale bar: $50 \mu\text{m}$.

6. SUMMARY OF RESULTS AND DISCUSSION

Covalent binding, on-command activation and deactivation of bisubstrate protein kinase (PK) inhibitors were explored via previously measured co-crystal structure-guided design. cAMP-dependent PK was used as the main enzyme target.

- 1) The first photocaged bisubstrate inhibitor was designed and synthesised displaying that bisubstrate tight-binding inhibitors could be effectively photocaged at the ATP-binding site targeting fragment that provides spatial and temporal control over the functionality of this type of compound. The observed 10^5 times affinity change upon irradiation highlights the importance of finding the best energetic "hot spots" for blocking the interaction of the ligand with the protein by the photocage, but also points to the importance of finding the most suitable photocaging group and avoiding premature photolysis of the photocaged ligand. The photocaged inhibitors possess no effect on the activity of PKA α at micromolar concentration range and the inhibitory potency of the uncaged compounds can be quickly (within 1 min) restored with irradiation at 400 nm.
- 2) The first photocleavable bisubstrate inhibitors were designed and synthesised. The conjugation irradiation- and reduction-responsive cleavable linkers yielded compounds with strong ability to bind to the catalytic site of PKA α (K_D values in one- to two-digit picomolar range). Cleavage of the linker in response to external stimuli (irradiation at 365 nm or chemical reduction, respectively) disassembled the compounds, which resulted in liberation of the active PKA α .
- 3) The first covalent bisubstrate inhibitors of PKs were designed and synthesised. The count of C-terminal D-arginine residues in the peptide fragment of the inhibitor was the key influencing factor of the reversible complex stability as well as of reaction rate of the inhibitor–PK adduct formation.
 - The reversible analogues of the covalent inhibitors revealed very high, picomolar binding affinity toward PKA α and slow to moderate dissociation kinetics of the complexes; in a panel of 140 PKs **6a** (ARC-2156) revealed its preference for PKA α inhibition.
 - **6b** (ARC-2158), the first in class cysteine-reactive bisubstrate inhibitor of PKs, was able to make a covalent thioether bridge specifically with Cys199 residue of PKA α . Covalent inhibitors revealed very high k_{inact}/K_I values (up to $6.2 \times 10^7 \text{ M}^{-1} \text{ s}^{-1}$), which mostly stem from the very high binding affinity of the bisubstrate inhibitors. The reaction of the inhibitor with Cys199 residue of PKA α was relatively slow (half-life of 19.0 ± 0.5 min), which suggests sub-optimal positioning of the electrophilic warhead.
 - Fluorescently TAMRA-labeled covalent inhibitor **8a** (ARC-2154) was able to tag PKAc in U2OS, HeLa, and PC3 cell lysates and labeled spiked PKs AKT3, Aurora A, and MSK1 in PC3 cell lysate, although

still preferring to form the adduct with the native PKAc. Cy5.5-labeled **8b** (ARC-2168) was able to penetrate the cell plasma membrane and react with PKAc inside the cell, although not as selectively as in the cell lysate.

7. REFERENCES

- Abbvie reports full-year and fourth-quarter 2021 financial results. **2022**, <https://news.abbvie.com/news/press-releases/abbvie-reports-full-year-and-fourth-quarter-2021-financial-results.htm> (accessed: 2022.10.01)
- Abdeldayem, A.; Raouf, Y. S.; Constantinescu, S. N.; Moriggl, R.; Gunning, P. T. Advances in covalent kinase inhibitors. *Chem. Soc. Rev.* **2020**, *49*, 2617–2687.
- Algorri, J. F.; Ochoa, M.; Roldán-Varona, P.; Rodríguez-Cobo, L.; López-Higuera, J. M. Photodynamic therapy: a compendium of latest reviews. *Cancers (Basel)* **2021**, *13*, 17, 4447.
- Attwood, M. M.; Fabbro, D.; Sokolov, A. V.; Knapp, S.; Schiöth, H. B. Trends in kinase drug discovery: targets, indications and inhibitor design. *Nat. Rev. Drug Discov.* **2021**, *20*, 11, 839–861; [published correction appears in *Nat. Rev. Drug Discov.* **2021**, *20*, 10, 798].
- Bartrop, J. A.; Schofield, P. Photosensitive protecting groups. *Tetrahedron Lett.* **1962**, *3*, 16, 697–699.
- Borsari, C.; Keles, E.; McPhail, J. A.; Schaefer, A.; Sriramaratnam, R.; Goch, W.; Schaefer, T.; De Pascale, M.; Bal, W.; Gstaiger, M.; Burke, J. E.; Wymann, M. P. Covalent proximity scanning of a distal cysteine to target PI3K α . *J. Am. Chem. Soc.* **2022**, *144*, 14, 6326–6342.
- Brieke, C.; Rohrbach, F.; Gottschalk, A.; Mayer, G.; Heckel, A. Light-controlled tools. *Angew. Chem. Int. Ed. Engl.* **2012**, *51*, 34, 8446–8476.
- Brinner, K.; Doughan, B.; Poon, D. J. Scalable synthesis of β -amino esters via reformatsky reaction with *N*-*tert*-butanesulfinyl imines. *Synlett*, **2009**, *6*, 991–993.
- Bum-Erdene, K.; Liu, D.; Gonzalez-Gutierrez, G.; Ghozayel, M. K.; Xu, D.; Meroueh, S. O. Small-molecule covalent bond formation at tyrosine creates a binding site and inhibits activation of Ral GTPases. *PNAS.* **2020**, *117*, 13, 7131–7139.
- Caldwell, J. J.; Davies, T. G.; Donald, A.; McHardy, T.; Rowlands, M. G.; Aherne, G. W.; Hunter, L. K.; Taylor, K.; Ruddle, R.; Raynaud, F. I.; Verdonk, M.; Workman, P.; Garrett, M. D.; Collins, I. Identification of 4-(4-aminopiperidin-1-yl)-7H-pyrrolo [2,3-d]pyrimidines as selective inhibitors of protein kinase B through fragment elaboration. *J. Med. Chem.* **2008**, *51*, 2147–2157.
- Chang, C.; Fernandez, T.; Panchal, R.; Bayley, H. Caged catalytic subunit of cAMP-dependent protein kinase. *J. Am. Chem. Soc.* **1998**, *120*, 7661–7662.
- Chen, C. T.; Kesselheim, A. S. Journey of generic imatinib: a case study in oncology drug pricing. *J. Oncol. Pract.* **2017**, *13*, 6, 352–355.
- Chen, Y.; Sabatini, B. L. The kinase specificity of protein kinase inhibitor peptide. *Front. Pharmacol.* **2021**, *12*, 632815.
- Cohen, M. S.; Hadjivassiliou, H.; Taunton, J. A clickable inhibitor reveals context-dependent autoactivation of p90 RSK. *Nat. Chem. Biol.* **2007**, *3*, 3, 156–160.
- Cohen, P. Protein kinases – the major drug targets of the twenty-first century? *Nat. Rev. Drug Discov.* **2002**, *1*, 309–315.
- Coover, R. A.; Luzi, N. M.; Korwar, S.; Casile, M. E.; Lyons, C. E.; Peterson, D. L.; Ellis, K. C. Design, synthesis, and *in vitro* evaluation of a fluorescently labeled irreversible inhibitor of the catalytic subunit of cAMP-dependent protein kinase (PKA α). *Org. Biomol. Chem.* **2016**, *14*, 4576–4581.
- Curley, K.; Lawrence, D. S. Photoactivation of a signal transduction pathway in living cells. *J. Am. Chem. Soc.* **1998**, *120*, 8573–8574.

- Dalton, G. D.; Dewey, W. L. Protein kinase inhibitor peptide (PKI): a family of endogenous neuropeptides that modulate neuronal cAMP-dependent protein kinase function. *Neuropeptides*. **2006**, *40*, 1, 23–34.
- de Boer, A. R.; Letzel, T.; Lingeman, H.; Irth, H. Systematic development of an enzymatic phosphorylation assay compatible with mass spectrometric detection. *Anal. Bioanal. Chem.* **2005**, *381*, 647–655.
- de Oliveira, P. S.; Ferraz, F. A.; Pena, D. A.; Pramio, D. T.; Morais, F. A.; Schechtman, D. Revisiting protein kinase-substrate interactions: toward therapeutic development. *Sci. Signal.* **2016**, *9*, 420, re3.
- de Wit, R. J.; Hekstra, D.; Jastorff, B.; Stec, W. J.; Baraniak, J.; Van Driel, R.; Van Haastert, P. J. Inhibitory action of certain cyclophosphate derivatives of cAMP on cAMP-dependent protein kinases. *Eur. J. Biochem.* **1984**, *142*, 2, 255–260.
- Demaille, J. G.; Peters, K. A.; Fischer, E. H. Isolation and properties of the rabbit skeletal muscle protein inhibitor of adenosine 3',5'-monophosphate dependent protein kinases. *Biochemistry*. **1977**, *16*, 14, 3080–3086.
- Deng, Z.; Hu, J.; Liu, S. Disulfide-based self-immolative linkers and functional bioconjugates for biological applications. *Macromol. Rapid Commun.* **2020**, *41*, e1900531.
- Dong, M.; Babalhavaeji, A.; Samanta, S.; Beharry, A. A.; Woolley, G. A. Red-shifting azobenzene photoswitches for in vivo use. *Acc. Chem. Res.* **2015**, *48*, 10, 2662–2670.
- Eichholtz, T.; de Bont, D. B.; de Widt, J.; Liskamp, R. M.; Ploegh, H. L. A myristoylated pseudosubstrate peptide, a novel protein kinase C inhibitor. *J. Biol. Chem.* **1993**, *268*, 3, 1982–1986.
- Ellis-Davies, G. C. R.; Kaplan, J. H. Nitrophenyl-EGTA, a photolabile chelator that selectively binds Ca²⁺ with high affinity and releases it rapidly upon photolysis. *Proc. Natl. Acad. Sci.* **1994**, *91*, 187–191.
- Engels, J.; Schlaeger, E. J. Synthesis, structure, and reactivity of adenosine cyclic 3',5'-phosphate-benzyltriesters. *J. Med. Chem.* **1977**, *20*, 7, 907–911.
- Enkvist, E.; Lavogina, D.; Raidaru, G.; Vaasa, A.; Viil, I.; Lust, M.; Viht, K.; Uri, A. Conjugation of adenosine and hexa-(d-arginine) leads to a nanomolar bisubstrate-analog inhibitor of basophilic protein kinases. *J. Med. Chem.* **2006**, *49*, 7150–7159.
- Enkvist, E.; Vaasa, A.; Kasari, M.; Kriisa, M.; Ivan, T.; Ligi, K.; Raidaru, G.; Uri, A. Protein-induced long lifetime luminescence of nonmetal probes. *ACS Chem. Biol.* **2011**, *6*, 1052.
- Enkvist, E.; Viht, K.; Bischoff, N.; Vahter, J.; Saaver, S.; Raidaru, G.; Issinger, O. G.; Niefind, K.; Uri, A. A subnanomolar fluorescent probe for protein kinase CK2 interaction studies. *Org. Biomol. Chem.* **2012**, *10*, 43, 8645–8653.
- Enns, L. C.; Pettan-Brewer, C.; Ladiges, W. Protein kinase A is a target for aging and the aging heart. *Aging (Albany NY)*. **2010**, *2*, 238–243.
- Fabbro, D.; Cowan-Jacob, S. W.; Moebitz, H. Ten things you should know about protein kinases: IUPHAR Review 14. *Br. J. Pharmacol.* **2015**, *172*, 11, 2675–2700.
- Fedoryak, O. D.; Dore, T. M. Brominated hydroxyquinoline as a photolabile protecting group with sensitivity to multiphoton excitation. *Org. Lett.* **2002**, *4*, 20, 3419–3422.
- Filevich, O.; Salierno, M.; Etchenique, R. A caged nicotine with nanosecond range kinetics and visible light sensitivity. *J. Inorg. Biochem.* **2010**, *104*, 12, 1248–1251.
- Flanagan, M. E.; Abramite, J. A.; Anderson, D. P.; Aulabaugh, A.; Dahal, U. P.; Gilbert, A. M.; Li, C.; Montgomery, J.; Oppenheimer, S. R.; Ryder, T.; Schuff, B. P.; Uccello, D. P.; Walker, G. S.; Wu, Y.; Brown, M. F.; Chen, J. M.; Hayward, M.

- M.; Noe, M. C.; Obach, R. S.; Philippe, L.; Shanmugasundaram, V.; Shapiro, M. J.; Starr, J.; Stroh, J.; Che, Y. Chemical and computational methods for the characterization of covalent reactive groups for the prospective design of irreversible inhibitors. *J. Med. Chem.* **2014**, *57*, 10072–10079.
- Gao, H. D.; Thanasekaran, P.; Chiang, C. W.; Hong, J. L.; Liu, Y. C.; Chang, Y. H.; Lee, H. M. Construction of a near-infrared-activatable enzyme platform to remotely trigger intracellular signal transduction using an upconversion nanoparticle, *ACS Nano* **2015**, *9*, 7, 7041–7051.
- Garske, A. L.; Peters, U.; Cortesi, A. T.; Perez, J. L.; Shokat, K. M. Chemical genetic strategy for targeting protein kinases based on covalent complementarity. *PNAS.* **2011**, *108*, 37, 15046–15052.
- Gehring, M.; Laufer, S. A. Emerging and re-emerging warheads for targeted covalent inhibitors: applications in medicinal chemistry and chemical biology. *J. Med. Chem.* **2019**, *62*, 5673–5724.
- Goeldner, M.; Givens, R. Dynamic Studies in Biology. WILEY-VCH Verlag GmbH & Co. KGaA, Weinheim: Federal Republic of Germany, **2005**.
- Gold, M. G. Swimming regulations for protein kinase A catalytic subunit. *Biochem. Soc. Trans.* **2019**, *47*, 5, 1355–1366.
- Gotoh, N.; Tojo, A.; Hino, M.; Yazaki, Y.; Shibuya, M. A Highly conserved tyrosine residue at codon 845 within the kinase domain is not required for the transforming activity of human epidermal growth factor receptor. *Biochem. Biophys. Res. Commun.* **1992**, *186*, 768–774.
- Gug, S.; Bolze, F.; Specht, A.; Bourgogne, C.; Goeldner, M.; Nicoud, J. F. Molecular engineering of photoremovable protecting groups for two-photon uncaging. *Angew. Chem. Int. Ed. Engl.* **2008**, *47*, 49, 9525–9529.
- Herberg, F. W.; Taylor, S. S. Physiological inhibitors of the catalytic subunit of cAMP-dependent protein kinase: effect of magnesium-ATP on protein-protein interactions. *Biochemistry* **1993**, *32*, 50, 14015–14022.
- Hofmann F. Apparent constants for the interaction of regulatory and catalytic subunit of cAMP-dependent protein kinase I and II. *J. Biol. Chem.* **1980**, *255*, 4, 1559–1564.
- Hossam, M.; Lasheen, D. S.; Abouzid, K. A. M. Covalent EGFR inhibitors: binding mechanisms, synthetic approaches, and clinical profile. *Arch. Pharm. Chem. Life Sci.* **2016**, *349*, 573–593.
- Isobe, K.; Jung, H. J.; Yang, C. R.; Claxton, J.; Sandoval, P.; Burg, M. B.; Raghuram, V.; Knepper, M. A. Systems-level identification of PKA-dependent signaling in epithelial cells. *PNAS.* **2017**, *114*, 42, E8875–E8884.
- Ivan, T.; Enkvist, E.; Viira, B.; Manoharan, G.; Raidaru, G.; Pflug, A.; Alam, K. A.; Zaccolo, M.; Engh, R. A.; Uri, A. *Bioconjugate Chem.* **2016**, *27*, 1900.
- Jackson, P. A.; Widen, J. C.; Harki, D. A.; Brummond, K. M.; Covalent modifiers: a chemical perspective on the reactivity of α,β -unsaturated carbonyls with thiols via hetero-michael addition reactions. *J. Med. Chem.* **2017**, *60*, 3, 839–885.
- Johnson, D.S.; Weerapana, E.; Cravatt, B.F. Strategies for discovering and derisking covalent, irreversible enzyme inhibitors. *Future Med. Chem.* **2010**, *2*, 6, 949–964.
- Kanev, G. K.; de Graaf, C.; de Esch, I.; Leurs, R.; Würdinger, T.; Westerman, B. A.; Kooistra, A. J. The Landscape of atypical and eukaryotic protein kinases. *Trends Pharmacol. Sci.* **2019**, *40*, 11, 818–832.
- Kaplan, J. H.; Forbush, B.; Hoffman, J. F. Rapid photolytic release of adenosine 5'-triphosphate from a protected analog: utilization by the sodium:potassium pump of human red blood cell ghosts. *Biochemistry.* **1978**, *17*, 10, 1929–1935.

- Klán, P.; Šolomek, T.; Bochet, C. G.; Blanc, A.; Givens, R.; Rubina, M.; Popik, V.; Kostikov, A.; Wirz, J. Photoremovable protecting groups in chemistry and biology: reaction mechanisms and efficacy. *Chem. Rev.* **2013**, *113*, 119–191.
- Klán, P.; Wirz, J. *Photochemistry of Organic Compounds*; Wiley: Great Britain, Chichester, Wiltshire, **2009**, p 8–10, 25–33, 39–40, 88, 236, 243, 265, 364–367.
- Knighton, D.R.; Zheng, J.H.; Ten Eyck, L.F.; Ashford, V.A.; Xuong, N.H.; Taylor, S.S.; Sowadski, J.M. Crystal structure of the catalytic subunit of cyclic adenosine monophosphate-dependent protein kinase. *Science* **1991**, *253*, 407–414.
- Koschinski, A.; Zaccolo, M. Activation of PKA in cell requires higher concentration of cAMP than in vitro: implications for compartmentalization of cAMP signalling. *Sci. Rep.* **2017**, *7*, 14090.
- Kou, J.; Dou, D.; Yang, L. Porphyrin photosensitizers in photodynamic therapy and its applications. *Oncotarget.* **2017**, *8*, 46, 81591–81603.
- Kriisa, M.; Sinijärvi, H.; Vaasa, A.; Enkvist, E.; Kostenko, S.; Moens, U.; Uri, A. Inhibition of CREB phosphorylation by conjugates of adenosine analogues and arginine-rich peptides, inhibitors of PKA catalytic subunit. *Chembiochem.* **2015**, *16*, 2, 312–319.
- Lakowicz, J. R.; Principles of fluorescence spectroscopy, third edition. Baltimore, Maryland, USA. **2006**. 1–18, 353–354.
- Lanning, B. R.; Whitby, L. R.; Dix, M. M.; Douhan, J.; Gilbert, A. M.; Hett, E. C.; Johnson, T. O.; Joslyn, C.; Kath, J. C.; Niessen, S.; Roberts, L. R.; Schnute, M. E.; Wang, C.; Hulce, J. J.; Wei, B.; Whiteley, L. O.; Hayward, M. M.; Cravatt, B. F. A road map to evaluate the proteome-wide selectivity of covalent kinase inhibitors. *Nat. Chem. Biol.* **2014**, *10*, 9, 760–767.
- Lavogina, D.; Enkvist, E.; Uri, A. Bisubstrate inhibitors of protein kinases: from principle to practical applications. *ChemMedChem.* **2010**, *5*, 1, 23–34.
- Lavogina, D.; Lust, M.; Viil, I.; König, N.; Raidaru, G.; Rogozina, J.; Enkvist, E.; Uri, A.; Bossemeyer, D. Structural analysis of ARC-type inhibitor (ARC-1034) binding to protein kinase A catalytic subunit and rational design of bisubstrate analogue inhibitors of basophilic protein kinases. *J. Med. Chem.* **2009**, *52*, 2, 308–21.
- Lee, S.; Kim, J.; Jo, J.; Chang, J. W.; Sim, J.; Yun, H. Recent advances in development of hetero-bivalent kinase inhibitors. *Eur. J. Med. Chem.* **2021**, *216*, 113318.
- Lerch, M. M.; Hansen, M. J.; van Dam, G. M.; Szymanski, W.; Feringa, B. L. Emerging targets in photopharmacology. *Angew. Chem. Int. Ed. Engl.* **2016**, *55*, 37, 10978–10999.
- Limbutara, K.; Kelleher, A.; Yang, C. R.; Raghuram, V.; Knepper, M. A. Phosphorylation changes in response to kinase inhibitor H89 in PKA-null cCells. *Sci. Rep.* **2019**, *9*, 1, 2814.
- Lindberg, P.; Nordberg, P.; Alminger, T.; Brändström, A.; Wallmark, B. The mechanism of action of the gastric acid secretion inhibitor omeprazole. *J. Med. Chem.* **1986**, *29*, 8, 1327–1329.
- Lipinski, C. A.; Lombardo, F.; Dominy, B. W.; Feeney, P. J. Experimental and computational approaches to estimate solubility and permeability in drug discovery and development settings. *Adv. Drug Deliv. Rev.* **2001**, *46*, 1–3, 3–26.
- Lissandron, V.; Terrin, A.; Collini, M.; D'alfonso, L.; Chirico, G.; Pantano, S.; Zaccolo, M. Improvement of a FRET-based indicator for cAMP by linker design and stabilization of donor-acceptor interaction. *J. Mol. Biol.* **2005**, *354*, 546.
- Liu, C.; Ke, P.; Zhang, J.; Zhang, X.; Chen, X. Protein kinase inhibitor peptide as a tool to specifically inhibit protein kinase A. *Front. Physiol.* **2020**, *11*, 574030.

- Mangubat-Medina, A. E.; Ball, Z. T. Triggering biological processes: methods and applications of photocaged peptides and proteins. *Chem. Soc. Rev.* **2021**, *50*, 10403–10421.
- Manning, G.; Whyte, D. B.; Martinez, R.; Hunter, T.; Sudarsanam, S. Protein Kinase Complement of the Human Genome. *Science.* **2002**, *298*, 5600, 1912–1934.
- Manschwetus, J. T.; Bendzunas, G. N.; Limaye, A. J.; Knape, M. J.; Herberg, F. W.; Kennedy, E. J. A stapled peptide mimic of the pseudosubstrate inhibitor PKI inhibits protein kinase A. *Molecules* **2019**, *24*, 1567.
- McClendon, C. L.; Kornev, A. P.; Gilson, M. K.; Taylor, S.S. Dynamic architecture of a protein kinase. *PNAS.* **2014**, *111*, 43, E4623–E4631. [published correction appears in *Proc. Natl. Acad. Sci. USA.* **2014**, *111*, 47, 16973.]
- McLeod, R.; Kumar, R.; Papadatos-Pastos, D.; Mateo, J.; Brown, J. S.; Garces, A.; Ruddle, R.; Decordova, S.; Jueliger, S.; Ferraldeschi, R.; Maiques, O.; Sanz-Moreno, V.; Jones, P.; Traub, S.; Halbert, G.; Mellor, S.; Swales, K. E.; Raynaud, F. I.; Garrett, M. D.; Banerji, U. First-in-human study of AT13148, a dual ROCK-AKT inhibitor in patients with solid tumors. *Clin Cancer Res.* **2020**, *26*, 18, 4777–4784.
- Meharena, H. S.; Chang, P.; Keshwani, M. M.; Oruganty, K.; Nene, A. K.; Kannan, N.; Taylor, S. S.; Kornev, A. P. Deciphering the structural basis of eukaryotic protein kinase regulation. *PLoS biology*, **2013**, *11*, 10.
- Miick, S. M.; Jalali, S.; Dwyer, B. P.; Havens, J.; Thomas, D.; Jimenez, M. A.; Simpson, M. T.; Zile, B.; Huss, K. L.; Campbell, R. M. Development of a microplate-based, electrophoretic fluorescent protein kinase A assay: comparison with filter-binding and fluorescence polarization assay formats. *J. Biomol. Screen.* **2005**, *10*, 4, 329–338.
- Miseta, A.; Csutora, P. Relationship between the occurrence of cysteine in proteins and the complexity of organisms. *Mol. Biol. Evol.* **2000**, *17*, 8, 1232–1239.
- Momotake, A.; Lindegger, N.; Niggli, E.; Barsotti, R. J.; Ellis-Davies, G. C. The nitro-dibenzofuran chromophore: a new caging group for ultra-efficient photolysis in living cells. *Nat. Methods.* **2006**, *3*, 1, 35–40.
- Murray, A. J. Pharmacological PKA inhibition: all may not be what it seems. *Sci. Signal.* **2008**, *1*, 22, re4.
- Nani, R. R.; Gorka, A. P.; Nagaya, T.; Kobayashi, H.; Schnermann, M. J. Near-IR light-mediated cleavage of antibody-drug conjugates using cyanine photocages. *Angew. Chem. Int. Ed. Engl.* **2015**, *54*, 46, 13635–13638.
- Nonga, O. E.; Lavogina, D.; Enkvist, E.; Kestav, K.; Chaikuad, A.; Dixon-Clarke, S. E.; Bullock, A. N.; Kopanchuk, S.; Ivan, T.; Ekambaram, R.; Viht, K.; Knapp, S.; Uri, A. Structure-guided design of bisubstrate inhibitors and photoluminescent probes for protein kinases of the PIM family. *Molecules* **2021**, *26*, 4353.
- Palma-Cerda, F.; Auger, C.; Crawford, D. J.; Hodgson, A. C.; Reynolds, S. J.; Cowell, J. K.; Swift, K. A.; Cais, O.; Vyklicky, L.; Corrie, J. E.; Ogden, D. New caged neurotransmitter analogs selective for glutamate receptor sub-types based on methoxynitroindoline and nitrophenylethoxycarbonyl caging groups. *Neuropharmacology.* **2012**, *63*, 4, 624–634.
- Patchornik, A.; Amit, B.; Woodward, R. B. Photosensitive protecting groups. *J. Am. Chem. Soc.* **1970**, *92*, 21, 6333–6335.
- Péczka, N.; Orgován, Z.; Ábrányi-Balogh, P.; Keserű, G. M. Electrophilic warheads in covalent drug discovery: an overview. *Expert Opin. Drug Discov.* **2022**, *17*, 4, 413–422.

- Perez, D. I.; Conde, S.; Pérez, C.; Gil, C.; Simon, D.; Wandosell, F.; Moreno, F. J.; Gelpí, J. L.; Luque, F. J.; Martínez, A. Thienylhalomethylketones: irreversible glycogen synthase kinase 3 inhibitors as useful pharmacological tools. *Bioorg. Med. Chem.* **2009**, *17*, 19, 6914–6925.
- Pettinger, J.; Jones, K.; Cheeseman, M. D. Lysine-targeting covalent inhibitors. *Angew. Chem. Int. Ed. Engl.* **2017**, *56*, 48, 15200–15209.
- Poelma, S. O.; Oh, S. S.; Helmy, S.; Knight, A. S.; Burnett, G. L.; Soh, H. T.; Hawker, C. J.; Read de Alaniz, J. Controlled drug release to cancer cells from modular one-photon visible light-responsive micellar system. *Chem. Commun. (Camb.)* **2016**, *52*, 69, 10525–10528.
- Rakauskaitė, R.; Urbanavičiūtė, G.; Simanavičius, M.; Lasickienė, R.; Vaitiekaitė, A.; Petraitytė, G.; Masevičius, V.; Žvirblienė, A.; Klimašauskas, S. Photocage-selective capture and light-controlled release of target proteins. *iScience* **2020**, *23*, 12, 101833.
- Ran, F.; Liu, Y.; Wang, C.; Xu, Z.; Zhang, Y.; Liu, Y.; Zhao, G.; Ling, Y. Review of the development of BTK inhibitors in overcoming the clinical limitations of ibrutinib. *Eur. J. Med. Chem.* **2022**, *229*, 114009.
- Rapp, T. L.; DeForest, C. A. Targeting drug delivery with light: a highly focused approach. *Adv. Drug Deliv. Rev.* **2021**, *171*, 94–107.
- Reed, J. L. Hard and soft acids and bases: atoms and atomic ions. *Inorg. Chem.* **2008**, *47*, 13, 5591–5600.
- Roskoski, R. Jr. A historical overview of protein kinases and their targeted small molecule inhibitors. *Pharmacological Research*, **2015**, *100*, 1–23.
- Roskoski, R. Jr. Classification of small molecule protein kinase inhibitors based upon the structures of their drug-enzyme complexes, *Pharmacol. Res.* **2016**, *103*, 26–48.
- Roskoski, R. Jr. Orally effective FDA-approved protein kinase targeted covalent inhibitors (TCIs). *Pharmacol Res.* **2021b**, *165*, 105422.
- Roskoski, R. Jr. Properties of FDA-approved small molecule protein kinase inhibitors: A 2022 update. *Pharmacol. Res.* **2022b**, *175*, 106037.
- Roskoski, R. Jr. Properties of FDA-approved small molecule protein kinase inhibitors: A 2021 update. *Pharmacological Research*. **2021a**, *165*, 105463.
- Roskoski, R. Jr., <http://www.brimr.org/PKI/PKIs.htm>, **2022a**. (accessed: 2022.08.31)
- Roth, B. L.; Sheffler, D. J.; Kroeze, W. K. Most Magic shotguns versus magic bullets: selectively non-selective drugs for mood disorders and schizophrenia. *Nat. Rev. Drug Discov.* **2004**, *3*, 353–359.
- Roth, G. J.; Stanford, N.; Majerus, P.W. Acetylation of prostaglandin synthase by aspirin. *Proc Natl Acad Sci. USA.* **1975**, *72*, 8, 3073–3076.
- Sardi, F.; Manta, B.; Portillo-Ledesma, S.; Knoop, B.; Comini, M. A.; Ferrer-Sueta, G. Determination of acidity and nucleophilicity in thiols by reaction with monobromobimane and fluorescence detection. *Anal. Biochem.* **2013**, *435*, 1, 74–82.
- Schwartz, P. A.; Kuzmic, P.; Solowiej, J.; Bergqvist, S.; Bolanos, B.; Almaden, C.; Nagata, A.; Ryan, K.; Feng, J.; Dalvie, D.; Kath, J. C.; Xu, M.; Wani, R.; Murray, B. W. Covalent EGFR inhibitor analysis reveals importance of reversible interactions to potency and mechanisms of drug resistance. *PNAS.* **2014**, *111*, 1, 173–178.
- Schwartz, P. A.; Murray, B. W. Protein kinase biochemistry and drug discovery. *Bioorg. Chem.* **2011**, *39*, 5–6, 192–210.
- Schwöbel, J. A.; Wondrousch, D.; Koleva, Y. K.; Madden, J. C.; Cronin, M. T.; Schüürmann, G. Prediction of michael-type acceptor reactivity toward glutathione. *Chem. Res. Toxicol.* **2010**, *23*, 10, 1576–1585.

- Shimokawa, T.; Smith, W. L. Prostaglandin endoperoxide synthase. The aspirin acetylation region. *J. Biol. Chem.* **1992**, 267, 17, 12387–12392.
- Shindo, N.; Fuchida, H.; Sato, M.; Watari, K.; Shibata, T.; Kuwata, K.; Miura, C.; Okamoto, K.; Hatsuyama, Y.; Tokunaga, K.; Sakamoto, S.; Morimoto, S.; Abe, Y.; Shiroishi, M.; Caaveiro, J. M. M.; Ueda, T.; Tamura, T.; Matsunaga, N.; Nakao, T.; Koyanagi, S.; Ohdo, S.; Yamaguchi, Y.; Hamachi, I.; Ono, M.; Ojida, A. Selective and reversible modification of kinase cysteines with chlorofluoroacetamides. *Nat. Chem. Biol.* **2019**, 15, 3, 250–258.
- Silva, J. M.; Silva, E.; Reis, R. L. Light-triggered release of photocaged therapeutics – where are we now? *J. Control Release.* **2019**, 298, 154–176.
- Sitkowska, K.; Hoes, M. F.; Lerch, M. M.; Lameijer, L. N.; van der Meer, P.; Szymański, W.; Feringa, B. L. Red-light-sensitive BODIPY photoprotecting groups for amines and their biological application in controlling heart rhythm. *Chem. Commun. (Camb.)* **2020**, 56, 41, 5480–5483.
- Skålhegg, B. S.; Huang, Y.; Su, T.; Idzerda, R. L.; McKnight, G. S.; Burton, K. A. Mutation of the Ca subunit of PKA leads to growth retardation and sperm dysfunction. *J. Mol. Endocrinol.*, **2002**, 16, 3, 630–639.
- Smith, F. D.; Esseltine, J. L.; Nygren, P. J.; Veessler, D.; Byrne, D. P.; Vonderach, M.; Strashnov, I.; Evers, C. E.; Evers, P. A.; Langeberg, L. K.; Scott, J. D. Local protein kinase A action proceeds through intact holoenzymes. *Science* **2017**, 356, 6344, 1288–1293.
- Søberg, K.; Skålhegg, B. S. The Molecular basis for specificity at the level of the protein Kinase a catalytic subunit. *Front. Endocrinol.* **2018**, 9, 538.
- Steichen, J. M.; Iyer, G. H.; Li, S.; Saldanha, S. A.; Deal, M. S.; Woods, V. L. Jr.; Taylor, S. S. Global consequences of activation loop phosphorylation on protein kinase A. *J. Biol. Chem.* **2010**, 285, 6, 3825–3832.
- Strelow, J. M. A perspective on the kinetics of covalent and irreversible inhibition. *SLAS Discov.* **2017**, 22, 1, 3–20.
- Sutanto, F.; Konstantinidou, M.; Dömling, A. Covalent inhibitors: a rational approach to drug discovery. *RSC Med. Chem.* **2020**, 11, 8, 876–884.
- Taskén, K.; Aandahl, E. M. Localized effects of cAMP mediated by distinct routes of protein kinase A. *Physiol Rev.* **2004**, 84, 137–167.
- Taylor, S. S.; Keshwani, M. M.; Steichen, J. M.; Kornev, A. P. Evolution of the eukaryotic protein kinases as dynamic molecular switches. *Phil. Trans. R. Soc. B.* **2012**, 367, 2517–2528.
- Taylor, S. S.; Yang, J.; Wu, J.; Haste, N. M.; Radzio-Andzelm, E.; Anand, G. PKA: a portrait of protein kinase dynamics. *Biochim Biophys Acta.* **2004**, 11, 1697, 259–269.
- Teo, S. L. Y.; Rennick, J. J.; Yuen, D.; Al-Wassiti, H.; Johnston, A.; Pouton, C. W. Unravelling cytosolic delivery of cell penetrating peptides with a quantitative endosomal escape assay. *Nat. Commun.* **2021**, 12, 1, 3721.
- Tumbrink, H. L.; Heimsoeth, A.; Sos, M. L. The next tier of EGFR resistance mutations in lung cancer. *Oncogene.* **2021**, 40, 1, 1–11.
- Turnbull, W. B. Divided We Fall? Studying low affinity fragments of ligands by ITC. School of Chemistry and Astbury Centre for Structural Molecular Biology – University of Leeds, Leeds, LS2 9JT, UK. **2005**
- Utrecht, J. Immune-mediated adverse drug reactions. *Chem. Res. Toxicol.* **2009**, 22, 24–34.

- Ung, P.M.; Rahman, R.; Schlessinger, A. Redefining the protein kinase conformational space with machine learning. *Cell Chem. Biol.* **2018**, *25*, 916–924.
- Vaasa, A.; Lust, M.; Terrin, A.; Uri, A.; Zaccolo, M. Small-molecule FRET probes for protein kinase activity monitoring in living cells. *Biochem. Biophys. Res. Commun.* **2010**, *397*, 750–755.
- Vaasa, A.; Viil, I.; Enkvist, E.; Viht, K.; Raidaru, G.; Lavogina, D.; Uri, A. High-affinity bisubstrate probe for fluorescence anisotropy binding/displacement assays with protein kinases PKA and ROCK. *Anal. Biochem.* **2009**, *385*, 1, 85–93.
- Velema, W. A.; van der Berg, J. P.; Hansen, M. J.; Szymanski, W.; Driessen, A. J.; Feringa, B. L. Optical control of antibacterial activity. *Nat. Chem.* **2013**, *5*, 11, 924–928.
- Vickerman, B. M.; Zywoot, E. M.; Tarrant, T. K.; Lawrence, D. S. Taking phototherapeutics from concept to clinical launch. *Nat. Rev. Chem.* **2021**, *5*, 11, 816–834.
- Viht, K.; Saaver, S.; Vahter, J.; Enkvist, E.; Lavogina, D.; Sinijärvi, H.; Raidaru, G.; Guerra, B.; Issinger, O. G.; Uri, A. Acetoxymethyl ester of tetrabromobenzimidazole-peptoid conjugate for inhibition of protein kinase CK2 in living cells. *Bioconjug. Chem.* **2015**, *26*, 12, 2324–2335.
- Viht, K.; Schweinsberg, S.; Lust, M.; Vaasa, A.; Raidaru, G.; Lavogina, D.; Uri, A.; Herberg, F. W. Surface-plasmon-resonance-based biosensor with immobilized bisubstrate analog inhibitor for the determination of affinities of ATP- and protein-competitive ligands of cAMP-dependent protein kinase. *Anal. Biochem.* **2007**, *362*, 2, 268–277.
- Walker-Gray, R.; Stengel, F.; Gold, M. G. Mechanisms for restraining cAMP-dependent protein kinase revealed by subunit quantitation and cross-linking approaches. *PNAS.* **2017**, *114*, 39, 10414–10419.
- Walsh, D. A.; Perkins, J. P.; Krebs, E. G. An adenosine 3',5'-monophosphate-dependant protein kinase from rabbit skeletal muscle. *J. Biol. Chem.* **1968**, *243*, 13, 3763–3765.
- Wang, Y.; Dai, Y.; Wu, X.; Li, F.; Liu, B.; Li, C.; Liu, Q.; Zhou, Y.; Wang, B.; Zhu, M.; Cui, R.; Tan, X.; Xiong, Z.; Liu, J.; Tan, M.; Xu, Y.; Geng, M.; Jiang, H.; Liu, H.; Ai, J.; Zheng, M. Discovery and development of a series of pyrazolo[3,4-d]pyridazinone compounds as the novel covalent fibroblast growth factor receptor inhibitors by the rational drug design. *J. Med. Chem.* **2019**, *62*, 7473–7488.
- Wang, Z. X. An exact mathematical expression for describing competitive binding of two different ligands to a protein molecule. *FEBS Lett.* **1995**, *360*, 111–114.
- Waxman, D. J.; Strominger, J. L. Penicillin-binding proteins and the mechanism of action of beta-lactam antibiotics. *Annu. Rev. Biochem.* **1983**, *52*, 825–869.
- Weisner, J.; Landel, I.; Reintjes, C.; Uhlenbrock, N.; Trajkovic-Arsic, M.; Dienstbier, N.; Hardick, J.; Ladigan, S.; Lindemann, M.; Smith, S.; Quambusch, L.; Scheinplflug, R.; Depta, L.; Gontla, R.; Unger, A.; Müller, H.; Baumann, M.; Schultz-Fademrecht, C.; Günther, G.; Maghnouj, A.; Müller, M. P.; Pohl, M.; Teschendorf, C.; Wolters, H.; Viebahn, R.; Tannapfel, A.; Uhl, W.; Hengstler, J. G.; Hahn, S. A.; Siveke, J. T.; Rauh, D. Preclinical efficacy of covalent-allosteric AKT inhibitor Borussertib in combination with Trametinib in KRAS-mutant pancreatic and colorectal cancer. *Cancer Res.* **2019**, *79*, 9, 2367–2378.
- Whitehouse, S.; Feramisco, J. R.; Casnellie, J. E.; Krebs, E. G.; Walsh, D. A. Studies on the kinetic mechanism of the catalytic subunit of the cAMP-dependent protein kinase. *J. Biol. Chem.* **1983**, *258*, 3693–3701.
- Wu, G.; Fang, Y. Z.; Yang, S.; Lupton, J. R.; Turner, N.D. Glutathione metabolism and its implications for health. *J. Nutr.* **2004**, *134*, 3, 489–492.

- Yi, J. J.; Wang, H.; Vilela, M.; Danuser, G.; Hahn, K. M. Manipulation of endogenous kinase activity in living cells using photoswitchable inhibitory peptides. *ACS Synth. Biol.* **2014**, *3*, 11, 788–795.
- Zaro, B. W.; Whitby, L. R.; Lum, K. M.; Cravatt, B. F. Metabolically labile fumarate esters impart kinetic selectivity to irreversible inhibitors. *J. Am. Chem. Soc.* **2016**, *138*, 49, 15841–15844.
- Zhai, X.; Ward, R. A.; Doig, P.; Argyrou, A. Insight into the therapeutic selectivity of the irreversible EGFR tyrosine kinase inhibitor osimertinib through enzyme kinetic studies. *Biochemistry.* **2020**, *59*, 14, 1428–1441.
- Zhang, J.; Gao, Z.; Ye, J. Phosphorylation and degradation of S6K1 (p70S6K1) in response to persistent JNK1 Activation. *Biochim. Biophys. Acta.* **2013**, 1832, 12, 1980–1988.
- Zhang, J.; Yang, P. L.; Gray, N. S. Targeting cancer with small molecule kinase inhibitors. *Nat. Rev. Cancer.* **2009**, *9*, 1, 28–39.
- Zhang, X.; Liu, F.; Chen, X.; Zhu, X.; Uetrecht, J. Involvement of the immune system in idiosyncratic drug reactions. *Drug Metab. Pharmacokinet.* **2011**, *26*, 47–59.
- Zhou, Z.; Song, J.; Nie, L.; Chen, X. Reactive oxygen species generating systems meeting challenges of photodynamic cancer therapy. *Chem. Soc. Rev.* **2016**, *45*, 23, 6597–6626.
- Zou, K.; Cheley, S.; Givens, R. S.; Bayley, H. Catalytic subunit of protein kinase A caged at the activating phosphothreonine, *J. Am. Chem. Soc.* **2002**, *124*, 8220–8229.
- Zuccotto, F.; Ardini, E.; Casale, E.; Angiolini, M. Through the “gatekeeper door”: exploiting the active kinase conformation. *J. Med. Chem.* **2010**, *53*, 7, 2681–2694.

8. SUMMARY IN ESTONIAN

Stiimulitundlike ja kovalentsete bisubstraatsete proteiinkinaasi inhibiitorite arendamine

Proteiinkinaasid on laialdaselt levinud ensüümid, mille ülesandeks katalüüsida valkude fosforüülimist. Proteiinkinaasid mõjutavad sel viisil arvukate mehhanismide kaudu pea kõiki raku funktsioone. Liigne või pikaajaline proteiinkinaasi aktiivsus põhjustab erinevaid haigusi, sealhulgas ka vähkkasvajaid. Viimaste kümnendite jooksul on uuritud proteiinkinaaside struktuure ja interaktsioone, mis on võimaldanud kasutusele võtta madalmolekulaarseid ühendeid proteiinkinaaside aktiivsuse reguleerimiseks. Nimelt on erinevad agentuurid viimase veerandsajandi jooksul ravimina kasutamiseks heaks kiitnud ligi sada proteiinkinaasi inhibiitorit. Enamik proteiinkinaasi inhibiitoreid, mis on ravimina tunnustatud, seonduvad proteiinkinaasi ATP-taskusse. Tartu Ülikoolis, Dr Asko Uri uurimisrühmas on välja töötatud bisubstraatsed ARC-inhibiitorid, mis seonduvad korrakahte proteiinkinaasi sidumispiirkonda ning saavutavad tänu sellele kõrgema seondumisvõime ning selektiivsuse. Käesolevas töös demonstreeriti, et optimeeritud struktuurimodifikatsioonidega oli ARC inhibiitoritele oli võimalik lisada täiendavaid omadusi. Nimelt konstrueeriti kõrge bioaktiivsusega inhibiitorid, mille bioaktiivsus ilmneb või kaob välise stiimuli rakendamisel (valgustamine, redutseeriv keskkond) ja inhibiitorid, mis seonduvad proteiinkinaasiga kovalentselt. Inhibiitorite struktuurid disainiti varasemalt mõõdetud valgus-inhibiitori kristallstruktuuride põhised.

- 1) Valgusega aktiveeritavad proteiinkinaasi inhibiitorid (ARC-2112 ja ARC-2113) seonduvad oma sihtmärkvalguga – cAMP-sõltuva proteiinkinaasi katalüütilise alaühikuga (PKA α) väga nõrgalt. Piisas üheminutilise kiiritamisest LED-valgustiga 400 nm juures, kui nende ühendite seondumisvõime oma sihtmärgiga suurenes viie suurusjärgu võrra. Nii suurt seondumistugevuse erinevust enne ja pärast valgustamist ei ole varem täheldatud. ARC-2113 dissotseeris valgustamise järgselt rakulüsaadis PKA holoensüümi.
- 2) Lagundatavate inhibiitorite struktuuri lisatud stiimulitundlik rühm ei alandanud oluliselt nende seondumisvõimet sihtmärkvalguga (PKA α). Valgustundliku inhibiitori, ARC-2121 kaheminutilise kiiritamisega LED-valgustitega 365 nm juures vähenes ühendi seondumisvõime oma sihtmärkvalgu suhtes 30 korda. Redutseerija-tundliku inhibiitori, ARC-2194 seondumisvõime vähenes redutseerija lisamisel lausa 4,5 suurusjärku.
- 3) Elektrofiiliga varustatud kovalentselt seonduvad inhibiitorid (nt ARC-2158) suutsid reageerida PKA α aktivatsiooniasas asuva tsüsteiinijäägiga (Cys199). Kuna Cys199 asub aktivatsiooniasas, siis ei ole sellega reageerimine nõrga elektrofiiliga varustatud väikeste ATP-taskusse seonduvate inhibiitorite jaoks võimalik. Muidu ei ole PKAc-I ATP-tasku piirkonnas ühtegi tsüsteiinijääki, nagu ka paljudel teistel proteiinkinaasidel, mistõttu on nende jaoks kovalentsete inhibiitorite väljatöötamine raskendatud. Kovalentsete inhibiitorite seondumisvõime ja reaktsiooni kiirus sihtmärkvalguga sõltus

tugevalt struktuuris olevate arginiinide arvust. Kovalentne inhibiitor ARC-2154 reageeris rakulüsaadis selektiivselt oma sihtmärkvalguga PKA α ning kovalentne inhibiitor ARC-2168 reageeris sihtmärkvalguga ka elusrakkudes, kuigi mitte nii selektiivselt.

Selles töös demonstreeriti esmakordselt kovalentsete inhibiitorite ja stiimulitundlike inhibiitorite põhimõtete rakendamist bisubstraatsete inhibiitorite korral. Töö illustreerib bisubstraatsete inhibiitorite modifitseerimise paindlikkust uute omaduste lisamiseks.

ACKNOWLEDGEMENTS

I would like to thank all my colleagues from the 3-rd and 4-th floor, especially Kaido Viht, Darja Lavõgina, Erki Enkvist, Katrin Kestav, Anu Teearu, Eva Lea Jääger, and Asko Uri. Thank you for your support, hard work, and for showing me what true scientists look like. Kaido should be specifically highlighted for being an excellent supervisor and a dear friend. I would also like to thank my friends and family, especially my grandparents, Gerda and Alo, for lighting a spark for science in me; my parents and three siblings, and of course Merit and Harlet for your never-ending love and support.

This research was supported by the Estonian Research Council (IUT20-17, PRG454, and PRG1198), the EU (TRANSCAN2-JTC2016; project PROSCANE-XO), and ASTRA project PER ASPERA Graduate School of Functional Materials and Technologies receiving funding from the European Regional Development Fund under project in University of Tartu, Estonia. I would like to thank The University of Tartu Foundation, and the Estonian Students Fund in USA for scholarships.

PUBLICATIONS

CURRICULUM VITAE

Name: Tanel Sõrmus
Date of birth: October 11, 1992
Citizenship: Estonian
Address: University of Tartu, Institute of Chemistry
Ravila 14a, 50411, Tartu, Estonia
Phone: +372 554 7335
E-mail: tanel.sormus@ut.ee

Education:

2018–... University of Tartu, PhD student in chemistry
2016–2018 University of Tartu, MSc in chemistry, *cum laude*
2012–2015 University of Tartu, BSc in chemistry
2000–2012 Miina Härma Gymnasium

Professional employment:

2022.09.01–... University of Tartu, Institute of Chemistry; Chemist
2017.07–08 Cambrex Tallinn; Chemist Trainee

Professional self-improvement:

2021.08.16–2021.11.14 Research stay in Tromsø, at the Norwegian Structural Biology Center (3 months)
2019.06.09–2021.06.15 FEBS Advanced course in Holland, Amsterdam: Functional imaging of nuclear organisation & signaling

Professional acknowledgement:

2018 National competition of student research projects, II prize within Master degree student's group

List of publications:

1. **Sõrmus, T.**; Lavogina, D.; Enkvist, E.; Uri, A.; Viht, K. Efficient photocaging of a tight-binding bisubstrate inhibitor of cAMP-dependent protein kinase. *Chem. Commun.* **2019**, 55, 11147–11150.
2. **Sõrmus, T.**; Lavogina, D.; Teearu, A.; Enkvist, E.; Uri, A.; Viht, K. Construction of covalent bisubstrate inhibitor of protein kinase reacting with cysteine residue at substrate-binding site. *J. Med. Chem.* **2022**, 65, 16, 10975–10991.
3. Lavogina, D.; Nasirova, N.; **Sõrmus, T.**; Tähtjärv, T.; Enkvist, E.; Viht, K.; Haljasorg, T.; Herodes, K.; Jaal, J.; Uri, A. Conjugates of adenosine mimetics and arginine-rich peptides serve as inhibitors and fluorescent probes but not as long-lifetime photoluminescent probes for protein arginine methyltransferases. *J. Pept. Sci.* **2022**, e3456.
4. **Sõrmus, T.**; Lavogina, D.; Enkvist, E.; Uri, A.; Viht, K. Deactivatable bisubstrate inhibitors of protein kinases. *Molecules* **2022**, 27, 6689.

ELULOOKIRJELDUS

Nimi: Tanel Sõrmus
Sünniaeg: 11 oktoober 1992
Kodakondsus: Eesti
Aadress: Tartu Ülikool, Keemia Instituut
Ravila 14a, 50411, Tartu, Eesti
Telefon: +372 554 7335
E-mail: tanel.sormus@ut.ee

Haridus:
2018–... Tartu Ülikool, Keemia Instituut, doktorantuur
2016–2018 Tartu Ülikool, Keemia Instituut, magistrantuur (*cum laude*)
2012–2015 Tartu Ülikool, Keemia Instituut, bakalaureus
2000–2012 Miina Härma Gümnaasium

Teenistuskäik:
2022.09.01–... Tartu Ülikool, Keemia Instituut, keemik
2017.07–08 Cambrex Tallinn, praktikant

Erialane enesetäiendus:
2021.08.16–2021.11.14 Õpiränne Tromsø, Norra; Norwegian Structural
Biology Center (kolm kuud)
2019.06.09–2021.06.15 FEBS kursus Amsterdamis, Hollandis:
Functional imaging of nuclear organisation &
signaling

Erialane tunnustus:
2018 Üliõpilaste teadustööde riiklik konkurss, II preemia magistriõppe
üliõpilaste astmes, Eesti Teaduste Akadeemia

Teaduspublikatsioonid:

1. **Sõrmus, T.**; Lavogina, D.; Enkvist, E.; Uri, A.; Viht, K. Efficient photocaging of a tight-binding bisubstrate inhibitor of cAMP-dependent protein kinase. *Chem. Commun.* **2019**, 55, 11147–11150.
2. **Sõrmus, T.**; Lavogina, D.; Teearu, A.; Enkvist, E.; Uri, A.; Viht, K. Construction of covalent bisubstrate inhibitor of protein kinase reacting with cysteine residue at substrate-binding site. *J. Med. Chem.* **2022**, 65, 16, 10975–10991.
3. Lavogina, D.; Nasirova, N.; **Sõrmus, T.**; Tähtjärv, T.; Enkvist, E.; Viht, K.; Haljasorg, T.; Herodes, K.; Jaal, J.; Uri, A. Conjugates of adenosine mimetics and arginine-rich peptides serve as inhibitors and fluorescent probes but not as long-lifetime photoluminescent probes for protein arginine methyltransferases. *J. Pept. Sci.* **2022**, e3456.
4. **Sõrmus, T.**; Lavogina, D.; Enkvist, E.; Uri, A.; Viht, K. Deactivatable bisubstrate inhibitors of protein kinases. *Molecules* **2022**, 27, 6689.

DISSERTATIONES CHIMICAE UNIVERSITATIS TARTUENSIS

1. **Toomas Tamm.** Quantum-chemical simulation of solvent effects. Tartu, 1993, 110 p.
2. **Peeter Burk.** Theoretical study of gas-phase acid-base equilibria. Tartu, 1994, 96 p.
3. **Victor Lobanov.** Quantitative structure-property relationships in large descriptor spaces. Tartu, 1995, 135 p.
4. **Vahur Mäemets.** The ^{17}O and ^1H nuclear magnetic resonance study of H_2O in individual solvents and its charged clusters in aqueous solutions of electrolytes. Tartu, 1997, 140 p.
5. **Andrus Metsala.** Microcanonical rate constant in nonequilibrium distribution of vibrational energy and in restricted intramolecular vibrational energy redistribution on the basis of Slater's theory of unimolecular reactions. Tartu, 1997, 150 p.
6. **Uko Maran.** Quantum-mechanical study of potential energy surfaces in different environments. Tartu, 1997, 137 p.
7. **Alar Jänes.** Adsorption of organic compounds on antimony, bismuth and cadmium electrodes. Tartu, 1998, 219 p.
8. **Kaido Tammeveski.** Oxygen electroreduction on thin platinum films and the electrochemical detection of superoxide anion. Tartu, 1998, 139 p.
9. **Ivo Leito.** Studies of Brønsted acid-base equilibria in water and non-aqueous media. Tartu, 1998, 101 p.
10. **Jaan Leis.** Conformational dynamics and equilibria in amides. Tartu, 1998, 131 p.
11. **Toonika Rinke.** The modelling of amperometric biosensors based on oxidoreductases. Tartu, 2000, 108 p.
12. **Dmitri Panov.** Partially solvated Grignard reagents. Tartu, 2000, 64 p.
13. **Kaja Orupõld.** Treatment and analysis of phenolic wastewater with microorganisms. Tartu, 2000, 123 p.
14. **Jüri Ivask.** Ion Chromatographic determination of major anions and cations in polar ice core. Tartu, 2000, 85 p.
15. **Lauri Vares.** Stereoselective Synthesis of Tetrahydrofuran and Tetrahydropyran Derivatives by Use of Asymmetric Horner-Wadsworth-Emmons and Ring Closure Reactions. Tartu, 2000, 184 p.
16. **Martin Lepiku.** Kinetic aspects of dopamine D_2 receptor interactions with specific ligands. Tartu, 2000, 81 p.
17. **Katrin Sak.** Some aspects of ligand specificity of P2Y receptors. Tartu, 2000, 106 p.
18. **Vello Pällin.** The role of solvation in the formation of iotsitch complexes. Tartu, 2001, 95 p.
19. **Katrin Kollist.** Interactions between polycyclic aromatic compounds and humic substances. Tartu, 2001, 93 p.

20. **Ivar Koppel.** Quantum chemical study of acidity of strong and superstrong Brønsted acids. Tartu, 2001, 104 p.
21. **Viljar Pihl.** The study of the substituent and solvent effects on the acidity of OH and CH acids. Tartu, 2001, 132 p.
22. **Natalia Palm.** Specification of the minimum, sufficient and significant set of descriptors for general description of solvent effects. Tartu, 2001, 134 p.
23. **Sulev Sild.** QSPR/QSAR approaches for complex molecular systems. Tartu, 2001, 134 p.
24. **Ruslan Petrukhin.** Industrial applications of the quantitative structure-property relationships. Tartu, 2001, 162 p.
25. **Boris V. Rogovoy.** Synthesis of (benzotriazolyl)carboximidamides and their application in relations with *N*- and *S*-nucleophiles. Tartu, 2002, 84 p.
26. **Koit Herodes.** Solvent effects on UV-vis absorption spectra of some solvatochromic substances in binary solvent mixtures: the preferential solvation model. Tartu, 2002, 102 p.
27. **Anti Perkson.** Synthesis and characterisation of nanostructured carbon. Tartu, 2002, 152 p.
28. **Ivari Kaljurand.** Self-consistent acidity scales of neutral and cationic Brønsted acids in acetonitrile and tetrahydrofuran. Tartu, 2003, 108 p.
29. **Karmen Lust.** Adsorption of anions on bismuth single crystal electrodes. Tartu, 2003, 128 p.
30. **Mare Piirsalu.** Substituent, temperature and solvent effects on the alkaline hydrolysis of substituted phenyl and alkyl esters of benzoic acid. Tartu, 2003, 156 p.
31. **Meeri Sassian.** Reactions of partially solvated Grignard reagents. Tartu, 2003, 78 p.
32. **Tarmo Tamm.** Quantum chemical modelling of polypyrrole. Tartu, 2003. 100 p.
33. **Erik Teinmaa.** The environmental fate of the particulate matter and organic pollutants from an oil shale power plant. Tartu, 2003. 102 p.
34. **Jaana Tammiku-Taul.** Quantum chemical study of the properties of Grignard reagents. Tartu, 2003. 120 p.
35. **Andre Lomaka.** Biomedical applications of predictive computational chemistry. Tartu, 2003. 132 p.
36. **Kostyantyn Kirichenko.** Benzotriazole – Mediated Carbon–Carbon Bond Formation. Tartu, 2003. 132 p.
37. **Gunnar Nurk.** Adsorption kinetics of some organic compounds on bismuth single crystal electrodes. Tartu, 2003, 170 p.
38. **Mati Arulepp.** Electrochemical characteristics of porous carbon materials and electrical double layer capacitors. Tartu, 2003, 196 p.
39. **Dan Cornel Fara.** QSPR modeling of complexation and distribution of organic compounds. Tartu, 2004, 126 p.
40. **Riina Mahlapuu.** Signalling of galanin and amyloid precursor protein through adenylate cyclase. Tartu, 2004, 124 p.

41. **Mihkel Kerikmäe.** Some luminescent materials for dosimetric applications and physical research. Tartu, 2004, 143 p.
42. **Jaanus Kruusma.** Determination of some important trace metal ions in human blood. Tartu, 2004, 115 p.
43. **Urmas Johanson.** Investigations of the electrochemical properties of polypyrrole modified electrodes. Tartu, 2004, 91 p.
44. **Kaido Sillar.** Computational study of the acid sites in zeolite ZSM-5. Tartu, 2004, 80 p.
45. **Aldo Oras.** Kinetic aspects of dATP α S interaction with P2Y₁ receptor. Tartu, 2004, 75 p.
46. **Erik Mölder.** Measurement of the oxygen mass transfer through the air-water interface. Tartu, 2005, 73 p.
47. **Thomas Thomborg.** The kinetics of electroreduction of peroxodisulfate anion on cadmium (0001) single crystal electrode. Tartu, 2005, 95 p.
48. **Olavi Loog.** Aspects of condensations of carbonyl compounds and their imine analogues. Tartu, 2005, 83 p.
49. **Siim Salmar.** Effect of ultrasound on ester hydrolysis in aqueous ethanol. Tartu, 2006, 73 p.
50. **Ain Uustare.** Modulation of signal transduction of heptahelical receptors by other receptors and G proteins. Tartu, 2006, 121 p.
51. **Sergei Yurchenko.** Determination of some carcinogenic contaminants in food. Tartu, 2006, 143 p.
52. **Kaido Tämm.** QSPR modeling of some properties of organic compounds. Tartu, 2006, 67 p.
53. **Olga Tšubrik.** New methods in the synthesis of multisubstituted hydrazines. Tartu, 2006, 183 p.
54. **Lilli Sooväli.** Spectrophotometric measurements and their uncertainty in chemical analysis and dissociation constant measurements. Tartu, 2006, 125 p.
55. **Eve Koort.** Uncertainty estimation of potentiometrically measured pH and pK_a values. Tartu, 2006, 139 p.
56. **Sergei Kopanchuk.** Regulation of ligand binding to melanocortin receptor subtypes. Tartu, 2006, 119 p.
57. **Silvar Kallip.** Surface structure of some bismuth and antimony single crystal electrodes. Tartu, 2006, 107 p.
58. **Kristjan Saal.** Surface silanization and its application in biomolecule coupling. Tartu, 2006, 77 p.
59. **Tanel Tätte.** High viscosity Sn(OBu)₄ oligomeric concentrates and their applications in technology. Tartu, 2006, 91 p.
60. **Dimitar Atanasov Dobchev.** Robust QSAR methods for the prediction of properties from molecular structure. Tartu, 2006, 118 p.
61. **Hannes Hagu.** Impact of ultrasound on hydrophobic interactions in solutions. Tartu, 2007, 81 p.
62. **Rutha Jäger.** Electroreduction of peroxodisulfate anion on bismuth electrodes. Tartu, 2007, 142 p.

63. **Kaido Viht.** Immobilizable bisubstrate-analogue inhibitors of basophilic protein kinases: development and application in biosensors. Tartu, 2007, 88 p.
64. **Eva-Ingrid Rõõm.** Acid-base equilibria in nonpolar media. Tartu, 2007, 156 p.
65. **Sven Tamp.** DFT study of the cesium cation containing complexes relevant to the cesium cation binding by the humic acids. Tartu, 2007, 102 p.
66. **Jaak Nerut.** Electroreduction of hexacyanoferrate(III) anion on Cadmium (0001) single crystal electrode. Tartu, 2007, 180 p.
67. **Lauri Jalukse.** Measurement uncertainty estimation in amperometric dissolved oxygen concentration measurement. Tartu, 2007, 112 p.
68. **Aime Lust.** Charge state of dopants and ordered clusters formation in CaF₂:Mn and CaF₂:Eu luminophors. Tartu, 2007, 100 p.
69. **Iiris Kahn.** Quantitative Structure-Activity Relationships of environmentally relevant properties. Tartu, 2007, 98 p.
70. **Mari Reinik.** Nitrates, nitrites, N-nitrosamines and polycyclic aromatic hydrocarbons in food: analytical methods, occurrence and dietary intake. Tartu, 2007, 172 p.
71. **Heili Kasuk.** Thermodynamic parameters and adsorption kinetics of organic compounds forming the compact adsorption layer at Bi single crystal electrodes. Tartu, 2007, 212 p.
72. **Erki Enkvist.** Synthesis of adenosine-peptide conjugates for biological applications. Tartu, 2007, 114 p.
73. **Svetoslav Hristov Slavov.** Biomedical applications of the QSAR approach. Tartu, 2007, 146 p.
74. **Eneli Härk.** Electroreduction of complex cations on electrochemically polished Bi(*hkl*) single crystal electrodes. Tartu, 2008, 158 p.
75. **Priit Möller.** Electrochemical characteristics of some cathodes for medium temperature solid oxide fuel cells, synthesized by solid state reaction technique. Tartu, 2008, 90 p.
76. **Signe Viggor.** Impact of biochemical parameters of genetically different pseudomonads at the degradation of phenolic compounds. Tartu, 2008, 122 p.
77. **Ave Sarapuu.** Electrochemical reduction of oxygen on quinone-modified carbon electrodes and on thin films of platinum and gold. Tartu, 2008, 134 p.
78. **Agnes Kütt.** Studies of acid-base equilibria in non-aqueous media. Tartu, 2008, 198 p.
79. **Rouvim Kadis.** Evaluation of measurement uncertainty in analytical chemistry: related concepts and some points of misinterpretation. Tartu, 2008, 118 p.
80. **Valter Reedo.** Elaboration of IVB group metal oxide structures and their possible applications. Tartu, 2008, 98 p.
81. **Aleksei Kuznetsov.** Allosteric effects in reactions catalyzed by the cAMP-dependent protein kinase catalytic subunit. Tartu, 2009, 133 p.

82. **Aleksei Bredihhin.** Use of mono- and polyanions in the synthesis of multisubstituted hydrazine derivatives. Tartu, 2009, 105 p.
83. **Anu Ploom.** Quantitative structure-reactivity analysis in organosilicon chemistry. Tartu, 2009, 99 p.
84. **Argo Vonk.** Determination of adenosine A_{2A}- and dopamine D₁ receptor-specific modulation of adenylate cyclase activity in rat striatum. Tartu, 2009, 129 p.
85. **Indrek Kivi.** Synthesis and electrochemical characterization of porous cathode materials for intermediate temperature solid oxide fuel cells. Tartu, 2009, 177 p.
86. **Jaanus Eskusson.** Synthesis and characterisation of diamond-like carbon thin films prepared by pulsed laser deposition method. Tartu, 2009, 117 p.
87. **Marko Lätt.** Carbide derived microporous carbon and electrical double layer capacitors. Tartu, 2009, 107 p.
88. **Vladimir Stepanov.** Slow conformational changes in dopamine transporter interaction with its ligands. Tartu, 2009, 103 p.
89. **Aleksander Trummal.** Computational Study of Structural and Solvent Effects on Acidities of Some Brønsted Acids. Tartu, 2009, 103 p.
90. **Eerold Vellemäe.** Applications of mischmetal in organic synthesis. Tartu, 2009, 93 p.
91. **Sven Parkel.** Ligand binding to 5-HT_{1A} receptors and its regulation by Mg²⁺ and Mn²⁺. Tartu, 2010, 99 p.
92. **Signe Vahur.** Expanding the possibilities of ATR-FT-IR spectroscopy in determination of inorganic pigments. Tartu, 2010, 184 p.
93. **Tavo Romann.** Preparation and surface modification of bismuth thin film, porous, and microelectrodes. Tartu, 2010, 155 p.
94. **Nadežda Aleksejeva.** Electrocatalytic reduction of oxygen on carbon nanotube-based nanocomposite materials. Tartu, 2010, 147 p.
95. **Marko Kullapere.** Electrochemical properties of glassy carbon, nickel and gold electrodes modified with aryl groups. Tartu, 2010, 233 p.
96. **Liis Siinor.** Adsorption kinetics of ions at Bi single crystal planes from aqueous electrolyte solutions and room-temperature ionic liquids. Tartu, 2010, 101 p.
97. **Angela Vaasa.** Development of fluorescence-based kinetic and binding assays for characterization of protein kinases and their inhibitors. Tartu 2010, 101 p.
98. **Indrek Tulp.** Multivariate analysis of chemical and biological properties. Tartu 2010, 105 p.
99. **Aare Selberg.** Evaluation of environmental quality in Northern Estonia by the analysis of leachate. Tartu 2010, 117 p.
100. **Darja Lavõgina.** Development of protein kinase inhibitors based on adenosine analogue-oligoarginine conjugates. Tartu 2010, 248 p.
101. **Laura Herm.** Biochemistry of dopamine D₂ receptors and its association with motivated behaviour. Tartu 2010, 156 p.

102. **Terje Raudsepp.** Influence of dopant anions on the electrochemical properties of polypyrrole films. Tartu 2010, 112 p.
103. **Margus Marandi.** Electroformation of Polypyrrole Films: *In-situ* AFM and STM Study. Tartu 2011, 116 p.
104. **Kairi Kivirand.** Diamine oxidase-based biosensors: construction and working principles. Tartu, 2011, 140 p.
105. **Anneli Kruve.** Matrix effects in liquid-chromatography electrospray mass-spectrometry. Tartu, 2011, 156 p.
106. **Gary Urb.** Assessment of environmental impact of oil shale fly ash from PF and CFB combustion. Tartu, 2011, 108 p.
107. **Nikita Oskolkov.** A novel strategy for peptide-mediated cellular delivery and induction of endosomal escape. Tartu, 2011, 106 p.
108. **Dana Martin.** The QSPR/QSAR approach for the prediction of properties of fullerene derivatives. Tartu, 2011, 98 p.
109. **Säde Viirlaid.** Novel glutathione analogues and their antioxidant activity. Tartu, 2011, 106 p.
110. **Ülis Sõukand.** Simultaneous adsorption of Cd²⁺, Ni²⁺, and Pb²⁺ on peat. Tartu, 2011, 124 p.
111. **Lauri Lipping.** The acidity of strong and superstrong Brønsted acids, an outreach for the “limits of growth”: a quantum chemical study. Tartu, 2011, 124 p.
112. **Heisi Kurig.** Electrical double-layer capacitors based on ionic liquids as electrolytes. Tartu, 2011, 146 p.
113. **Marje Kasari.** Bisubstrate luminescent probes, optical sensors and affinity adsorbents for measurement of active protein kinases in biological samples. Tartu, 2012, 126 p.
114. **Kalev Takkis.** Virtual screening of chemical databases for bioactive molecules. Tartu, 2012, 122 p.
115. **Ksenija Kisseljova.** Synthesis of aza-β³-amino acid containing peptides and kinetic study of their phosphorylation by protein kinase A. Tartu, 2012, 104 p.
116. **Riin Rebane.** Advanced method development strategy for derivatization LC/ESI/MS. Tartu, 2012, 184 p.
117. **Vladislav Ivaništšev.** Double layer structure and adsorption kinetics of ions at metal electrodes in room temperature ionic liquids. Tartu, 2012, 128 p.
118. **Irja Helm.** High accuracy gravimetric Winkler method for determination of dissolved oxygen. Tartu, 2012, 139 p.
119. **Karin Kipper.** Fluoroalcohols as Components of LC-ESI-MS Eluents: Usage and Applications. Tartu, 2012, 164 p.
120. **Arno Ratas.** Energy storage and transfer in dosimetric luminescent materials. Tartu, 2012, 163 p.
121. **Reet Reinart-Okugbeni.** Assay systems for characterisation of subtype-selective binding and functional activity of ligands on dopamine receptors. Tartu, 2012, 159 p.

122. **Lauri Sikk.** Computational study of the Sonogashira cross-coupling reaction. Tartu, 2012, 81 p.
123. **Karita Raudkivi.** Neurochemical studies on inter-individual differences in affect-related behaviour of the laboratory rat. Tartu, 2012, 161 p.
124. **Indrek Saar.** Design of GalR2 subtype specific ligands: their role in depression-like behavior and feeding regulation. Tartu, 2013, 126 p.
125. **Ann Laheäär.** Electrochemical characterization of alkali metal salt based non-aqueous electrolytes for supercapacitors. Tartu, 2013, 127 p.
126. **Kerli Tõnurist.** Influence of electrospun separator materials properties on electrochemical performance of electrical double-layer capacitors. Tartu, 2013, 147 p.
127. **Kaija Põhako-Esko.** Novel organic and inorganic ionogels: preparation and characterization. Tartu, 2013, 124 p.
128. **Ivar Kruusenberg.** Electroreduction of oxygen on carbon nanomaterial-based catalysts. Tartu, 2013, 191 p.
129. **Sander Piiskop.** Kinetic effects of ultrasound in aqueous acetonitrile solutions. Tartu, 2013, 95 p.
130. **Ilona Faustova.** Regulatory role of L-type pyruvate kinase N-terminal domain. Tartu, 2013, 109 p.
131. **Kadi Tamm.** Synthesis and characterization of the micro-mesoporous anode materials and testing of the medium temperature solid oxide fuel cell single cells. Tartu, 2013, 138 p.
132. **Iva Bozhidarova Stoyanova-Slavova.** Validation of QSAR/QSPR for regulatory purposes. Tartu, 2013, 109 p.
133. **Vitali Grozovski.** Adsorption of organic molecules at single crystal electrodes studied by *in situ* STM method. Tartu, 2014, 146 p.
134. **Santa Veikšina.** Development of assay systems for characterisation of ligand binding properties to melanocortin 4 receptors. Tartu, 2014, 151 p.
135. **Jüri Liiv.** PVDF (polyvinylidene difluoride) as material for active element of twisting-ball displays. Tartu, 2014, 111 p.
136. **Kersti Vaarmets.** Electrochemical and physical characterization of pristine and activated molybdenum carbide-derived carbon electrodes for the oxygen electroreduction reaction. Tartu, 2014, 131 p.
137. **Lauri Tõntson.** Regulation of G-protein subtypes by receptors, guanine nucleotides and Mn²⁺. Tartu, 2014, 105 p.
138. **Aiko Adamson.** Properties of amine-boranes and phosphorus analogues in the gas phase. Tartu, 2014, 78 p.
139. **Elo Kibena.** Electrochemical grafting of glassy carbon, gold, highly oriented pyrolytic graphite and chemical vapour deposition-grown graphene electrodes by diazonium reduction method. Tartu, 2014, 184 p.
140. **Teemu Näykki.** Novel Tools for Water Quality Monitoring – From Field to Laboratory. Tartu, 2014, 202 p.
141. **Karl Kaupmees.** Acidity and basicity in non-aqueous media: importance of solvent properties and purity. Tartu, 2014, 128 p.

142. **Oleg Lebedev.** Hydrazine polyanions: different strategies in the synthesis of heterocycles. Tartu, 2015, 118 p.
143. **Geven Piir.** Environmental risk assessment of chemicals using QSAR methods. Tartu, 2015, 123 p.
144. **Olga Mazina.** Development and application of the biosensor assay for measurements of cyclic adenosine monophosphate in studies of G protein-coupled receptor signaling. Tartu, 2015, 116 p.
145. **Sandip Ashokrao Kadam.** Anion receptors: synthesis and accurate binding measurements. Tartu, 2015, 116 p.
146. **Indrek Tallo.** Synthesis and characterization of new micro-mesoporous carbide derived carbon materials for high energy and power density electrical double layer capacitors. Tartu, 2015, 148 p.
147. **Heiki Erikson.** Electrochemical reduction of oxygen on nanostructured palladium and gold catalysts. Tartu, 2015, 204 p.
148. **Erik Anderson.** *In situ* Scanning Tunnelling Microscopy studies of the interfacial structure between Bi(111) electrode and a room temperature ionic liquid. Tartu, 2015, 118 p.
149. **Girinath G. Pillai.** Computational Modelling of Diverse Chemical, Biochemical and Biomedical Properties. Tartu, 2015, 140 p.
150. **Piret Pikma.** Interfacial structure and adsorption of organic compounds at Cd(0001) and Sb(111) electrodes from ionic liquid and aqueous electrolytes: an *in situ* STM study. Tartu, 2015, 126 p.
151. **Ganesh babu Manoharan.** Combining chemical and genetic approaches for photoluminescence assays of protein kinases. Tartu, 2016, 126 p.
152. **Carolin Siimenson.** Electrochemical characterization of halide ion adsorption from liquid mixtures at Bi(111) and pyrolytic graphite electrode surface. Tartu, 2016, 110 p.
153. **Asko Laaniste.** Comparison and optimisation of novel mass spectrometry ionisation sources. Tartu, 2016, 156 p.
154. **Hanno Evard.** Estimating limit of detection for mass spectrometric analysis methods. Tartu, 2016, 224 p.
155. **Kadri Ligi.** Characterization and application of protein kinase-responsive organic probes with triplet-singlet energy transfer. Tartu, 2016, 122 p.
156. **Margarita Kagan.** Biosensing penicillins' residues in milk flows. Tartu, 2016, 130 p.
157. **Marie Kriisa.** Development of protein kinase-responsive photoluminescent probes and cellular regulators of protein phosphorylation. Tartu, 2016, 106 p.
158. **Mihkel Vestli.** Ultrasonic spray pyrolysis deposited electrolyte layers for intermediate temperature solid oxide fuel cells. Tartu, 2016, 156 p.
159. **Silver Sepp.** Influence of porosity of the carbide-derived carbon on the properties of the composite electrocatalysts and characteristics of polymer electrolyte fuel cells. Tartu, 2016, 137 p.
160. **Kristjan Haav.** Quantitative relative equilibrium constant measurements in supramolecular chemistry. Tartu, 2017, 158 p.

161. **Anu Teearu.** Development of MALDI-FT-ICR-MS methodology for the analysis of resinous materials. Tartu, 2017, 205 p.
162. **Taavi Ivan.** Bifunctional inhibitors and photoluminescent probes for studies on protein complexes. Tartu, 2017, 140 p.
163. **Maarja-Liisa Oldekop.** Characterization of amino acid derivatization reagents for LC-MS analysis. Tartu, 2017, 147 p.
164. **Kristel Jukk.** Electrochemical reduction of oxygen on platinum- and palladium-based nanocatalysts. Tartu, 2017, 250 p.
165. **Siim Kukk.** Kinetic aspects of interaction between dopamine transporter and *N*-substituted nortropine derivatives. Tartu, 2017, 107 p.
166. **Birgit Viira.** Design and modelling in early drug development in targeting HIV-1 reverse transcriptase and Malaria. Tartu, 2017, 172 p.
167. **Rait Kivi.** Allostery in cAMP dependent protein kinase catalytic subunit. Tartu, 2017, 115 p.
168. **Agnes Heering.** Experimental realization and applications of the unified acidity scale. Tartu, 2017, 123 p.
169. **Delia Juronen.** Biosensing system for the rapid multiplex detection of mastitis-causing pathogens in milk. Tartu, 2018, 85 p.
170. **Hedi Rahnel.** ARC-inhibitors: from reliable biochemical assays to regulators of physiology of cells. Tartu, 2018, 176 p.
171. **Anton Ruzanov.** Computational investigation of the electrical double layer at metal–aqueous solution and metal–ionic liquid interfaces. Tartu, 2018, 129 p.
172. **Katrin Kestav.** Crystal Structure-Guided Development of Bisubstrate-Analogue Inhibitors of Mitotic Protein Kinase Haspin. Tartu, 2018, 166 p.
173. **Mihkel Ilisson.** Synthesis of novel heterocyclic hydrazine derivatives and their conjugates. Tartu, 2018, 101 p.
174. **Anni Allikalt.** Development of assay systems for studying ligand binding to dopamine receptors. Tartu, 2018, 160 p.
175. **Ove Oll.** Electrical double layer structure and energy storage characteristics of ionic liquid based capacitors. Tartu, 2018, 187 p.
176. **Rasmus Palm.** Carbon materials for energy storage applications. Tartu, 2018, 114 p.
177. **Jürgen Metsik.** Preparation and stability of poly(3,4-ethylenedioxythiophene) thin films for transparent electrode applications. Tartu, 2018, 111 p.
178. **Sofja Tšepelevitš.** Experimental studies and modeling of solute-solvent interactions. Tartu, 2018, 109 p.
179. **Märt Lõkov.** Basicity of some nitrogen, phosphorus and carbon bases in acetonitrile. Tartu, 2018, 104 p.
180. **Anton Mastitski.** Preparation of α -aza-amino acid precursors and related compounds by novel methods of reductive one-pot alkylation and direct alkylation. Tartu, 2018, 155 p.
181. **Jürgen Vahter.** Development of bisubstrate inhibitors for protein kinase CK2. Tartu, 2019, 186 p.

182. **Piia Liigand.** Expanding and improving methodology and applications of ionization efficiency measurements. Tartu, 2019, 189 p.
183. **Sigrid Selberg.** Synthesis and properties of lipophilic phosphazene-based indicator molecules. Tartu, 2019, 74 p.
184. **Jaanus Liigand.** Standard substance free quantification for LC/ESI/MS analysis based on the predicted ionization efficiencies. Tartu, 2019, 254 p.
185. **Marek Mooste.** Surface and electrochemical characterisation of aryl film and nanocomposite material modified carbon and metal-based electrodes. Tartu, 2019, 304 p.
186. **Mare Oja.** Experimental investigation and modelling of pH profiles for effective membrane permeability of drug substances. Tartu, 2019, 306 p.
187. **Sajid Hussain.** Electrochemical reduction of oxygen on supported Pt catalysts. Tartu, 2019, 220 p.
188. **Ronald Väli.** Glucose-derived hard carbon electrode materials for sodium-ion batteries. Tartu, 2019, 180 p.
189. **Ester Tee.** Analysis and development of selective synthesis methods of hierarchical micro- and mesoporous carbons. Tartu, 2019, 210 p.
190. **Martin Maide.** Influence of the microstructure and chemical composition of the fuel electrode on the electrochemical performance of reversible solid oxide fuel cell. Tartu, 2020, 144 p.
191. **Edith Viirlaid.** Biosensing Pesticides in Water Samples. Tartu, 2020, 102 p.
192. **Maike Käärrik.** Nanoporous carbon: the controlled nanostructure, and structure-property relationships. Tartu, 2020, 162 p.
193. **Artur Gornischeff.** Study of ionization efficiencies for derivatized compounds in LC/ESI/MS and their application for targeted analysis. Tartu, 2020, 124 p.
194. **Reet Link.** Ligand binding, allosteric modulation and constitutive activity of melanocortin-4 receptors. Tartu, 2020, 108 p.
195. **Pilleriin Peets.** Development of instrumental methods for the analysis of textile fibres and dyes. Tartu, 2020, 150 p.
196. **Larisa Ivanova.** Design of active compounds against neurodegenerative diseases. Tartu, 2020, 152 p.
197. **Meelis Härmas.** Impact of activated carbon microstructure and porosity on electrochemical performance of electrical double-layer capacitors. Tartu, 2020, 122 p.
198. **Ruta Hecht.** Novel Eluent Additives for LC-MS Based Bioanalytical Methods. Tartu, 2020, 202 p.
199. **Max Hecht.** Advances in the Development of a Point-of-Care Mass Spectrometer Test. Tartu, 2020, 168 p.
200. **Ida Rahu.** Bromine formation in inorganic bromide/nitrate mixtures and its application for oxidative aromatic bromination. Tartu, 2020, 116 p.
201. **Sander Ratso.** Electrocatalysis of oxygen reduction on non-precious metal catalysts. Tartu, 2020, 371 p.
202. **Astrid Darnell.** Computational design of anion receptors and evaluation of host-guest binding. Tartu, 2021, 150 p.

203. **Ove Korjus.** The development of ceramic fuel electrode for solid oxide cells. Tartu, 2021, 150 p.
204. **Merit Oss.** Ionization efficiency in electrospray ionization source and its relations to compounds' physico-chemical properties. Tartu, 2021, 124 p.
205. **Madis Lüsi.** Electroreduction of oxygen on nanostructured palladium catalysts. Tartu, 2021, 180 p.
206. **Eliise Tammekivi.** Derivatization and quantitative gas-chromatographic analysis of oils. Tartu, 2021, 122 p.
207. **Simona Selberg.** Development of Small-Molecule Regulators of Epi-transcriptomic Processes. Tartu, 2021, 122 p.
208. **Olivier Etebe Nonga.** Inhibitors and photoluminescent probes for in vitro studies on protein kinases PKA and PIM. Tartu, 2021, 189 p.
209. **Riinu Härmas.** The structure and H₂ diffusion in porous carbide-derived carbon particles. Tartu, 2022, 123 p.
210. **Maarja Paalo.** Synthesis and characterization of novel carbon electrodes for high power density electrochemical capacitors. Tartu, 2022, 144 p.
211. **Jinfeng Zhao.** Electrochemical characteristics of Bi(hkl) and micro-mesoporous carbon electrodes in ionic liquid based electrolytes. Tartu, 2022, 134 p.
212. **Alar Heinsaar.** Investigation of oxygen electrode materials for high-temperature solid oxide cells in natural conditions. Tartu, 2022, 120 p.
213. **Jaana Lilloja.** Transition metal and nitrogen doped nanocarbon cathode catalysts for anion exchange membrane fuel cells. Tartu, 2022, 202 p.
214. **Maris-Johanna Tahk.** Novel fluorescence-based methods for illuminating transmembrane signal transduction by G-protein coupled receptors. Tartu, 2022, 200 p.
215. **Eerik Jõgi.** Development and Applications of E. coli Immunosensor. Tartu, 2022, 103 p.
216. **Alo Rüütel.** Design principles of synthetic molecular receptors for anion-selective electrodes. Tartu, 2022, 109 p.